2015

QUARTZ CRYSTAL MICROBALANCE STUDIES ON FRICTION MODIFIERS FOR LUBRICANT APPLICATIONS

Carey Lehner
Virginia Commonwealth University

QUARTZ CRYSTAL MICROBALANCE STUDIES ON FRICTION MODIFIERS FOR LUBRICANT APPLICATIONS

A thesis submitted in partial fulfillment of the requirements for the degree of Master of Science at Virginia Commonwealth University.

by

CAREY REBECCA GARBER LEHNER
Chemistry and Anthropology, University of Mary Washington, VIRGINIA, 2005

Director: Julio C Alvarez
PROFESSOR, DEPARTMENT OF CHEMISTRY

Virginia Commonwealth University
Richmond, Virginia
December 2015

Table of Contents

Page

List of Figures

Page

List of Tables

Page

List of Abbreviations

AFM	Atomic Force Microscopy
CMC	Critical Micelle Concentration
CoF	Coefficient of Friction
D	Dissipation
Δf	Change in frequency
FM	Friction Modifier
GDO	Glycerol Dioleate
GMO	Glycerol Monoleate
HFRR	High Frequency Reciprocating Rig
k	Boltzmann constant
N	Newtons
Q	Quality Factor
QCM-D	Quartz Crystal Microbalance with Dissipation
ZDDP	Zinc Dialkyldithiophosphate

Abstract

QUARTZ CRYSTAL MICROBALANCE STUDIES ON FRICTION MODIFIERS FOR LUBRICANT APPLICATIONS

By Carey Lehner, M.S.

A thesis submitted in partial fulfillment of the requirements for the degree of Master of Science at Virginia Commonwealth University.

Virginia Commonwealth University, 2015

Major Director: Dr. Julio C Alvarez, Associate Professor, Department of Chemistry

Lubricants are used in numerous applications to control friction and protect moving parts from fatigue. These fluids consist of a variety of surface active chemistries competing for the surface to provide performance. In order to develop fluids that meet the ever-increasing requirements (from legislation and manufacturers), techniques that can provide insight into surface adsorption, in real time, and relate it back to performance are critical.

The objective of this work is to determine if Quartz Crystal Microbalance with Dissipation (QCM-D) is an effective technique to investigate surfactant adsorption in regimes that are common to the transportation lubricant industry. QCM-D is employed to quantify the

mass, characterize the morphology, and quantify the kinetics of adsorption of common friction modifiers. The adsorption information is then compared to macroscopic properties (friction and corrosion prevention) to determine if this technique can aid in formulating future lubricants.

CHAPTER 1: Introduction

1.1 **Overview of Lubricants:** A wide variety of applications mandate the need for fluids to protect moving parts and control friction. Examples include (but are not limited to) aerospace, over-the-road and off-road transportation, food machinery, shipping and boating, wind turbines, metal shaping, and oil exploration and recovery. Many of these applications require high temperatures and minimal rust, making petroleum-based lubricants an obvious choice. Due to the numerous applications, and nuisances associated with each of them, this thesis will focus on factors important to the transportation industry, but the application of this work extends to numerous other industries.

Transportation lubricants consist of two parts: a base oil and the additive system. The base oil provides a heat sink, some lubricity, and transport for the additive. The additive system consists of the other components added into the base oil to protect the moving parts and extend the life of the machine. A multitude of chemicals of different functionality are used to provide bulk fluid performance (reduce oxidation, foam, etc.) as well as condition the surface to provide proper friction, protect from fatigue and minimize corrosion. A delicate balance of chemicals is required to optimize the performance characteristics, because many of the additives compete for the surface. Figure 1 is a simplified illustration of the composition of common additives.

Detergents, dispersants and anti-oxidants prevent oxidation, formation of sludge deposits and maintain soot in suspension. Detergents are typically oil soluble acids neutralized with metal oxides that are capable of neutralizing acidic products formed while vehicles are in operation. Dispersants consist of polar functional groups, typically oxygen or nitrogen based, and large

nonpolar hydrocarbon groups. The polar group associates with the polar degradation products and the nonpolar regions keeps the particles suspended in solution. Hindered phenols are typical antioxidants that serve as free radical traps to prevent oxidation of the oil.

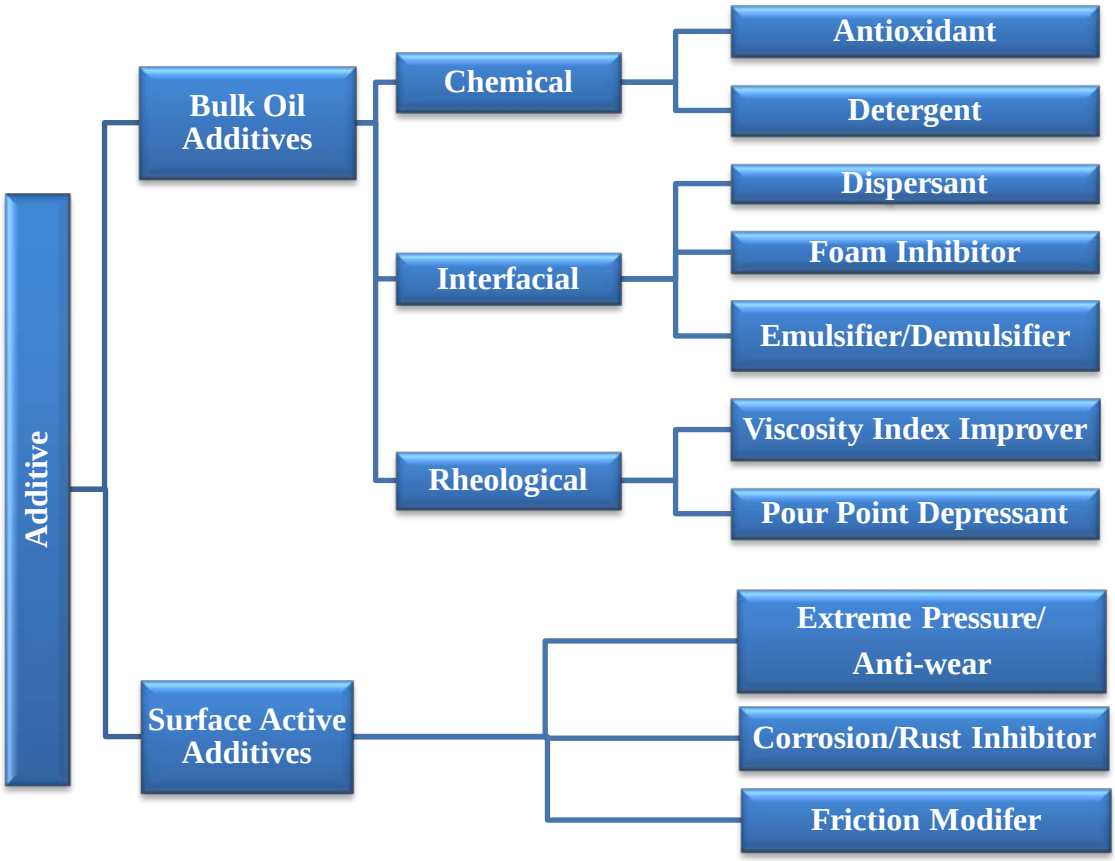

Figure 1: Classification of components contained in common additive packages

Components are also added to control the presence of water and air in lubricant systems. If not properly controlled, water can generate corrosion and entrained air can generate foam (which is a poor lubricant). Polydimethylsiloxane (PDMS) is a common foam inhibitor that lowers surface tension, collapsing air bubbles formed during aeration. Surfactants are added to manage water introduced during operation of the equipment/vehicles. Depending on the application water may

need to be emulsified or demulsified, so there is not a characteristic structure. Rheological properties are controlled by long chain polymers that serve to maintain consistent viscosity over a wide temperature range. In order for vehicles to operate efficiently, at very cold temperatures the lubricant needs to be pumpable. At high temperatures the lubricant needs to be viscous enough to separate the moving parts and operate pumps.

The surface active components are the chemicals added to protect the surface from wear (or other fatigue), control friction and prevent corrosion. Zinc dialkyldithiophosphates (ZDDPs) are one of the most established anti-wear additives in the industry and are present within virtually all engine oils. The ZDDP decomposes and forms polyphosphate glass on the steel surface, reducing wear. Transmission, hydraulic and gear applications in transportation vehicles may use other anti-wear additives but the majority of them contain sulfur and phosphorus. Surface active short chain oligomers are commonly used as friction modifiers and corrosion inhibitors. These oligomers adsorb to steel to protect the surface from corrosion and separate the two surfaces in order to reduce friction, but can also out-compete the anti-wear components leading to increased fatigue of parts. Understanding the nature of adsorption of these surface active chemicals (and relating them back to performance) is advantageous in attaining a strong, well balanced lubricant needed for the next generation of transportation vehicles. As mentioned previously, friction and corrosion performance strongly depends on the interactions that occur at surfaces and will be the focus of this work.

1.2 **Friction:** In the broadest sense, friction is the resistance to sliding and motion. This resistance is typically quantified by the unitless coefficient (CoF). In real systems, friction is dependent on viscosity, sliding speed and normal force. The magnitude of these parameters defines the regime: boundary, hydrodynamic or mixed. Hydrodynamic friction is defined by

higher sliding speed and lower loads, allowing enough fluid in the interface such that asperities on the surface are not in direct contact with one another. Under higher loads or slower speeds minimal fluid is present in the interface and the two surfaces are close enough that asperities are in contact, leading to higher friction. In this regime additives are needed to reduce friction and wear to prevent seizure of the moving parts. The transition between boundary and hydrodynamic is described as mixed. The Stribeck curve in Figure 2 illustrates how friction is influenced over these three regimes.[1] Dry friction, located on the left side of the graph, is the point where two surfaces are in direct contact with one another and friction is at its highest. As the viscosity of the lubricant increases the two surfaces are pushed apart; consequently, lowering friction. In addition, increasing the sliding speed or decreasing the force pushing the surfaces together has the same effect. At some point, the fluid between the surfaces becomes so large that internal friction is generated from the viscosity of the lubricant and the friction begins to increase. In general, these trends are consistent throughout systems, although the magnitudes may vary.

Engine oils aim to minimize friction to increase fuel economy. As much as 3-8% of fuel consumption can be attributed to internal friction.[2] Improving fuel economy is becoming more and more critical as legislation continues to introduce more stringent fuel economy requirements. Transmissions have more complex friction needs. In these applications, it is not ideal to simply lower friction overall since high static friction is necessary to prevent clutch slippage. Instead, it is critical to control and maintain friction to eliminate shudder in the transmission. This is done by ensuring friction (μ) decreases as velocity (υ) decreases ($d\mu/d\upsilon>0$).[3] Without modification, low speed friction is typically higher than high speed friction, so molecules such as surfactants are added to in an effort to lower the coefficient of friction in the low speed region.

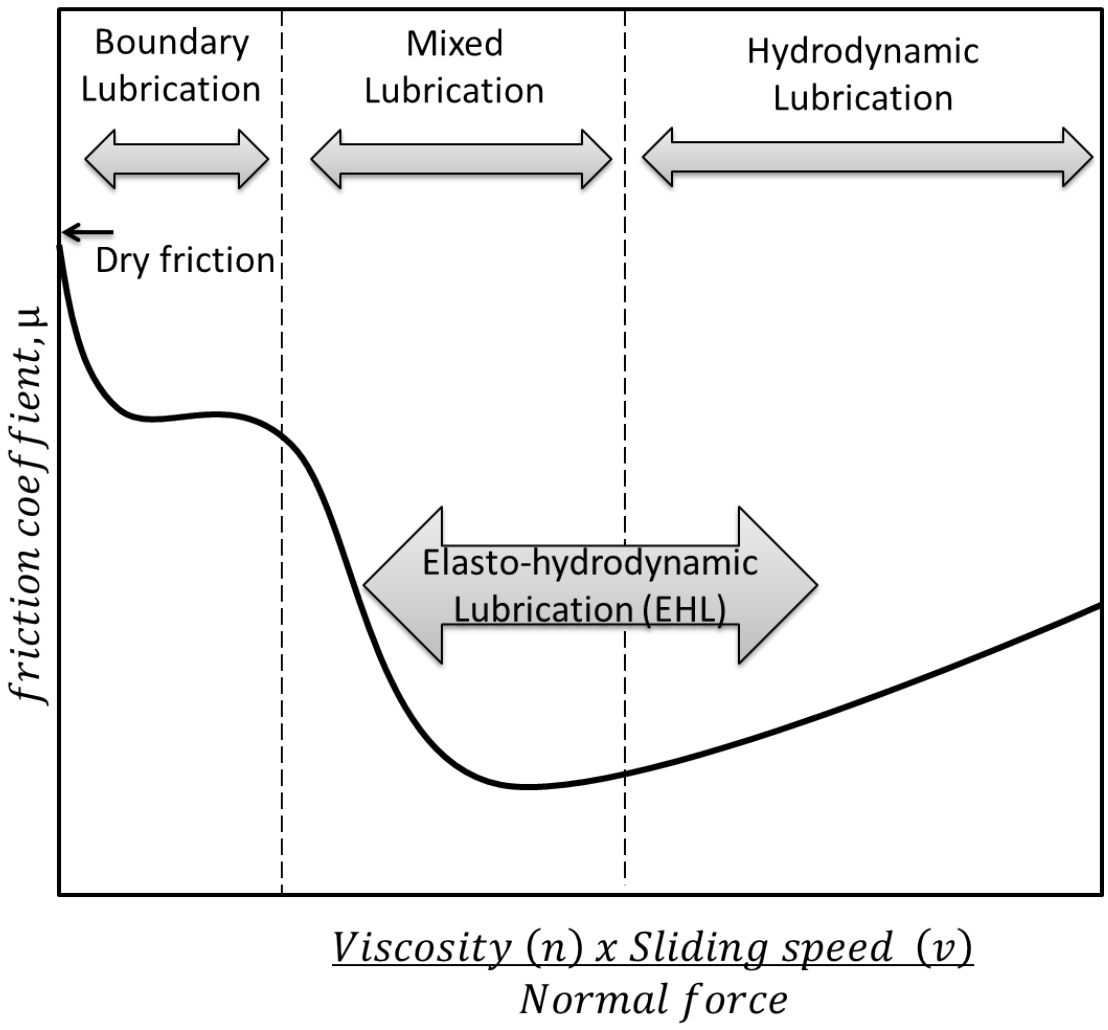

Figure 2: Stribeck curve: Illustrates the different tribological regimes and how friction is a function of viscosity, sliding speed and normal force.

1.3 **Surfactants:** Boundary friction can be reduced by surface active molecules that are classified as friction modifiers. These components need to be oil soluble as well as surface active. As a result, many of the common friction modifiers are surfactants. Surfactants are characterized by their distinct polar and nonpolar regions, the latter being commonly a hydrocarbon chain. More specifically, oleyl-based surfactants are often used since they are naturally occurring, economical, and efficient in lowering friction. The polar head group varies

but some common functional groups are sulfonates, amides, glycerols, amines, and acids. These surface active oligomers are commonly used to improve corrosion and lower boundary friction; however, they can also increase wear, scuffing or other surface fatigue phenomena.

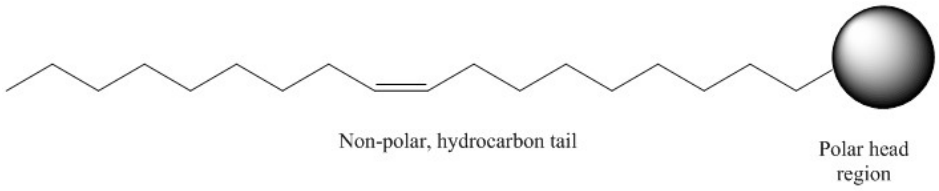

Figure 3: General diagram of common oleyl friction modifier/surfactant

1.3.1 Micelles: In polar environments and low concentrations, surfactants arrange at interfaces with their nonpolar hydrocarbon tails towards oil or air and polar head group oriented towards the solvent; thus, lowering the surface tension. At higher concentrations, the surfactants begin to form aggregates with their hydrophobic tails oriented towards the center and polar head group toward the solvent. This orientation, known as micelles, serves to shield the nonpolar region from the polar solvent. In this configuration, hydrocarbon tails are slightly more restricted compared to in the bulk solution, but still mobile. Often micelles are pictured as spherical, but in reality are often times elongated or odd in shape.

The minimum concentration at which micelles begin to form is known as the critical micelle concentration (CMC). The average number of monomers that make up a micelle and the CMC values are dependent on a number of factors, such as hydrocarbon chain length, polar head group, solvent and temperature. Compared to nonionic surfactants, ionic surfactants tend to form smaller micelles due to the electrostatic repulsion from their head group.[4] CMCs can be determined experimentally by surface tension, conductivity, and light scattering methods.[5]

1.3.2 Reverse Micelles: In nonpolar solvents, surfactants aggregate in the opposite direction with their polar head group oriented towards the interior and hydrophobic tail outward. These aggregates are labeled inverted or reverse micelles. The CMC decreases with increasing chain length, due to the increase in tendency of monomers to aggregate with increasing chain length.[6] The driving force for inverted micelles is different than normal micelles and CMCs are often more difficult to experimentally measure. Water present in these non-polar systems can be shielded from the non-polar solvent by sequestering in the interior of the inverted micelle. As with normal micelles, they are depicted as static structures but in reality the surfactant molecules are dynamic.

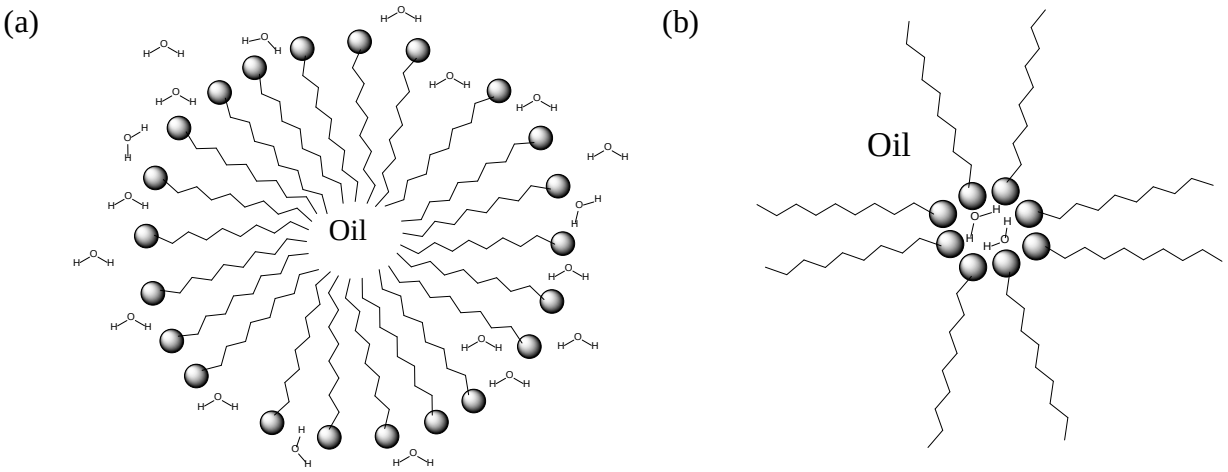

Figure 4: (a) Illustration of normal micelle in polar solvent and (b) reverse micelle in oil

1.3.3. Self Assembled Monolayers (SAMs): In addition to aggregating in the bulk, surfactants also adsorb to surfaces. SAMs are formed when surfactants spontaneously adsorb from solutions into a monomolecular layer on surfaces. In these monolayers, van der Waals interactions exist between the hydrocarbon chains because they are in registry. Adsorption can be chemical or physical. Differentiating between the two adsorption methods is defined by the enthalpy of

adsorption and/or residence time. Chemisorption is defined by the higher binding energy (typically more negative than -40kJ/mol) or long residence time. The residence time is long, so the molecules are considered to not depart from the surface after adsorption. The weaker adsorption, physisorption, is defined by a very small residence time and lower binding energy.[7] Comparing the enthalpy of bonding to kT (k is the Boltzmann constant and T the absolute temperature) provides an indication of molecular motion. If the binding energy is an order of magnitude greater than kT, the SAM is very stable over a long period of time and a wider temperature range. Alkanethiol SAMs on Au(111) are one such example. These SAMs have been heavily studied and form very stable monolayers due to their high bonding energies (ΔH_{abs}=-83.7$\pm$4.2 kJ/mol).[8]

1. 4 Surface Analysis: The amount of friction and corrosion observed in applications can be controlled by the SAMs that are formed on solid surfaces. Due to its strong mechanical properties and cost-effectiveness, steel is typically the substrate in transportation applications. Surfactant molecules, with an affinity for steel, form friction reducing layers increasing the lifetime of mechanical devices. Iron oxide surfaces are not atomically flat nor chemically uniform making highly ordered monolayers unlikely. Also, relative to thiol on gold, many of the typical friction modifiers and corrosion inhibitors used in the industry have lower binding energies. In these systems it is likely the surfactants exchange between the surface and bulk fluid on very fast timescales. Molecular dynamic simulations conducted by Greenfield of weakly adsorbed surfactants desorbed from the surface on the timeframe of 200 picoseconds.[9] For engines, steel-on-steel friction is the only friction of concern but in transmissions multiple materials are in contact with the steel (i.e., paper, sintered bronze and elastomers).

Understanding interactions with these surfaces is also important, but since steel is the most copious material it will be the focus of this thesis.

Understanding the chemical and physical interactions that occur at surfaces is essential, but is often difficult to follow *in-situ*. There are a variety of techniques to measure surface phenomena (mechanical, optical, and electrical) each with their own advantages and disadvantages (Table 1). The majority of the techniques are *ex-situ* (i.e., ellipsometry, Atomic Force Microscopy, etc.); thus, incapable of providing kinetic information. Surface plasma resonance (SPR) and Quartz Crystal Microbalance (QCM) are the principal techniques for measuring *in-situ* adsorption of SAMs. SPR is an optical technique that utilizes light to resonate electrons (within the sensor chip) that are sensitive to their surrounding environment. These electrons are referred to as surface plasmons. Dynamic processes are measured through the decrease in intensity of reflected light observed upon adsorption to the surface. The disadvantage with this technique is the substrate must be capable of generating surface plasmons in the detectable region (typically gold or silver). In contrast, Quartz Crystal Microbalances (QCM) are capable of measuring dynamic processes on steel substrates at high sensitivities (ng/cm^2).

Table 1: Summary of some common surface analysis techniques. High sensivity, in-situ measuremnents, and ability to measure adsorption on steel substrates were requirements for this application.

Techniques	Method	*In-situ*	Steel Substrate	Quantitative	High Sensitivity	Other
Spectroscopic Ellipsometry[10]	Optical	✗	✓	✓	✓	• Surface roughness of sample needs to be quite small • Data analysis complicated
Quartz Crystal Microbalance with dissipation (QCM-D)[11]	Gravimetric/ Mechanical	✓	✓	✓	✓	• Non-specific (responds to all analytes) • Complex modeling necessary for highly dissipative films • Provides conformational information
Attenuated Total Reflectance (ATR-IR)[12]	Optical	✗	✗	✗	✗	• Lacks sensitivity (scattering makes difficult to quantify) • Evanescent effect works if the crystal is made of an optical material with a higher refractive index than sample • Provides conformational changes
Surface Plasmon Resonance (SPR)[13]	Optical	✓	✗	✓	✓	• Substrate must be capable of generating surface plasmons in detectable region
Atomic Force Microscopy (AFM)[14]	Electrostatic/ Mechanical	✗	✓	✓	✗	• Provides topography of surface • Assumes substrate is smooth • Also capable of measuring friction • Measures small surface area (~5μm)
Polarization-Modulation Infrared Reflection Absorption Spectroscopy (PM-IRRAS)[15]	Optical	✗	✓	✗	✓	• Provides information on bonding occurring at surfaces and molecular orientation • Eliminates need for separate background spectrum

1.4.1 Quartz Crystal Microbalance (QCM): QCMs have been applied to various applications over the last few decades: gas phase detection, immunosensors, DNA biosensors and drug analysis to name a few.[16] Quartz is a piezoelectric material; therefore, an accumulation of

electrical charge occurs when mechanical stresses are applied along a defined axis. The converse is true as well. A piece of quartz is plated with two electrodes (typically gold) on each surface and an electrical potential applied that results in an internal mechanical stress, leading to the oscillation of the crystal at its natural or resonant frequency (Figure 5).

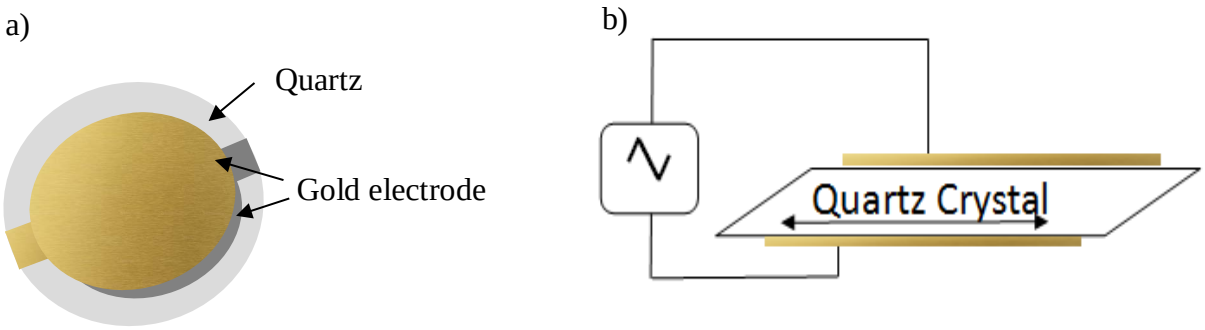

Figure 5: (a) Piezoelectric quartz crystal (b) piezoelectric quartz crystal after applying electrical potential.

Another way to define resonance is the frequency (or frequencies) at which the amplitude of a wave is the largest. Multiple resonant frequencies for a single system are depicted in Figure 6. Resonance is achieved in all three of the waves depicted, but the frequency of each wave is different. The left wave is the lowest frequency at which resonance is attained, known as the fundamental frequency. Overtone is the term used to describe any resonant frequency above the fundamental frequency. Frequency is inversely proportional to wavelength; therefore, the frequency of overtones increases incrementally by the fundamental frequency. Because of this, frequency of higher harmonics can be reduced to the fundamental frequency simply by dividing by the overtone. In QCM-D this is often done to normalize all frequency data to the same scale.[17]

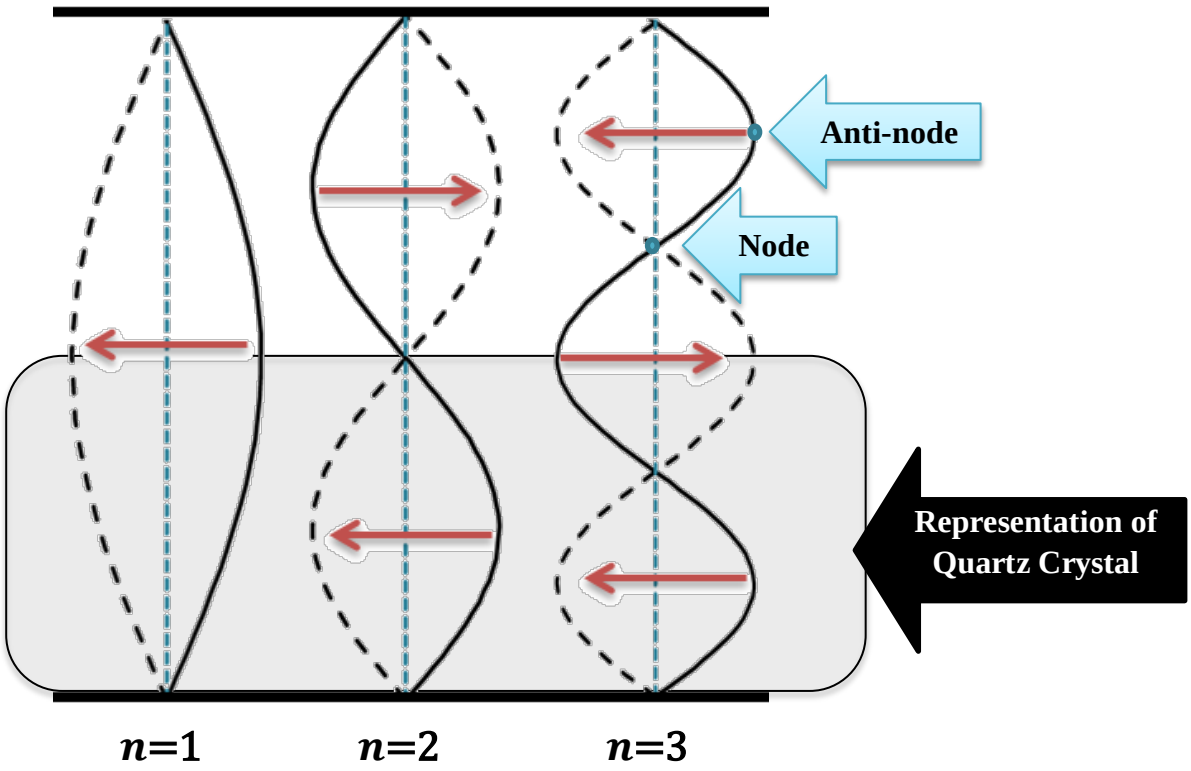

Figure 6: Illustration of multiple resonant frequencies (harmonics). The boundary conditons of the system are defined by the thick black lines. The wave on the left represents the lowest frequency at which resonance is achieved. Nodes are present in the higher frequency overtones, but the maximun amplitude is still reached. The wavelength of the fundamental frequency is twice the thickness of the quartz crystal. In order for the QCM to be able to excite oscillating waves at resonance, a node must be present at one surface and an anti-node at the other surface. As a result, only odd harmonics are measured.

The wavelength of the fundamental frequency is twice the thickness of the crystal. In order for the quartz crystal to excite a standing wave at resonance, a node (points on the wave with no displacement) must be present on one surface and an anti-node (points on the wave with maximum displacement) on the other. As the Figure 6 illustrates, this is only true in the case of odd harmonics. Nodes are located on both surfaces for even harmonics, so they cannot be measured using this technique.

The fundamental frequency of the crystal is dependent on the thickness, density, temperature and shear modulus of the quartz as well as the density or viscosity of the surrounding air or liquid. Since the properties of the quartz are constant for a given crystal/experiment, if variation in temperature is minimized any change in frequency can be related to changes in the surrounding air or liquid, as proven by Sauerbrey in 1959 (Equation 1)[18].

$$\Delta f = -\frac{2{f_0}^2 n}{A\sqrt{\rho_q \mu_q}}\,\Delta m \tag{1}$$

f_0 = fundamental resonant frequency (Hz)
Δf = frequency change (Hz)
Δm = mass change (g)
A = piezoelectrically active crystal area (area between electrodes, cm^2)
ρ_q = density of quartz (2.648 g/cm^3)
μ_q = shear modulus of AT cut quartz (2.947×10^{11} $gcm^{-1}s^{-2}$)
n = overtone

This equation regards the deposited mass as an extension of the thickness of the underlying quartz. It assumes the deposited mass is rigid, evenly distributed, and small relative to the mass of the crystal. This equation can be used for measurements in vacuum, but in a liquid the solvent can couple with the resonator, dampening the crystal and leading to an underestimation of the mass.[19] In the 1980s, QCMs become more widely applicable when Kanazawa modified the Sauerbrey equation to account for liquid environments (Equation 2).[20]

$$\Delta f_{liqload} = -f_0^{\frac{3}{2}}\left(\frac{n_L \rho_L}{\pi \mu_Q \rho_Q}\right)^{1/2} \tag{2}$$

n_L = absolute viscosity
ρ_L = density of liquid

Since the frequency of the crystal can be dampened by the liquid environment, it is also vital to measure the dissipation. The dissipation (D) is defined by Equation 3, where E_d is the energy dissipated and E_s is the energy stored during a period of oscillation. In addition to dampening from the liquid environment, any adsorbed film that is not rigid and contains viscoelastic character may contribute to the dampening of the crystal. Dissipation is sometimes referred to as the inverse of the quality factor (Q). Q is a dimensionless parameter widely used in circuits to quantify the ratio of energy stored in a resonator to the energy supplied by it.

$$D = \frac{1}{Q} = \frac{E_d}{2\pi E_s} \tag{3}$$

The QCM with Dissipation (QCM-D) shuts off the driving frequency for an infinitesimal time after the oscillation stabilizes and records the decay curve (Figure 8). This process occurs multiple times in a second.

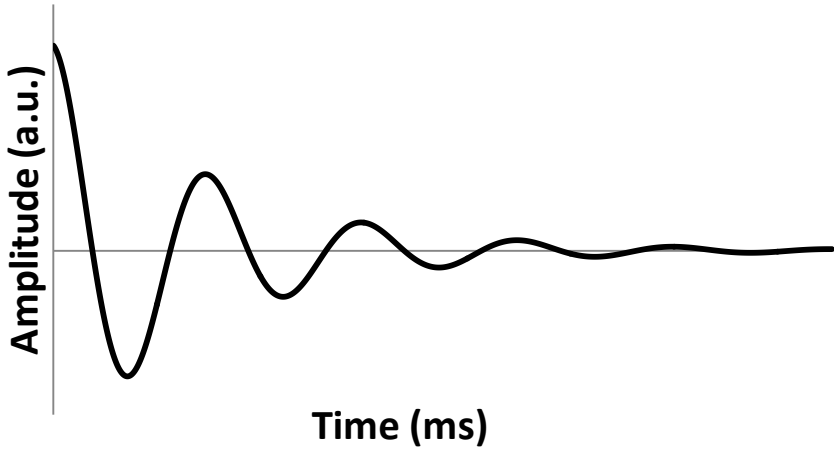

Figure 7: Depiction of typical decay curve

The dissipation is then calculated by fitting the decay curve to an exponentially damped, sinusoidal equation.

$$A = A_0 e^{-t/\tau} \sin(\omega t + \varphi) \tag{4}$$

$$D_{tot} = \frac{2}{\omega t} \tag{5}$$

The dissipation due to the dampening of the bulk liquid can be estimated from the density and viscosity of the liquid.[21]

$$\Delta D = \frac{2 f_0^{\frac{1}{2}}}{\sqrt{n\pi}} \frac{\sqrt{\rho_l \, n_l}}{\mu_Q \rho_Q} \tag{6}$$

A typical frequency and dissipation plot for the formation of a rigid monolayer is illustrated in Figure 7. Upon addition of the sample, the frequency (blue) decreases to a steady value and there is no measurable change in dissipation (red). Starting around 43 minutes, the initial solvent is pumped across the crystal to remove any loosely adsorbed material (physical adsorption). At this point, labeled rinse, the frequency increases then quickly plateaus. Since there is no change in dissipation, the Sauerbrey equation is valid and the mass (green) is directly proportional to the change in frequency.

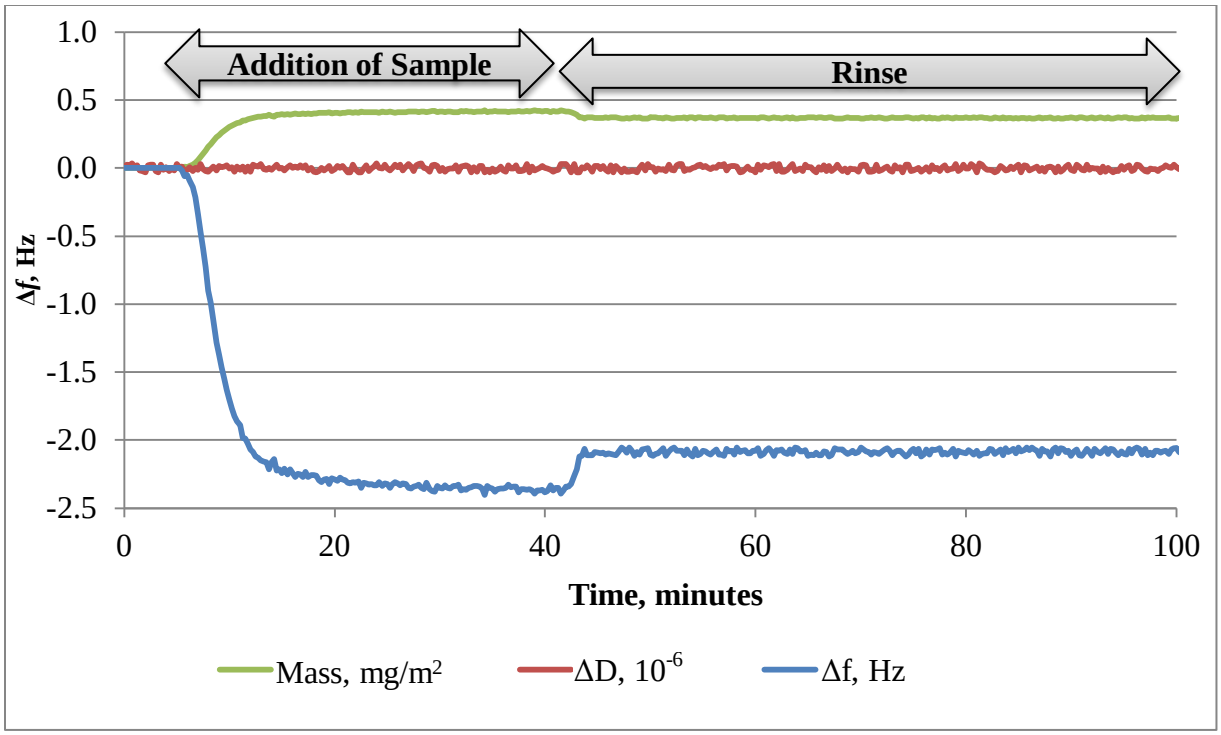

Figure 8: Example frequency and dissipation shift for rigid monolayer and calculated mass

Equations 2 and 6 can also be utilized to estimate correction factors, if there is significant change in viscosity and density of solutions compared to the solvent.[22] At low concentration of solute, the viscosity and density of solution is not much different from the baseline measurement, which is the pure solvent. However, at the higher concentrations of solute corrections are necessary. For example, viscosity and density values for various solutions of oleylamine in isooctane (at 25°C) are listed in Table 2. These values can be plugged into equation 2 and 6 as the density and viscosity of the liquid (ρ_l n_l). The difference between calculated frequency and dissipation for the pure solvent and the oleylamine solutions provides the correction factors.

Table 2: Viscosity and density values for various concentrations of olelylamine in isooctane used to calculate frequency and dissipation changes due to differences in bulk properties. The frequency correction values have been divided by the overtone, 9, to normalize the data.

Concentration, mM	**Viscosity, kg/ms**	**Density, kg/m^3**	**Correction Factors for 9^{th} overtone**	
			Frequency, Hz	**Dissipation, 10^{-6}**
0	0.0004730	692.00	---	---
0.25	0.0004731	692.00	0.01	0.00
2.00	0.0004734	692.04	0.07	0.03
100	0.0004949	693.91	3.25	1.31

At the lowest concentration (0.25 mM) minimal corrections are required, but at the highest concentration (100 mM) very large corrections are required. Looking at the raw data measured at this concentration and overtone using the QCM (Figure 9), odd behavior in the frequency measurement is observed upon addition of the solution. The first inflection at about ~3.2Hz corresponds to the calculated frequency correction of 3.25Hz, providing a reasonable explanation for the odd behavior. The corrected frequency and dissipation values are depicted as dotted lines in Figure 9 as well. Neglecting these corrections will lead to a large overestimation of deposited mass. All data reported hereafter will be corrected if required.

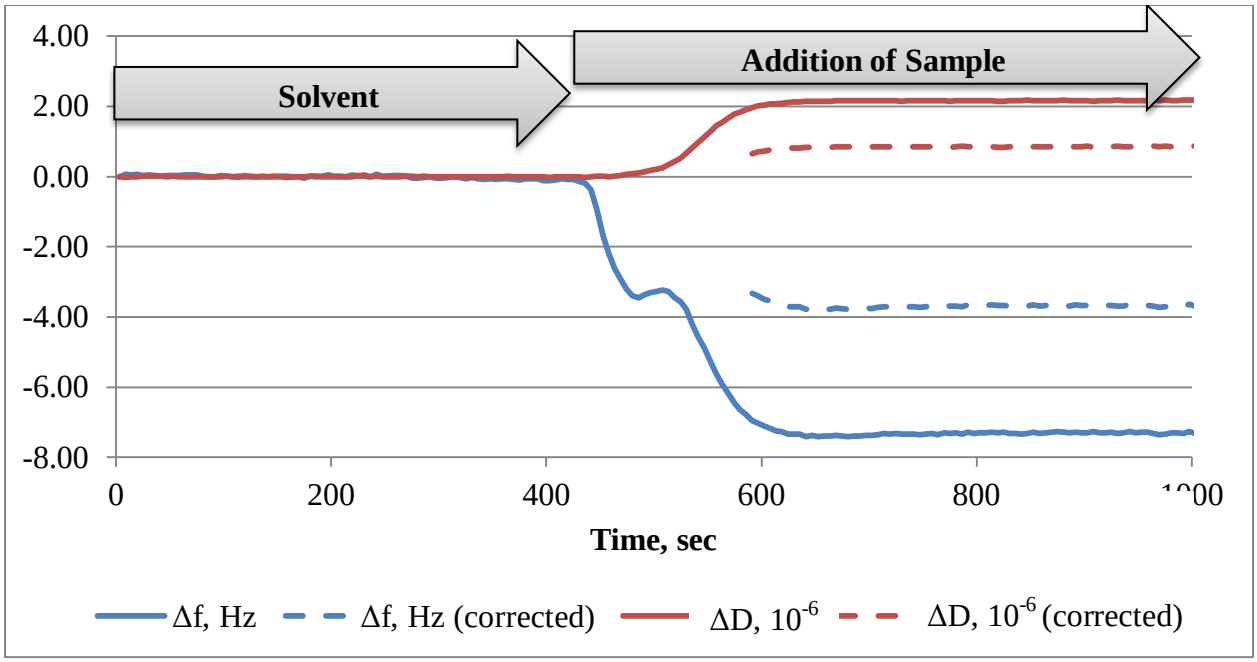

Figure 9: Frequency and dissipation measurements at the 9th overtone in real time for 100mM oleylamine in isooctane. Due to the large change in density and viscosity, corrections are required for frequency and dissipation at this concentration.

1.4.1.1 Viscoelastic Adsorption: If the adsorbed layer exhibits any viscoelastic character, (measured dissipation) the Sauerbrey equation is no longer valid and using it will underestimate the true mass adsorbed to the surface. In practice, if the dissipation is minimal, the Sauerbrey equation is recognized as an acceptable estimation. In cases where a high dissipation is measured viscoelastic models can be used to determine the mass. In order to most effectively use this model, data is recorded at multiple overtones. If the magnitude of the frequency shift at each harmonic is not proportional to the overtone number, it is another indication that the adsorbed layer is viscoelastic.[23] Figure 10 illustrates typical frequency and dissipation shifts observed for viscoelastic systems at multiple overtones. The first overtone is typically not utilized due to the small signal-to-noise ratio. For simplicity, the frequency values were normalized by dividing the measured frequency value by the overtone number. Upon addition of sample, the frequency

decreases and the overtones begin to separate. The dissipation increases, relative to the frequency, indicating a soft, viscoelastic film. In these systems, the adsorbed layer behaves like a viscoelastic solid leading to dampening of the measured frequency. In order to accurately determine the mass, complicated viscoelastic models (i.e., Voigt) must be employed. In these models, the data is fitted to solve for multiple unknowns (density, viscosity, shear, and thickness of adsorbed mass).[24] Due to the large number of unknowns, this can be problematic and can lead to serious misinterpretation of data without a corroborating experimental method for at least one of the unknowns.

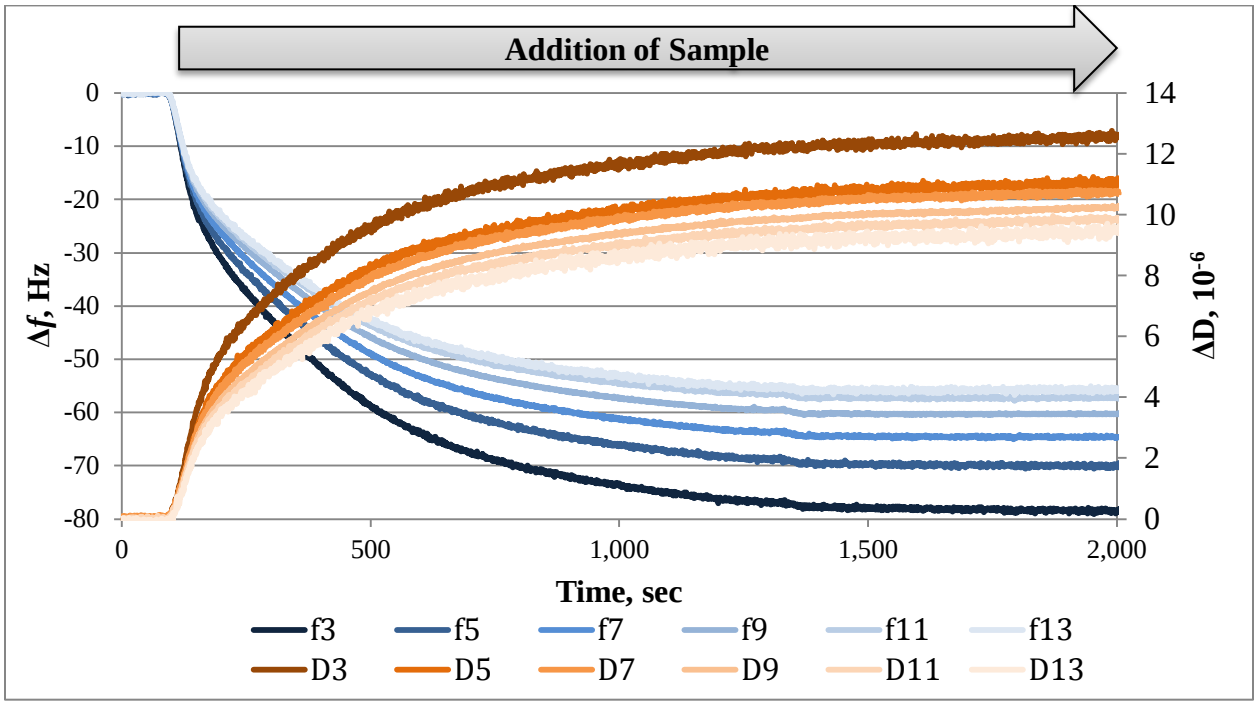

Figure 10: Example of frequency (f) and dissipation (D) shift measured for viscoelastic system at multiple overtones (3, 5, 7, 9, 11 and 13).

1.4.1.2 Penetration Depth of Overtones: As mentioned previously, the fundamental frequency is not often used due to the high signal to noise ratio. Figure 11 illustrates the varying penetration depth of each overtones. The fundamental frequency measures ~250nm from the quartz crystal.

This is an order of magnitude larger than most molecular interactions occurring at the surface, so its signal is largely dictated by the viscous medium and not as sensitive to adsorption characteristics. As the overtone increases, the shear wave's penetration into the medium decreases, so while the overall signal decreases, the signal-to-noise ratio increases. Thus, typically the higher overtones are reported due to the lower noise. It is important to note this is not infinite, if the frequency is too high spurious vibrations other than shear mode may be excited. This may lead to misinterpretation of the data since all models assume in-plane shear motion only.

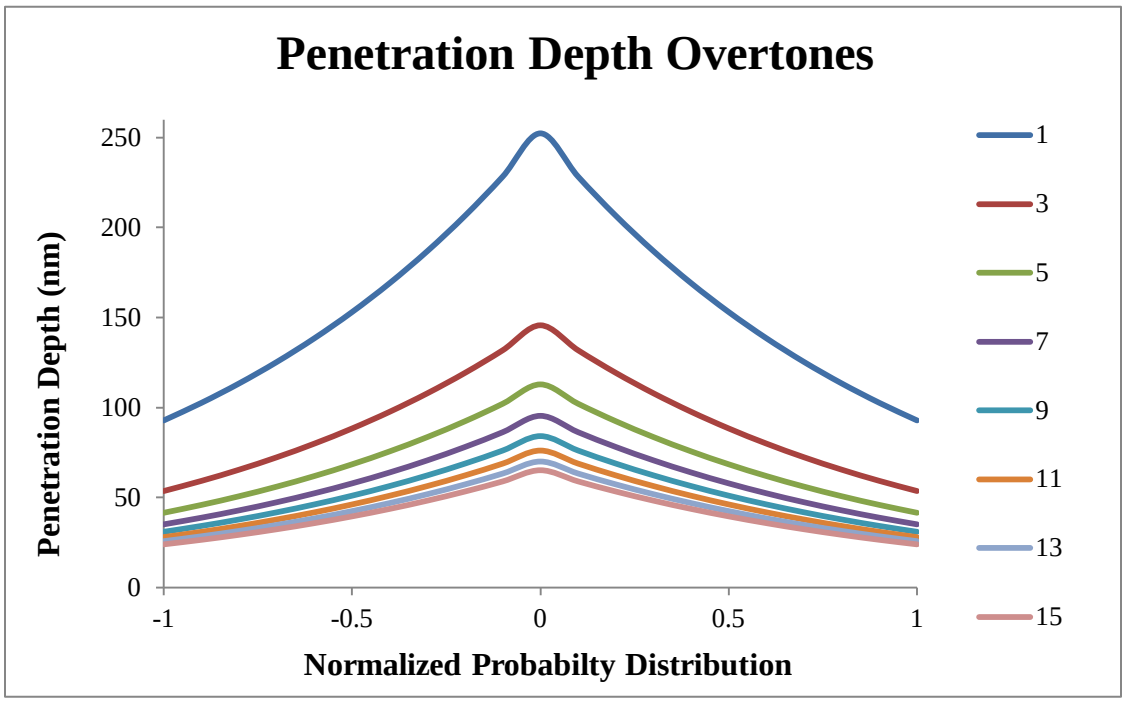

Figure 11: Nomalized probabiltiy distribution (provided by Qsense) illustrating the penetration depth for each overtone. [25]

1.4.1.3 Character of Adsorbed Layer: Plotting frequency and dissipation provides information on the adsorption process, irrespective of time. The frequency and dissipation values (from example datasets illustrated in Figures 6 and 8) are plotted in Figure 9. Type I illustrates the rigid

monolayer, where a change in frequency occurs but no change in dissipation. A greater slope is observed for the dissipative monolayer illustrated by Type II. A larger slope is indicative of a more viscoelastic film. This qualitative analysis provides notable insight into the adsorption process. Some curves may change slope over the course of adsorption, suggesting a multi-step adsorption processes are occurring, as in the case of thiols on gold.[26]

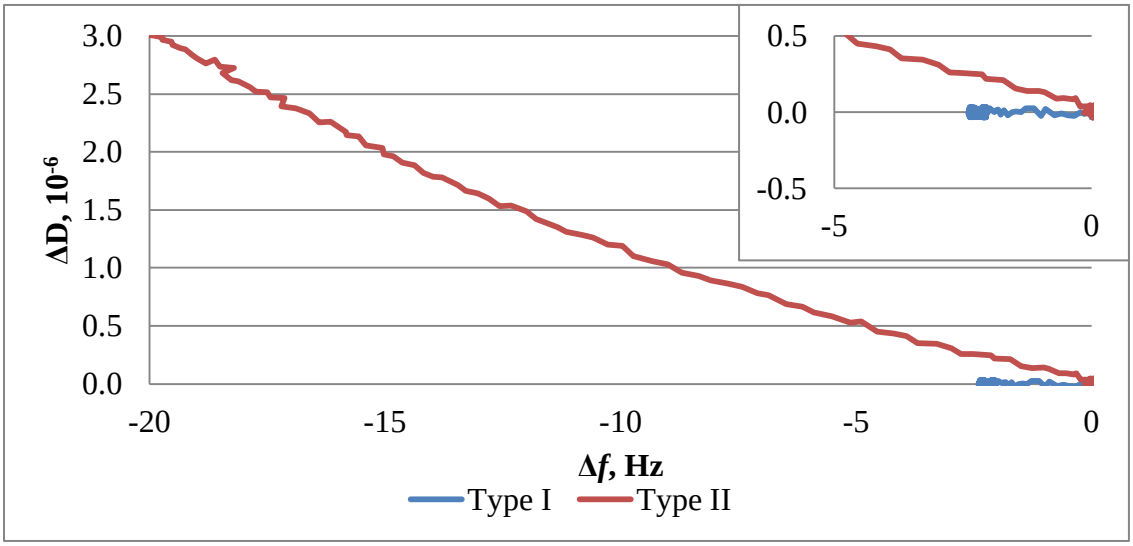

Figure 12: Representative frequency and dissipation plots for rigid monolayer (Type I) and dissipative films (Type II).

1.5 Statement of Thesis Research Objective: In the transportation industry, much of the testing (especially engine testing) can be very expensive and quite time-consuming. Gaining a good understanding of the interactions occurring on steel surfaces and relating it to performance could reduce the timeline and expense of evaluating new additives. Due to environmental concerns, legislation on improving fuel economy continues to become more stringent requiring the industry to move to lower viscosity lubricants. As viscosity of base oils continues to decrease, the demand for high performance additives capable of protecting moving parts under boundary conditions and controlling friction will become more critical. In addition to the fuel

economy legislation, more environmental regulations on metals and degradation products present in additives are being introduced globally. As a result, reducing the amount of metals, sulfur and phosphorous has become another area of interest. These requirements enforce the need for more complex lubricant formulations.

Additives based largely on carbon, hydrogen, and oxygen (with no environmental regulations) are the focus of this thesis (specifically fatty acids, glycerol oleates, amides, and amines). Using QCM-D the adsorption of these surfactants, from solution, will be measured in situ. The effectiveness of an additive depends on its affinity toward the material surface as well as the bulk solution. The data obtained on the nature and kinetics of the adsorbed films are then compared to friction and corrosion bench tests to determine if QCM-D is a useful technique in understanding difference observed in performance.

CHAPTER 2: Methods and Materials

2.1 Reagents: 1-monopalmitoleoyl-*rac*-glycerol (≥99%), 1-Stearoyl-*rac*-glycerol (≥99%), 1-Oleoyl-*rac*-glycerol (≥99%), Oleamide (≥99%), Oleic acid (≥99.0%), Octanoic acid(≥99.0%), and 2,2,4-Trimethylpentane (≥99.5%) were obtained from Sigma Aldrich. Oleyl amine was purchased from Akzo Nobel under the trade name Armeen OL. Glycerol dioleate (GDO) was purchased from Lambert Technologies and glycerol monooleate (GMO) from PMC Biogenix. All chemicals were used as received. GDO and GMO are often made from the natural fatty acids and sold as mixtures so the samples were further characterized by IR and ^{13}C NMR to determine the distribution (Table 3, Spectra shown in Appendix). Water can be measured as part of the mass using QCM-D, so Karl Fischer titrations (coulometric method) were utilized to quantify the amount of water in the GMO and GDO samples. Water in the GMO sample, 2128 ppm, was almost double the amount present in the GDO sample, 1194 ppm. These surfactants were chosen due to their common use as friction modifiers and/or steel corrosion inhibitors.

Table 3: Mole fraction of glycerol monooleate, diolate, trioleate in GMO and GDO determined by ^{13}C NMR and IR

	Glycerol	Glycerol Monooleate		Glycerol Dioleate		Glycerol Trioleate
		1-monolein	2-monolein	1,2-diolein	1,3-diolein	
GMO	0.08	0.57	0.06	0.09	0.18	0.02
GDO	0.03	0.22	0.02	0.14	0.29	0.29

2.2 **QCM:** The QCM-D is employed to quantify the mass and structure of various surfactants, in real time, as they adsorb to steel surfaces. The Qsense E4 model, QCM-D was purchased from Qsense, Gothenburg, Sweden. This model is comprised of four flow modules made of an aluminum shell and titanium (liquid contacting surfaces) mounted in a parallel configuration (Figure 13). Temperature stabilization loops are located within each module to control temperature within ± 0.02°C.

Figure 13: E4 Model QCM-D with four flow modules

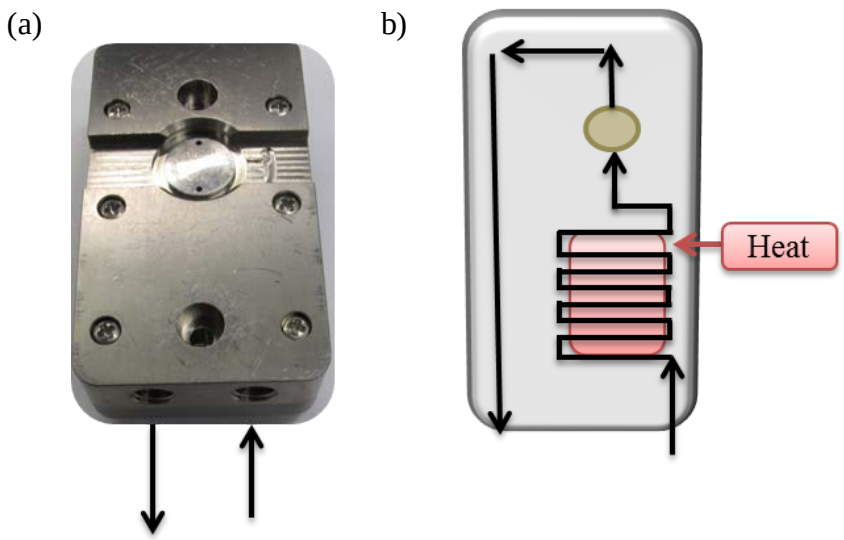

Figure 14: (a) QCM chamber and (b) diagram depicting the stabilization loop located within the chamber

AT cut quartz sensors (also purchased from Qsense) with a fundamental frequency of 5 MHz, are mounted within the modules. The sensors were 14 mm in diameter, and the active side was coated with Swedish standard steel 2343, which is comparable to US standard 316. The volume above the sensor was 40 µL. Based on the properties of the purchased crystal, the equation for the calculation of mass could be reduced to the following equation:

$$\Delta m = (-17.7 \text{ngcm}^{-2}\text{Hz}^{-1})\frac{1}{n}\Delta f \tag{7}$$

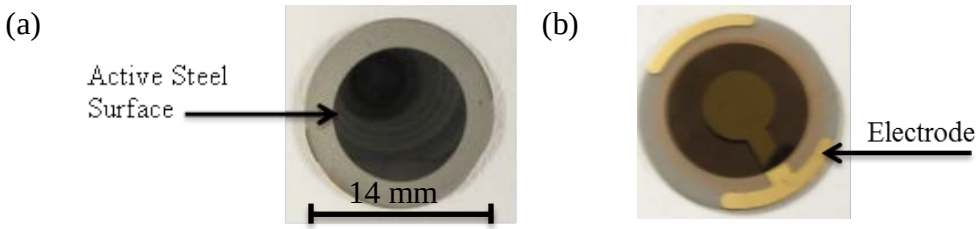

Figure 15: (a) Front and (b) back of stainless steel quartz sensor

The E4 model measures frequency and dissipation at 7 different overtones that probe various penetration depths and radial distributions. The first overtone has the greater penetration (~250 nm) and radial distribution and as a result suffers with a high amount of noise due the sensitivity. Often the higher overtones are reported because they exhibit a cleaner signal.

2.2.1 Cleaning the Sensors: The manufacturer's recommended procedure was followed for cleaning the crystals prior to use. The sensors were submerged in a solution of 1% Hellmanex® II (alkaline liquid concentrate) and ultrapure water (Type I). After 30 minutes, the sensors were rinsed with water, dried with nitrogen gas, and sonicated in 99 % ethanol for 10 minutes. The sensors were then rinsed with water and dried with nitrogen gas for a second time and finally treated with UV/ozone to oxidize the surface. Once the crystals were cleaned, they were immediately placed in the chamber of the flow module with the active side facing the flow chamber. Great care was taken to place the crystals evenly on the O-ring with the electrode facing the correct direction. The module was reassembled and placed on the QCM-D platform. The modules were taken apart after every experiment and the portion that was exposed to the sample (including the seals) were rinsed with heptane, sonicated in heptane and then dried with nitrogen gas. In order to verify the cleaning procedure was working effectively, at the end of testing, crystals were cleaned using the above procedure and compared to the theoretical frequency and dissipation values. The frequency and dissipation values were within 0.9% and 0.4%, respectively (Figure 48 in Appendix).

2.2.2 Adsorption Measurements: QCM-D was employed to measure the adsorption of a variety of surfactants, from solution (2,2,4-trimethylpentane) onto iron oxide surfaces. Solutions were made at various concentrations and sonicated for 30 minutes. First the frequency and

dissipation for each crystal and overtone was found in air, to ensure the quality of the crystal and that it was properly mounted within the module. Next solvent was added to the QCM-D at a pump speed of 90 µl/min and temperature of 25.00 ± 0.02°C until the frequency and dissipation leveled off. Multiple solvents and pump speeds were initially evaluated, but many of the higher viscosity solvents (i.e., squalane and low viscosity base oils) produced a high amount of noise that appeared to correlate with the pump speed. In order to best simulate the application, the minimum pump speed to maintain consistent temperature was selected.

After a stable base line was obtained surfactant solutions were added (maintaining the same pump speed and temperature) and the frequency and dissipation change measured in real time. (The GDO solutions were also measured at 50.00 ± 0.02°C to characterize the kinetics.) Each experiment was repeated a minimum of two times. After the frequency plateaued, the sensors were rinsed with solvent to differentiate the chemisorbed mass to the mass loosely physisorbed. In experiments that did not reach a plateau, the rinse was initiated after 2 to 3 hours. Friction and dissipation measurements were taken at the 3^{rd}, 5^{th}, 7^{th}, 9^{th}, 11^{th} and 13^{th} harmonic, but the 9^{th} and 11^{th} will be the primary data reported here due to their higher quality.

2.3 **High Frequency Reciprocating Rig (HFRR):** Steel on steel CoF values were measured using the High Frequency Reciprocating Rig (HFRR) to determine the relationship between the adsorbed layers to the friction of the system. The HFRR, purchased from PCS Instruments, measures boundary friction by sliding a 6 mm steel ball against a steel stationary disk. The set-up is illustrated in Figure 16 below.

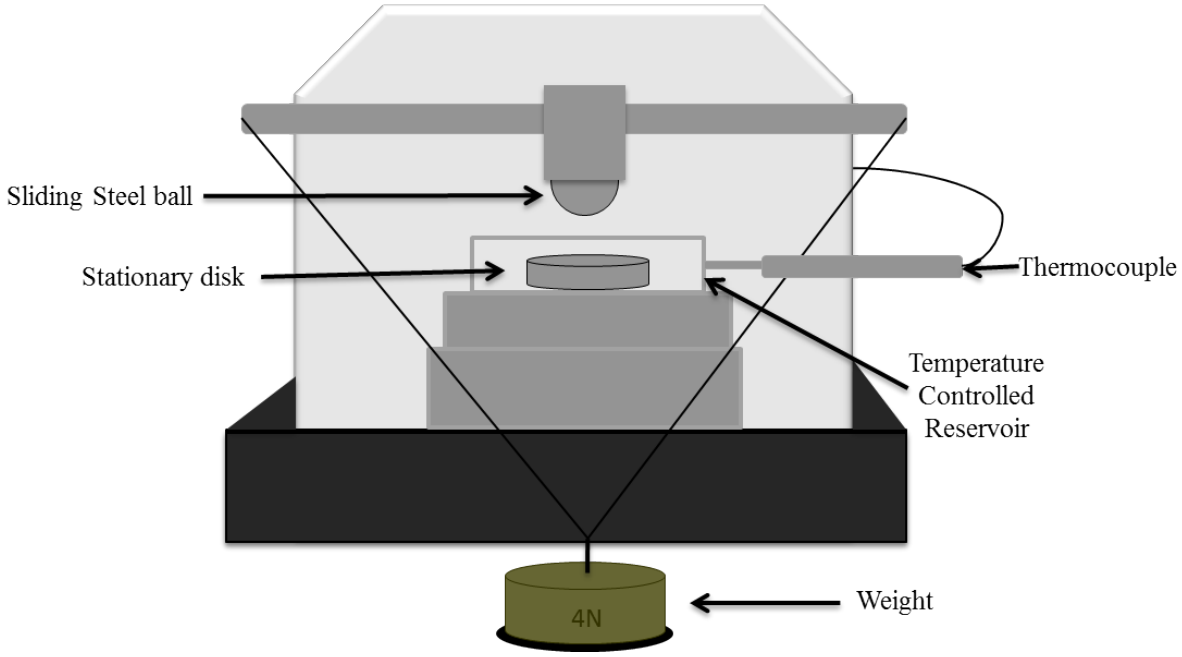

Figure 16: Illustration of HFRR Set-up

Both specimens were purchased from PCS Instruments and the specifications are listed in Table 4.

Table 4: Specifications for HFRR specimens

	Steel	Hardness	Surface Roughness, R_a
Ball	Grade 28	58-66 HRC	<0.05 µm
Disc	AISI E-5210 steel machined from annealed rod	190-210 HV30	<0.02 µm

2.3.1 Friction Measurements: Due to the low flash point of 2, 2, 4-trimethylpentane (10.4°F), low viscosity poly-α-olefin (PAO) base oil was used as the solvent for the HFRR friction measurements. The surfactant solution was added to the reservoir housing the stationary steel disk, ensuring the disk was completely submerged. The steel ball was attached above the steel disk and a thermocouple was inserted into the steel reservoir to measure the temperature of

the specimen during the experiment. Lastly, weight is added to the fixture housing the steel ball to place the ball and disk into contact and generate pressure. The conditions can be varied, but for our purposes the conditions were 4 Newtons (N) of pressure, a reciprocating frequency of 20 Hz, and 1 mm path length. After the reservoir temperature stabilized at 25 °C for 90 seconds, the rig began to reciprocate and friction measurements were taken every 5 seconds for 3 minutes. The fluid temperature was then raised to 50 °C and the procedure and measurements repeated.

2.4 Steel Corrosion: The ability of a surfactant to inhibit corrosion was measured by exposing steel coupons to 100% humidity environment and measuring the amount of corrosion present after a specific time. The steel coupons, purchased from Q-lab (Westlake, Ohio), were 150 mm in length, 75 mm in width and 0.8 mm thick. In the top of the coupon is a hole in the shape of a 'Q'. We define the right and left side by the direction the Q is pointing (Figure 17). The surface preparation for this testing is crucial, so a consistent procedure was followed. The left and right side of each panel was polished with a cotton ball soaked in iso-octane and then dried in air for 15 minutes. The plates were then soaked in the surfactant/base oil solutions for 10 minutes. After ten minutes the panels were placed in a dust free environment to hang for 24 hours. After this time period, the plates were hung 14 cm apart in a humidity cabinet maintained at 48.0 $\pm$1.5°C. Ten millimeters of deionized water is contained in the bottom of the humidity cabinet to maintain 100% relative humidity. After 48 hours in this environment, the plates were removed and rated for corrosion. After every run, the humidity cabinet was drained and cleaned out completely to avoid contamination between runs.

(a) (b)

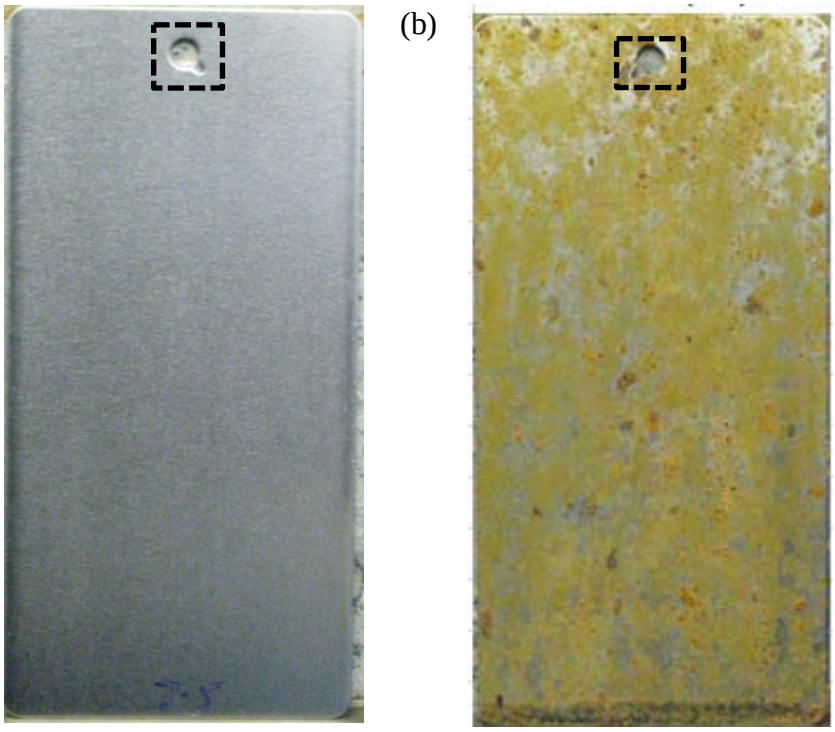

Figure 17: Photograph of steel coupon (a) before test (b) end of test with only base oil. The dotted line boxes highlighted the 'Q' shaped hole at the top of the coupon. The direction of the tail of the coupon helps to differentiate the right (a) and left (b) side of the coupon.

2.5 Software: All linear and non-linear regression modeling was performed using GraphPad Prism version 6.07 for Windows, GraphPad Software, La Jolla California USA, www.graphpad.com.

2.6 Summary of Reagents and Testing: For clarity, Table 5 summarizes the testing completed on each reagent. Limited testing was completed on the first three reagents due to limited quantity. Oleylamine, 1-Oleoyl-rac-glycerol, and oleic acid all contain the same alky chain but the polar head varies: amine, glycerol ester and carboxylic acid respectively. Comparison of oleic acid and octanoic acid were constrasted to investigate the effect of varying

the alkyl chain in steel corrosion. It is well documented in literature that shorter alkyl (<10 carbons) chains are not effective at lowering friction, so friction testing was not completed on octanoic acid. 1-Oleoyl-rac-glycerol (≥99%), GMO and GDO were compared to investigate the effect of increasing the esterification on adsorption.

Table 5: Reagents and Test

Reagent	Structure	Testing (Solvent)		
		QCM-D (isooctane)	Steel Corrosion (Yubase 6)	Friction (2cst PAO)
1-monopalmitoleoyl-rac-glycerol (≥99%)	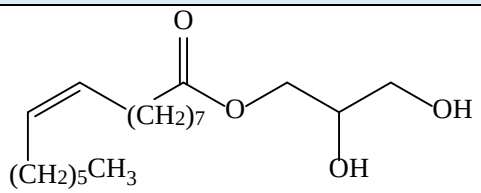	✓	✗	✗
1-Stearoyl-rac-glycerol (≥99%)	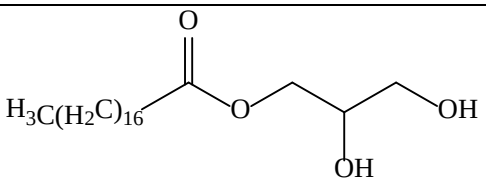	Insoluble		
1-Oleoyl-rac-glycerol (≥99%)	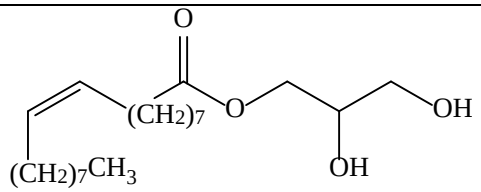	✓	✗	✓
GDO Mixture	See Table 3	✓	✓	✓
GMO Mixture	See Table 3	✓	✓	✓
Oleylamide	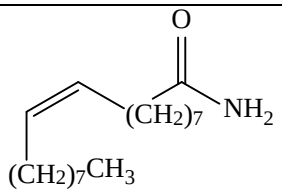	Insoluble		
Oleylamine (≥99%)	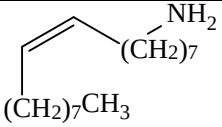	✓	✓	✓
Oleic acid (≥99.0%)	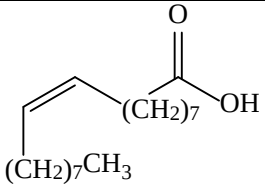	✓	✓	✓
Octanoic acid(≥99.0%)	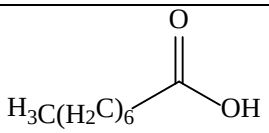	✓	✓	✗

CHAPTER 3: Results and Discussion

The focus of this work is to determine if QCM-D is an effective technique to investigate surfactant adsorption in concentration regimes that are common to the transportation lubricant industry. In order for this technique to be useful, it is essential the QCM provide better insight into differences we see in macroscopic properties. The first section summarizes the adsorption data obtained using QCM-D. The adsorption data is utilized to characterize the structure of the adsorbed film and determine kinetic information of the surfactants. Since many of the additive chemistries compete for the surface, understanding kinetics can aid in understanding interactions occurring in these systems that may lead to positive or negative behavior in the field. The second section explores the potential links between macroscopic behavior (corrosion/friction) and the characteristics of the adsorbed layer measured via QCM-D. While the QCM experimental set-up does not replicate the exact test conditions in these cases, it is hoped that understanding of film coverage, kinetics, and rigidity can be factors in understanding macroscopic performance of these additives. If the QCM-D can predict results observed in rig testing (or the field) the expense and time required for the development of new lubricants could be reduced.

3.1 Adsorption Measurements using Quartz Crystal Microbalance with Dissipation (QCM-D):

In the lubricant industry, surfactants with alkyl chains containing 18 carbons are typically used as friction modifiers and/or corrosion inhibitors. Some of the most widely used surfactants in the industry contain polar head group with carboxylic acid, amine, amide, or glycerol functionality; therefore, these were the focus for this work. Adsorption of 2 mM solutions of oleic acid, oleylamine, 1-oleoyl-glycerol (≥99%), 1-monopalmitoleoyl-glycerol

(≥99%), GMO and GDO mixtures (described previously) on iron oxide were measured at 25°C. The goal was to also consider oleamide and 1-stearoyl-glycerol, but neither was soluble in iso-octane at 2 mM.

3.1.1 Fatty Acids in the Literature: Fatty acids, particularly saturated fatty acids, have been heavily studied in literature and are known to adsorb to iron oxide through physical and chemical interactions, depending on the activation energy. Due to exposure of air and moisture, steel surfaces are partly covered with oxides and hydroxide providing a variety of adsorption schemes for carboxylic acids (mono-dentate, bi-dentate and bridging). In literature, the measured enthalpy of adsorption values for carboxylic acids on steel are greater than 70 times kT at 25°C, indicating a very stable monolayer.[27] Recent molecular simulations of stearic acid at 50 °C found the orientation of the fatty acid impacted the adsorption behavior. Chemisorption through the acid group was favored by molecules oriented parallel to the surfaces, but when the surfactant was oriented upward in solution, chemisorption through the carboxyl group was stronger. This work also found the presence of friction favors the formation of iron carboxylates.[28] Much of the molecular modeling work was completed on stearic acid, but due to poor solubility of stearic acid in base oil its unsaturated analogue, oleic acid, is more commonly used in real systems. In addition, the QCM-D is looking at real surfaces that are neither atomically flat nor orient molecules in perfect registry. Despite these differences, it is instructive to see similarities in qualitative behavior to provide a framework for understanding the QCM-D data.

Of the molecules tested in the QCM-D adsorption experiments, only oleic acid and oleylamine exhibited typical rigid monolayer behavior at this temperature and concentration. Upon addition of the surfactant solutions, a small change in mass was measured, with minimal to no change in dissipation. The systems reached equilibrium within 5 minutes and upon rinse with

solvent, a small loss in mass was measured. Varying the concentration of oleic acid did not have a significant impact on the adsorption behavior. A rigid monolayer was formed regardless of concentration. Representative plots of frequency versus dissipation are pictured in Figure 18. These further illustrate the one stage adsorption process resulting in a rigid monolayer for both oleylamine and oleic acid.

In contrast, the frequency and dissipation measured for the glycerol oleate compounds never plateaued over the length of the experiment, suggesting the formation of additional layers (at this concentration and temperature). In the frequency and dissipation plots, the change in slope indicates the glycerol esters chemistries exhibit at least two stages of self-assembly under these conditions. The first stage is rigid with minimal dissipation, making the Sauerbrey equation a valid estimation for this stage. The maximum frequency value for this stage was used to calculate the physisorbed and chemisorbed mass associated with the surface. Using the molecular weight of the surfactant and Avogodro's number mass could be converted to area per molecule. Figure 19 compares these values for all six surfactants.

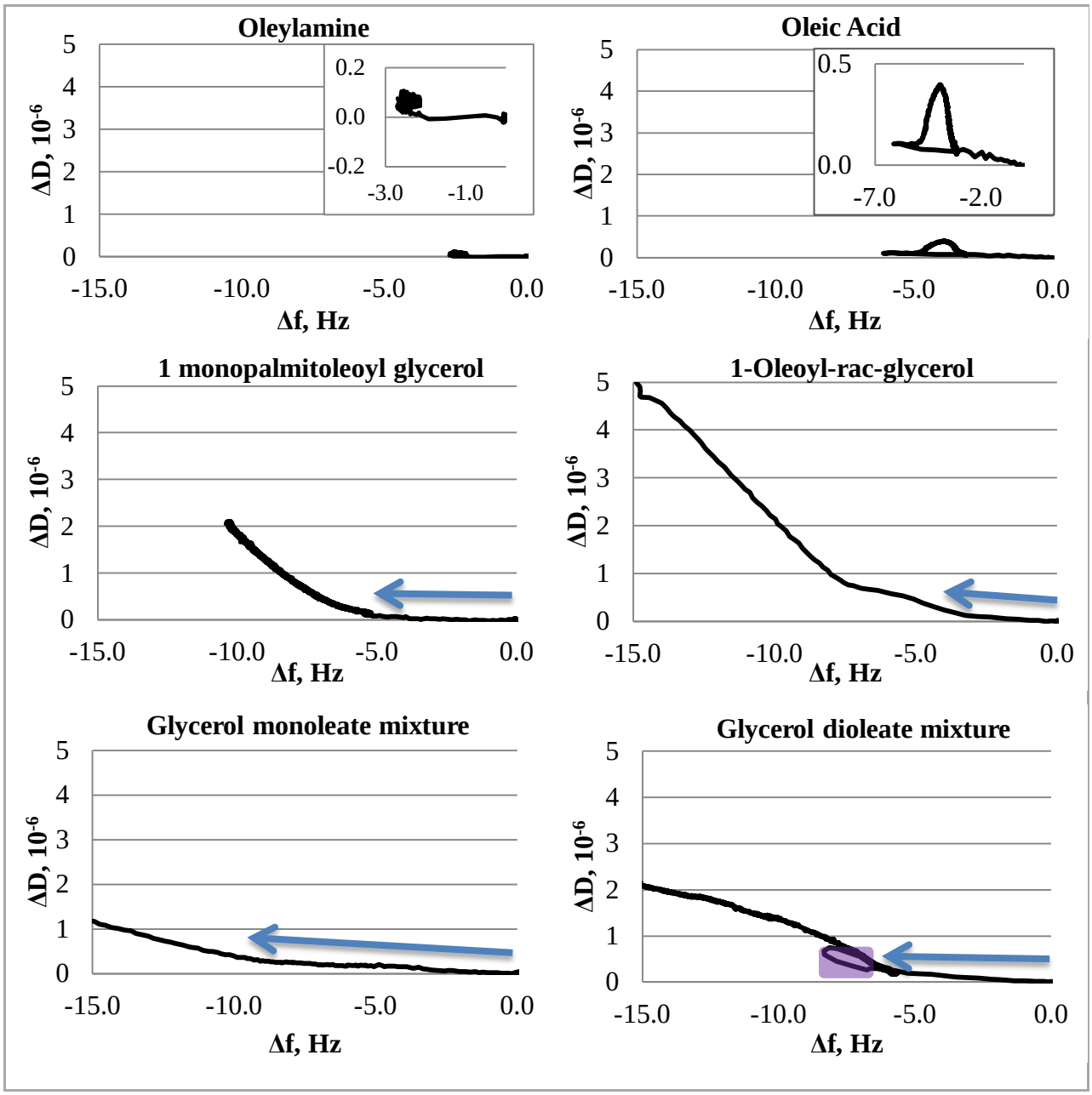

Figure 18: Representative frequency and dissipation plots for 2mM solutions of surfactants on iron oxide at 25°C. Changes in slope indicate multiple stages of adsorption. Arrows represent first stage where the Sauerbrey equation is still valid. Hysteresis in curves highlighted in purple.

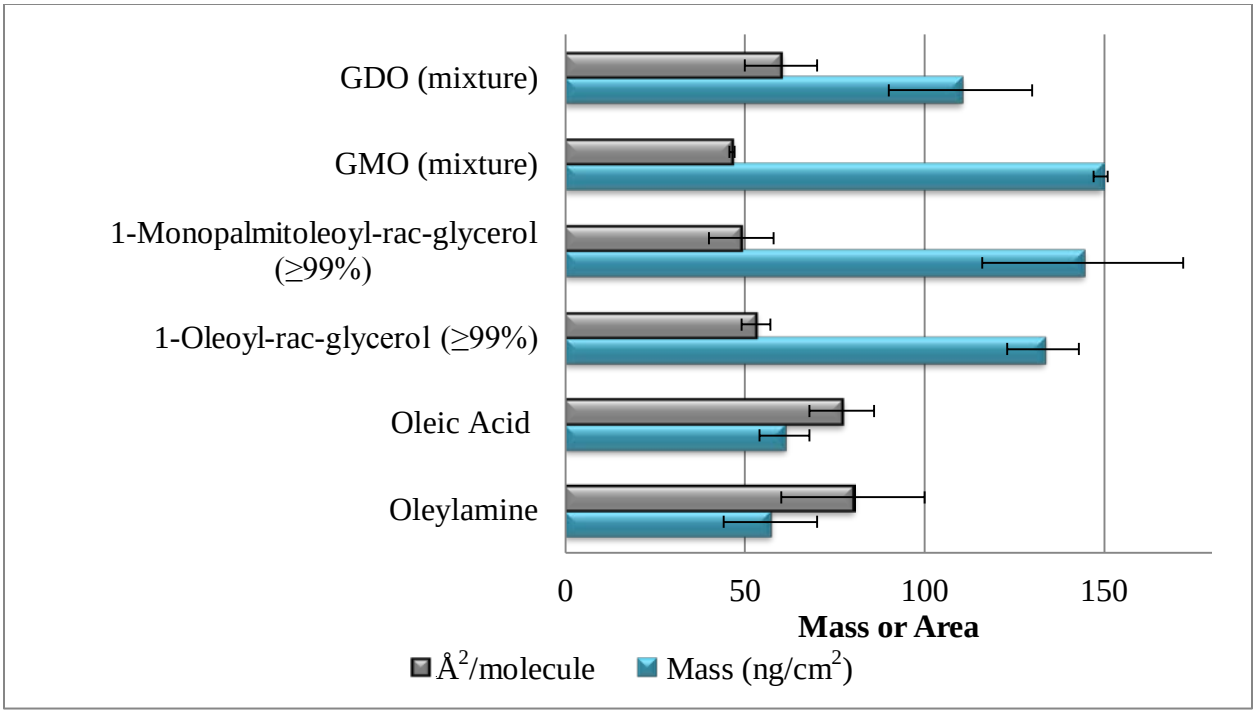

Figure 19: Mass and area per molecule calculated for rigid monolayer adsorption of surfactants after corrections for viscosity and density of solutions. If adsorption occurred through a two stage process, the maximum frequency change for the first stage was used to calculate mass and molecule per area. The error bars represent +/- 1σ.

Glycerol monoleate formed a more compact (46.4±0.7 Å^2/molecule) monolayer in the first stage of adsorption compared to glycerol dioleate (60±10 Å^2/molecule). This increase in area corresponds with the additional oleyl group in GDO. Molecular dynamic simulations conducted by Davidson at the University of Edinburgh, demonstrated that 1-monolein and 1,3-diolein interact with steel through hydrogen bonding.[29] Hydroxyl group present on the steel surface acted as a donor to the ester. Due to multiple hydroxyl groups, 1-monolein was capable of forming multiple hydrogen bonds with neighboring groups resulting in a stable, organized monolayer. Less hydrogen bonding was present in 1,3-diolein and due to the single hydroxyl group intermolecular hydrogen bonding resulted in the formation of dimers. Figure 20 illustrates the difference in intermolecular hydrogen bonding between GMO and GDO.

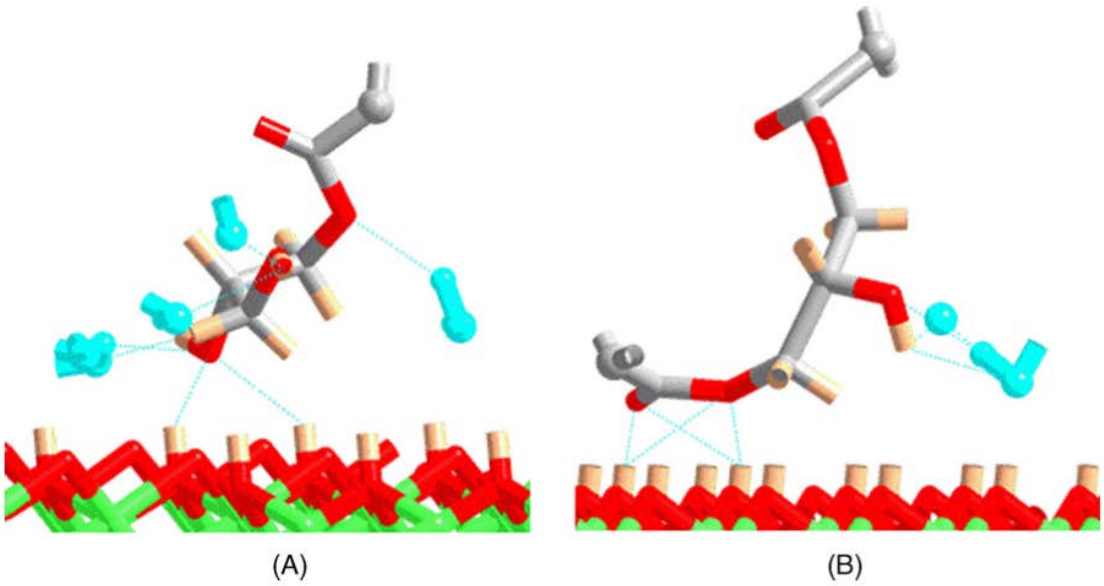

Figure 20: Snapshot from Davidson's simulation illustrating the hydrogen bonding interactions with neighboring ester moelcules (in blue) (A) GMO (B) GDO (Reprinted from Journal of Molecular Graphics and Modeling with permission from Elsevier.)[29]

The average area per molecule calculated in these simulations was 22.5 $Å^2$ for 1-monolein and 46.13 $Å^2$ for 1,3-diolein. These values are about half the value determined experimentally using the QCM-D. In Davidson's work he mentioned the simulation was extensive enough to provide confidence in the relative surface area per molecule but not necessarily the absolute numbers. Another possible explanation for the difference seen in the QCM-D results versus Davidson's simulations is that the QCM-D calculated values were based solely on the first step of adsorption (rigid monolayer). This would exclude any adlayer of molecules not tightly bound to the surface, so the mass may be underestimated.[29] Even without clarity on the absolute number, both the QCM-D and molecular simulations suggest that GMO forms more stable, compact monolayers compared to GDO.

Various concentrations were also tested for the glycerol oleates to determine if their more complicated adsorption behavior could be impacted by varying the concentration. Adsorption of pure 1-oleoyl-*rac*-glycerol was tested at three different concentrations over three orders of magnitude. At 0.01 and 0.1 wt%, adsorption occurred through a multi-step process; conversely, at the highest concentration adsorption occurred through a single process and formed a rigid monolayer. Upon rinse, there is no sign of hysteresis. Minimal loss of mass or dissipation occurs at the highest concentration and the other two desorption curves follow the slope of the adsorption curve. Testing was repeated for the GMO and GDO mixtures and similar trends were seen. At higher concentration only a rigid monolayer is formed and lower concentration result in multi-step adsorption processes.

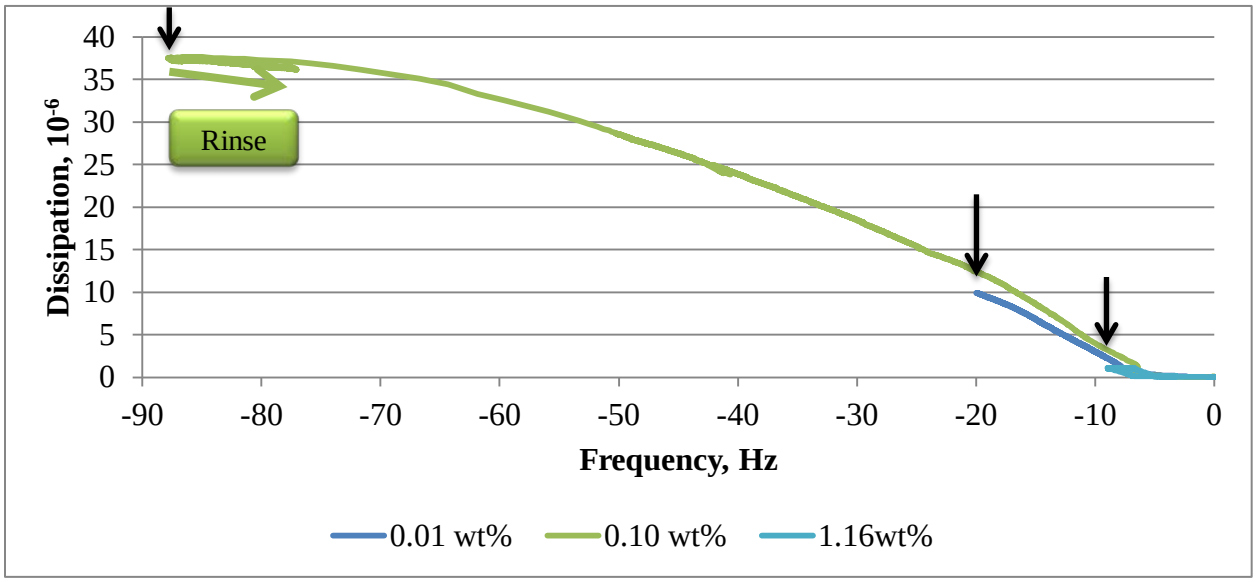

Figure 21: Frequency and dissipation curves for 1-Oleoyl-*rac*-glycerol at three different concentrations. Black arrows indicate point of rinse. The green arrow indicates change in dissipation and frequency that is occurring during rinse.

The first stage of adsorption proved to be quite repeatable (+/-2 Hz); however, the frequency and dissipation measured for the second stage was much more variable. This more dissipative mass could be due to the incorporation of solvent, formation of more complex adlayers of glycerol oleates or both. Ascertaining which mechanism is correct is impossible without a secondary technique capable of visualizing the surface.

In a few of the higher concentration GMO and GDO mixture experiments, odd behavior was observed upon addition of solutions. Large, sudden shifts in frequency and dissipation (relative to the solvent) were observed. Just as quickly as the shift occurred, the change decreased and plateaued immediately (Figure 22).

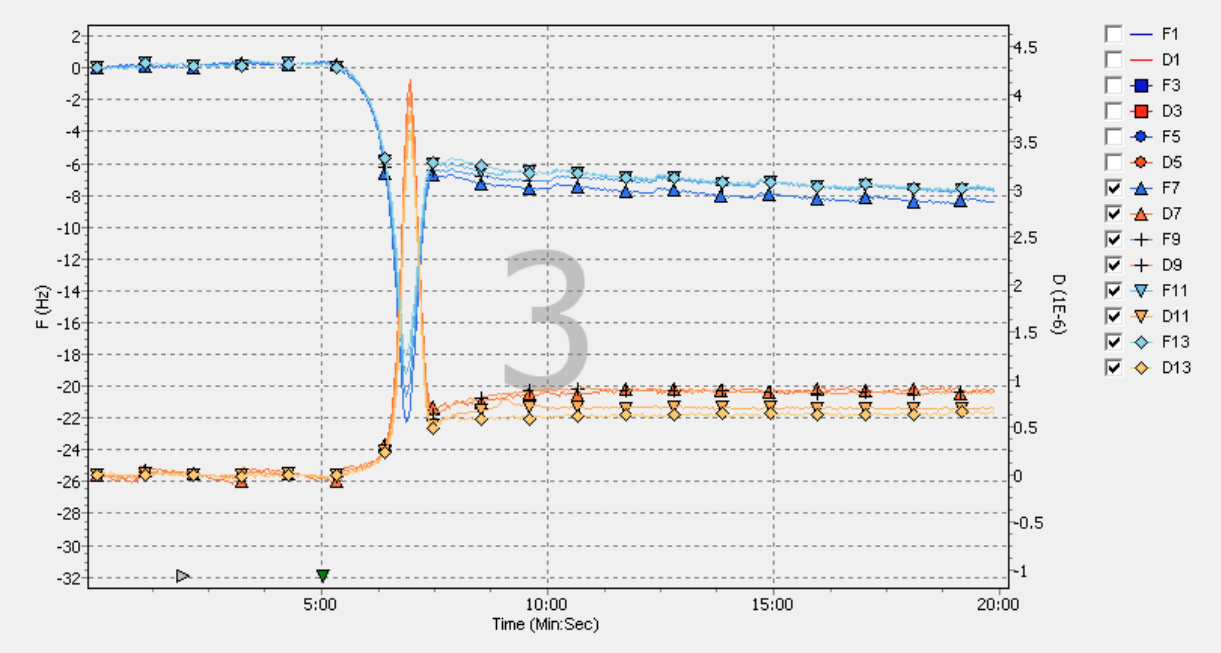

Figure 22: Frequency and dissipation measured upon addition of 0.3 wt% glycerol dioleate mixture at multiple overtones. (Image taken from instrument. Legend at the right is the frequency and dissipation at multiple overtones. The 3 indicates the 3rd chamber of the QCM-D).

Similar behavior has been noted in QCM literature and explained by the adsorption of intact vesicles followed by their rupture to form a rigid bilayer.[30] The adsorption of the vesicle created a rapid variation in frequency as well as dissipation. When the vesicle ruptures, a rigid bilayer is formed reducing the dissipation. The reduction is mass is attributed to the release of water previously contained in the interior of the vesicle. This explanation is reasonable in water systems where vesicles or normal micelles are present (polar head groups facing outward). In oil systems reverse micelles are formed, so the surface active polar head groups are located in the interior of micelle obstructing them from interacting with iron oxide making this explanation seem less logical. In the literature, Shrestha et al. used small-angle X-ray scattering (SAXS) to demonstrate the ability of glycerol monoleate to form spontaneous reverse micelles in the shape of elongated spheres. These reversed micelles tended to increase in size as the amount of water or chain length of oil increased.[31] Values in literature indicate 1-monolein begins to aggregate in heptane at concentrations of 0.05 wt% at 25 °C and 0.14 wt% at 50 °C, so at the concentrations tested, it is likely reverse micelles are present.[32] Also, as mentioned earlier, water is present in the GMO and GDO mixtures, making the presence of reverse micelles at these higher concentrations more probable. The odd behavior observed for the GMO and GDO mixtures was not observed with the pure reagent (1-Oleyl-*rac*-glycerol). One possible explanation is the absence of water in the pure system making the formation of reverse micelles less probable. Explaining how these reverse micelles diffuse and preferentially interact with the iron oxide is unknown but QCM literature suggests the macroscopic behavior of aggregates in solution may contribute to the odd shift in frequency and dissipation behavior observed.[33]

3.2 Kinetic Measurements: The ability to measure kinetic information is one of the biggest advantages of QCM-D over other techniques. The adsorption of a ligand onto a solid surface, such as in the QCM experiments, can be described by the equation:

$$rate = k[surfactant][surface\ sites] \tag{8}$$

In this set of experiments the concentration of surfactant remains constant throughout a given measurement owing to the flow through set-up of the QCM apparatus. As more and more surfactant adsorbs to iron oxide, the concentration of surface sites decreases. Due to the size limitations of the quartz crystal, the initial concentration of surface sites cannot be varied. In order to probe the rate constant, a series of concentrations was made for each surfactant in isooctane.

3.2.1 Oleic Acid: Due to its simplicity, the Langmuir isotherm model is commonly used to describe the adsorption of surfactants on solid surfaces. Adsorption is treated as equilibrium between the concentration of surfactant, (in this case oleic acid) [OA], free sites on the surface [S*] and adsorbed surfactant $[S - OA_{ads}]$. The Langmuir model assumes adsorption is limited to a monolayer, all surface sites are equivalent, and no interactions occur between surfactant molecules on adjacent sites. Overall, the Langmuir assumptions largely hold for the oleic acid data over the concentrations studied.

$$[S^*][OA] \rightleftharpoons [S - OA_{ads}]$$

$$K = \frac{[S - OA_{ads}]}{[S^*][OA]} \tag{9}$$

The concentration of adsorbed surfactants is expressed as the surface coverage, θ, and is always between 0 (no coverage) and 1 (complete monolayer). At equilibrium the rate of adsorption and desorption become equivalent. The change in surface coverage over time is described in terms of kinetics in the equation below where k_{ads} is the rate constant for adsorption and k_{des} is the rate constant for desorption

$$\frac{d\theta}{dt} = k_{ads}(1-\theta)\mathrm{C} - k_{des}\theta \tag{10}$$

This equation can be integrated to provide the time dependence.

$$\theta(\mathrm{t}) = \frac{C}{C + (k_{des}/k_{ads})}[1 - e^{(-k_{ads}C + k_{des})t}]$$

The objective is not to quantify mass, so the equation can be further simplified by substituting k' for $C/(C + (k_{des}/k_{ads}))$ and replacing $\theta(\mathrm{t})$ with $\Delta f(\mathrm{t})$. Also, a single observed rate constant,k_{obs}, is substituted for $k_{ads}C + k_{des}$ to further simply the equation.

$$\Delta f(\mathrm{t}) = \mathrm{k}'[1 - e^{(-k_{obs})t}]$$

This reduced equation was input into GraphPad Prism and fit to raw frequency versus time QCM-D data to determine the observed rate constant (Figure 23). Before the raw data was fit into the model, corrections needed to be made for changes in bulk properties and poor mixing due to laminar flow using equations 2 and 6. [8a, 34] Experimentally determined rates for oleic acid and corresponding 95% confidence intervals are listed in Table 6.

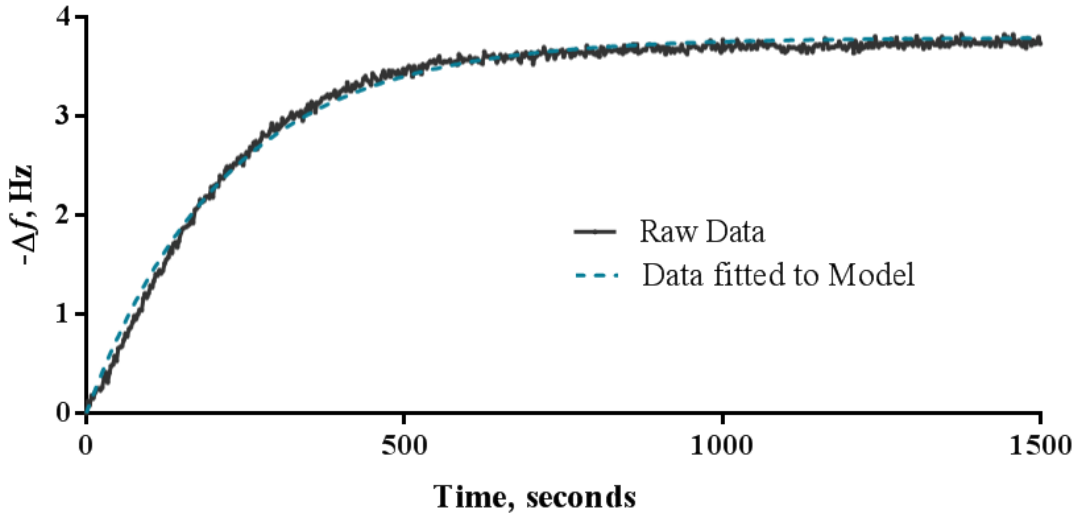

Figure 23: Change in frequency versus time for 3 mM oleic acid at 25°C. Frequency data measured at 9th overtone and normalized (divided by 9). Two parameter fit data displayed as dotted line.

Table 6: Observed rate constants at 25°C as a function of oleic acid concentration

oleic acid concentration, mM	k_{obs} ± 95% C.I., s^{-1}
0.25	0.00051 ± 0.00002
1.22	0.0033 ± 0.0002
2.45	0.0074 ± 0.0003
3.00	0.0067 ± 0.0001
7.35	0.019 ± 0.001

It is also important to note oleic acid is known to form dimeric hydrogen bonded structures similar to other carboxylic acids in hydrocarbon solvents, as shown in Figure 24.

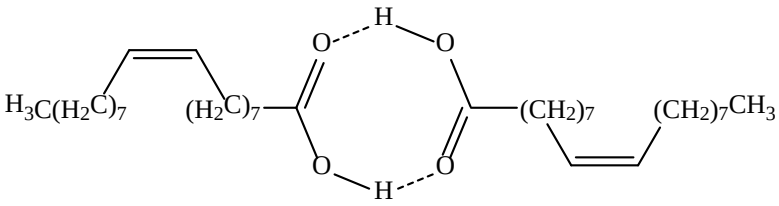

Figure 24: Depiction of hydrogen bonded oleic acid

Benzoic acid and lauric acid are reported to have dimerization constants, K_{dimer}, at *25°C* of 2340 M^{-1} and 1950 M^{-1}, respectively.[35] If we approximate a dimerization constant of 2000 M^{-1} for oleic acid in isooctane, then we can calculate the concentration of monomeric oleic acid present in each of the individual QCM experiments. This is important to consider in the event that the monomeric form of oleic acid is directly responsible for adsorption in the QCM experiments as in equations 11 and 12. If this is the case, than the proper graphical representation of the initial rate data is to plot it as a function of [monomeric oleic acid].

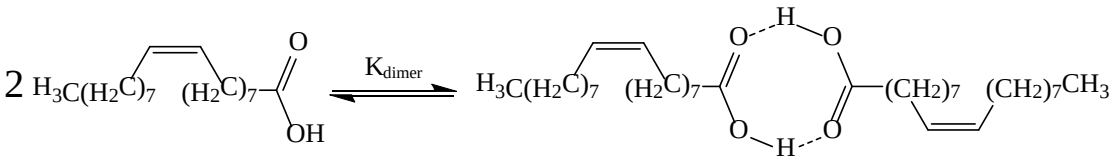

(11)

$$[\text{monomeric oleic acid}] \xrightarrow{k'} (\text{oleic acid})_{adsorbed} \tag{12}$$

The concentration of oleic acid existing in a monomeric form can be calculated directly using equations 13-17.

$$K^{dimer} = \frac{[dimer]}{[monomer]^2} \quad (13)$$

$$[total\ oleic\ acid] = [monomer] + [dimer] \quad (14)$$

Solving for [dimer] in equation 13 and substituting into equation 14 provides:

$$[total\ oleic\ acid] = [monomer] + K^{dimer}[monomer]^2 \quad (15)$$

Equation 15 can be rearranged into the more familiar form of a quadratic equation as in equation 16 and the [monomer] solved for at each [oleic acid] using equation 17.

$$0 = K^{dimer}[monomer]^2 + [monomer] - [oleic\ acid] \quad (16)$$

$$[monomer] = \frac{-1 \pm \sqrt{1^2 + 4K^{dimer}[oleic\ acid]}}{2K^{dimer}} \quad (17)$$

Using equation 17 the [monomer] was calculated for each treat rate of the QCM experiments.

Table 7: Observed rates and monomer concentrations for oleic acid adsorption

Total oleic acid, mM	Monomeric oleic acid, mM	k_{obs} ± 95% C.I., s^{-1}
0.25	0.18	0.00051 ± 0.00002
1.22	0.570	0.0033 ± 0.0002
2.45	0.884	0.0074 ± 0.0003
3.00	1.00	0.0067 ± 0.0001
7.35	1.68	0.019 ± 0.001

Since $k_{obs}=k_{ads}C + k_{des}$, graphing concentration versus observed rate constant provides the adsorption (slope) and desorption (y-intercept) rate constants. The linear regression fit and 95% confidence interval is shown in Figure 25. Across the concentrations tested, there was no

deviation from linearity suggesting a second order process dependent on total oleic acid concentration not just monomer concentration. There are three possible explanations: 1. Dimerization is not occurring. (This is unlikely due to the multiple accounts in literature of oleic acid forming dimers in petroleum based solvents.) 2. Oleic acid can adsorb as a monomer or dimer. 3. The square root dependence of the reaction rate is aliased by a second order process. Regardless of the explanation, it was possible to experimentally determine the rate constants of oleic acid using the Langmuir model.

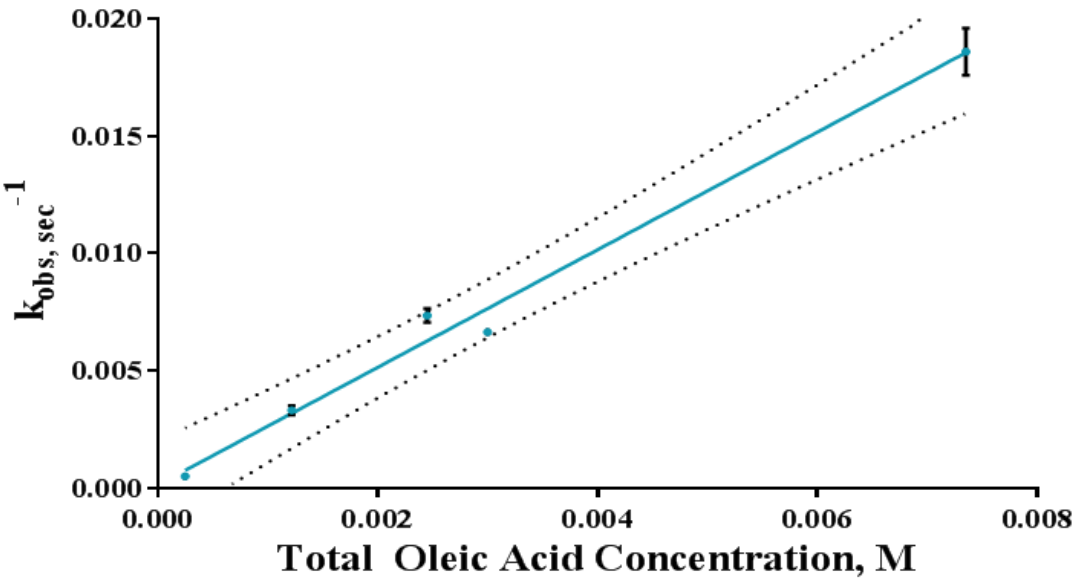

Figure 25: Observed rate constants at 25°C for the adsorption of oleic acid (from isooctane) to iron oxide versus concentration. The slope of the best fit line equals k_{ads}=2.5±0.2 $M^{-1}s^{-1}$ and y-intercept is k_{des}=0.0001±0.0006 s^{-1}. Error bars depict 95% confidence interval. 95% confidence band for linear regression line represented by dashed lines. At the highest concentration, some of the adsorption curves begin to deviate from typical Langmuir behavior leading to much larger confidence intervals.

The rate constant of adsorption (k_{ads} = 2.5±0.5 $M^{-1}s^{-1}$) was much greater than that of desorption (k_{des} = 0.0001±.0006 s^{-1}). From the rate constants, the equilibrium constant (K_{eq})

can be determined. The very small rate constant of desorption and large equilibrium constant confirms the strong adsorption of oleic acid to iron oxide and indicates minimal desorption of oleic acid.

$$K_{eq} = \frac{k_{ads}}{k_{des}} \tag{18}$$

The equilibrium constant can be utilized to determine the fraction coverage at equilibrium (θ_{eq}) by substituting surface coverage into equation 9 and rearranging the equation.

$$\theta_{eq} = \frac{[OA]}{[OA] + (1/Keq)} \tag{19}$$

The calculated surface coverage for oleic acid at different concentrations is shown in Table 8. At very low concentrations 100% surface coverage is attained. Considering the confidence interval, it is statistically probable that k_{des}=0 and there is no equilibrium because the adsorption of oleic acid to iron oxide is irreversible under these conditions. The kinetic data determined experimentally using QCM-D mirrors accounts in literature describing oleic acid's strong binding to steel.

Table 8: Estimated surface coverage at equilbrium determined using Equation 19.

oleic acid concentration, M	θ_{eq} ± 95% C.I., s^{-1}
2.50×10^{-4}	0.86 ± 0.04
1.22×10^{-3}	0.97 ± 0.01
2.45×10^{-3}	0.984 ± 0.005
3.00×10^{-3}	0.987 ± 0.004
7.35×10^{-3}	0.995 ± 0.002

3.2.2 Glycerol Dioleate: One of the assumptions of the Langmuir model is the adsorbate forms a single monolayer and not multiple adlayers. The high dissipation measured for glycerol dioleates suggests adsorption occurs in two stages. First a rigid monolayer forms, followed by formation of additional dissipative layers (possibly due to the incorporation of solvent). The Langmuir model falls short of explaining multilayer formation, so only the initial part of the adsorption curve (that corresponds to a single monolayer) was modeled. Also, as mentioned previously, glycerol oleates form intermolecular hydrogen bonds which violate another requirement of the Langmuir model. The concentration of GDO mixture above 0.1 wt% did not display typical Langmuir behavior (Figure 26) which could be attributed to these intermolecular interactions. At concentrations below 0.1 wt%, the adsorption curve followed more typical Langmuir behavior. At these lower concentrations, the intermolecular interactions may be minimal making the Langmuir model a valid approximation. Rate constants were determined for

GDO by fitting the first phase of adsorption (negligible or no dissipation) at low concentrations (0.1 to 0.5mM). These values are listed in Table 9.

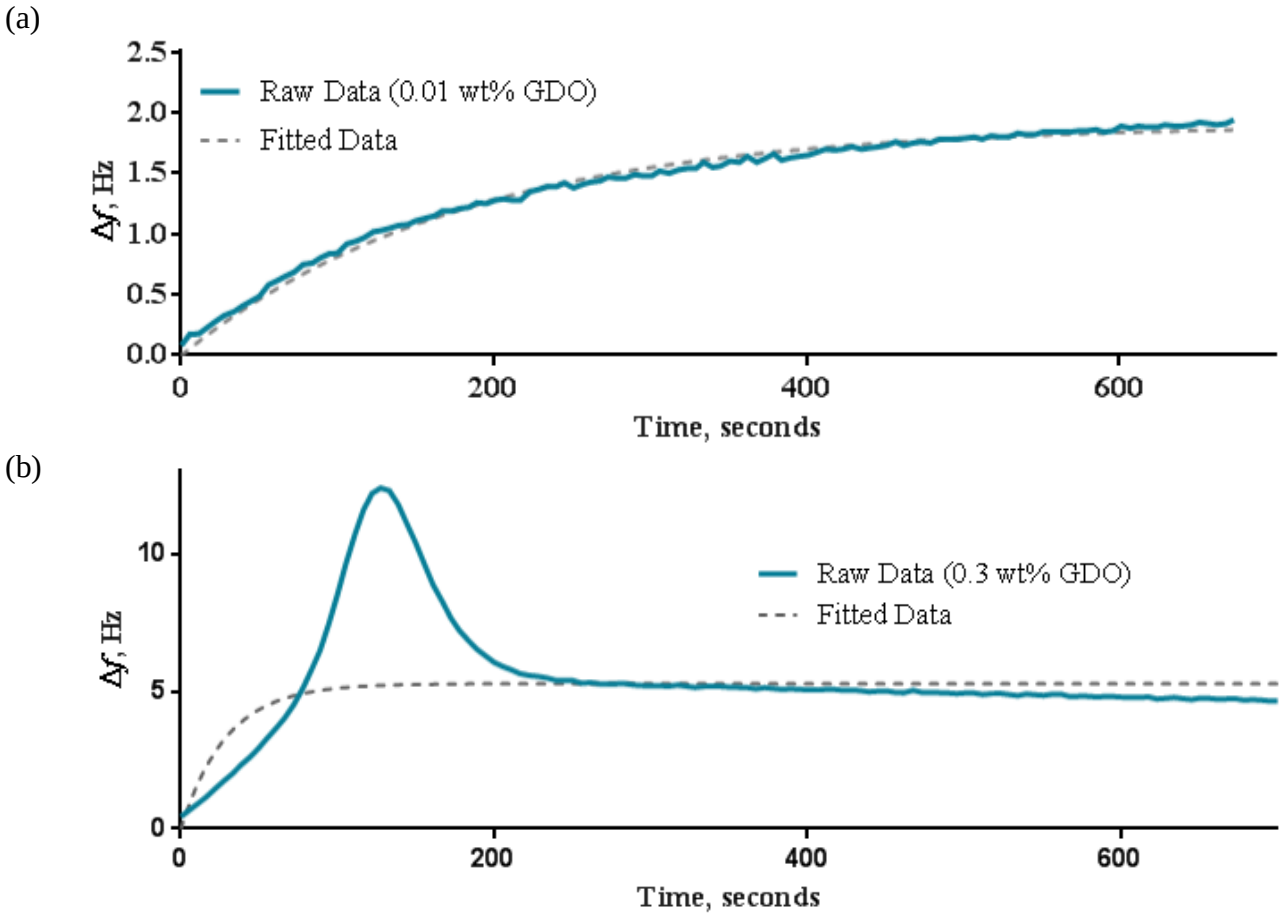

Figure 26: Change in frequency measurement over the intial 700 seconds of adsorption of (a) 0.01 wt% GDO and (b) 0.3 wt% GDO. The dotted line displays the fited data. At the lower concentrations(0.1 to 0.5mM) the data adheres to the typical Langmuir behavior. At concentration above 0.5mM, the intial 200 seconds does not dissplay typical Langmuir behavior possibly due to intermolecular interactions (i.e. hydrogen bonding) or reverse micelle formation. As a result, kinetics at this concentration could not be determined using this model.

Table 9: Experimentally determined rate constants and 95% C.I. for GDO. Rate constants were experimentally determined at low concentraitons (0.1 to 0.5mM) for the first stage of adsorption (rigid monolayer).

	25°C	**50°C**
k_{ads}	2.4±0.2 $M^{-1}s^{-1}$	1.5±0.4 $M^{-1}s^{-1}$
k_{des}	0.00540±0.00007 s^{-1}	0.006±0.002 s^{-1}

3.2.3 Summary of Kinetic: QCM-D experiments for oleylamine suggested it forms a rigid monolayer, signifying that the Langmuir model is appropriate. The calculations detailed previously for oleic acid were repeated for oleylamine. Calculated rate and equilibrium constants for oleylamine and other surfactants are listed in Table 10. The rate constant for adsorption is almost an order of magnitude smaller than that of desorption suggesting oleylamine is very weakly bound to the iron oxide. It is important to note, the confidence intervals for the rate and equilibrium constants are very large due to the very minimal dependence of concentration on observed rate.

Comparing the rate and equilibrium constants, the rate of adsorption for oleylamine is three orders of magnitude smaller than oleic acid, GDO and 1-oleoyl-*rac*-glycerol suggesting it may deliver inferior friction reduction and protection from steel corrosion. The equilibrium constants communicate a similar narrative. The relative numbers suggest oleic acid would provide superior performance, followed by 1-oleoyl-*rac*-glycerol and GDO.

Table 10: Summary of experimentally determined rate constants and 95% confidence interval for surfactants at 25°C

Surfactant	k_{ads}, $M^{-1}s^{-1}$	k_{des}, s^{-1}	K_{eq}. M^{-1}
Oleic Acid	2.5±0.6	0.0001±0.0006	25000±6000
GDO Mixture	2.4±0.2	0.00540±0.00007	450±50
1-Oleoyl-*rac*-glycerol	5.5±0.3	0.0022±0.0005	2500±700
Oleylamine	0.004±0.008	0.03±0.01	0.2±0.6

3.3 Competitive Adsorption: Up to this point, all experiments measured adsorption of a single surfactant. Transportation lubricant systems contain upwards of 10 components, so for the QCM-D to be effective for these applications it will need to provide insight into multi-component interactions. Data analysis for QCM-D is complicated, so it is important to analyze simple systems (single component) first before adding the complexity of additional components. Previously, oleic acid and GDO were characterized at various concentrations individually. In the competitive adsorption experiments, adsorption of GDO and oleic acid was investigated sequentially and simultaneously using QCM-D (Figure 27). Solutions of 0.01 and 0.3 wt% GDO were added to the QCM-D and after 60 minutes switched to 0.3 wt% oleic acid. The low concentration did not reach equilibrium during the adsorption of GDO, but quickly reach equilibrium when 0.3 wt% oleic acid was added. In both experiments, the dissipation values stayed low suggesting only a rigid monolayer was formed. Upon rinse, a small amount of mass was lost and equilibrium was quickly reached. Next, the experiment was completed in reverse. Oleic acid was added at 0.3 wt% for 60 minutes, followed by the addition of 0.3 wt% GDO. This experiment did not produce significantly different frequency and dissipation changes from the

previous sequential experiments. After rinse, the adsorbed mass was relatively the same for all experiments. Frequency versus dissipation curves also show similar behavior (Figure 28). Next, 0.3 wt% oleic acid and 0.3 wt% GDO were added into one mixture and adsorption measured. This binary system produced very different curves. The adsorbed mass and the dissipation were much larger compared to the sequential experiments. Also, the frequency versus dissipation curve indicates adsorption is a two-step process that after rinse reduces to a more rigid monolayer, greater in mass than the other systems. The differences in these experiments suggest cooperative binding may be present in the binary system, but QCM-D is not specific to a single analyte. Due to this disadvantage, it is impossible to elucidate the QCM-D response without a secondary technique capable of visualizing the surface of the crystal. These experiments suggest QCM-D may be helpful in understanding complex competitive adsorption in combination with a secondary technique or by comparing kinetic and thermodynamic data of single systems.

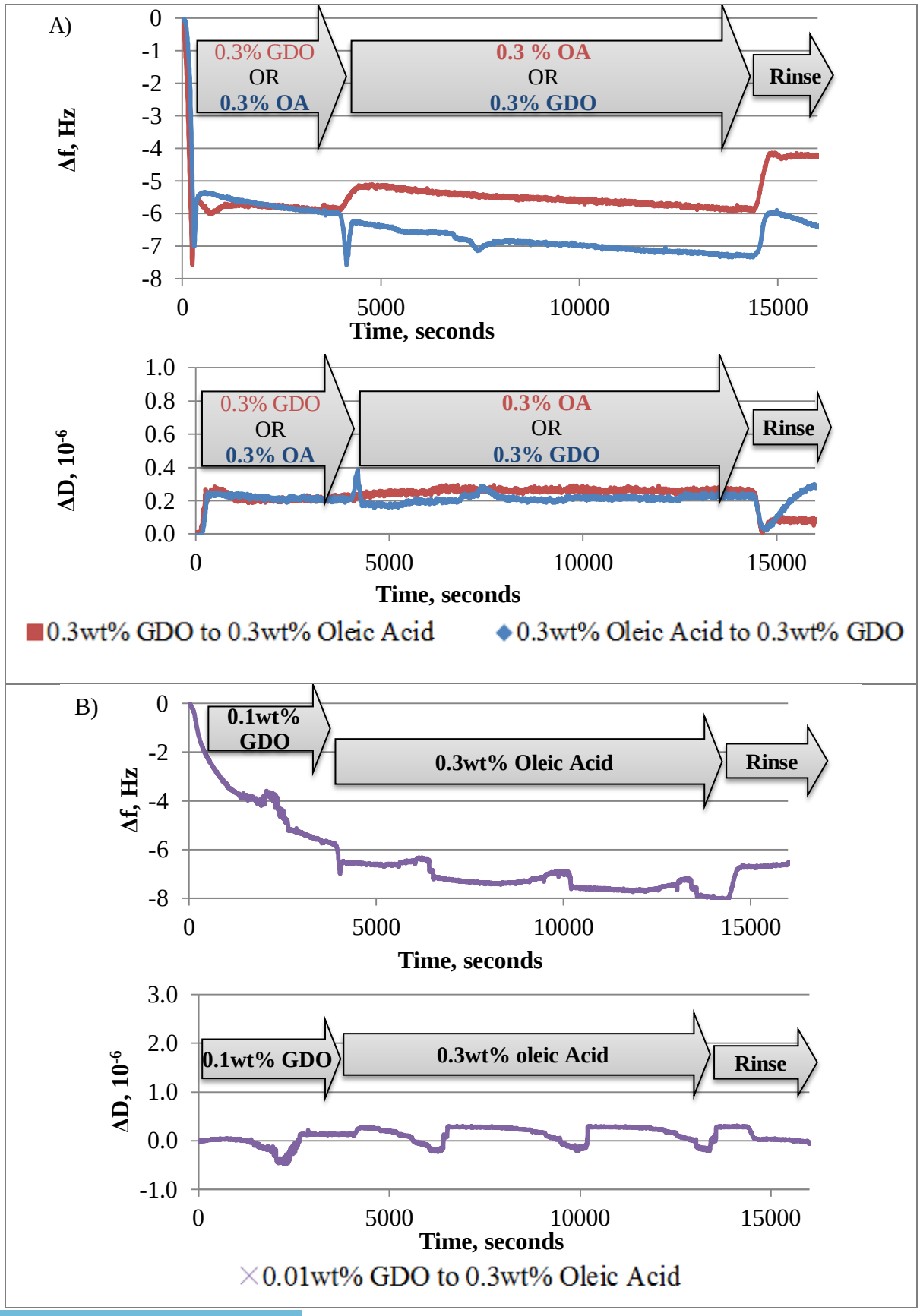

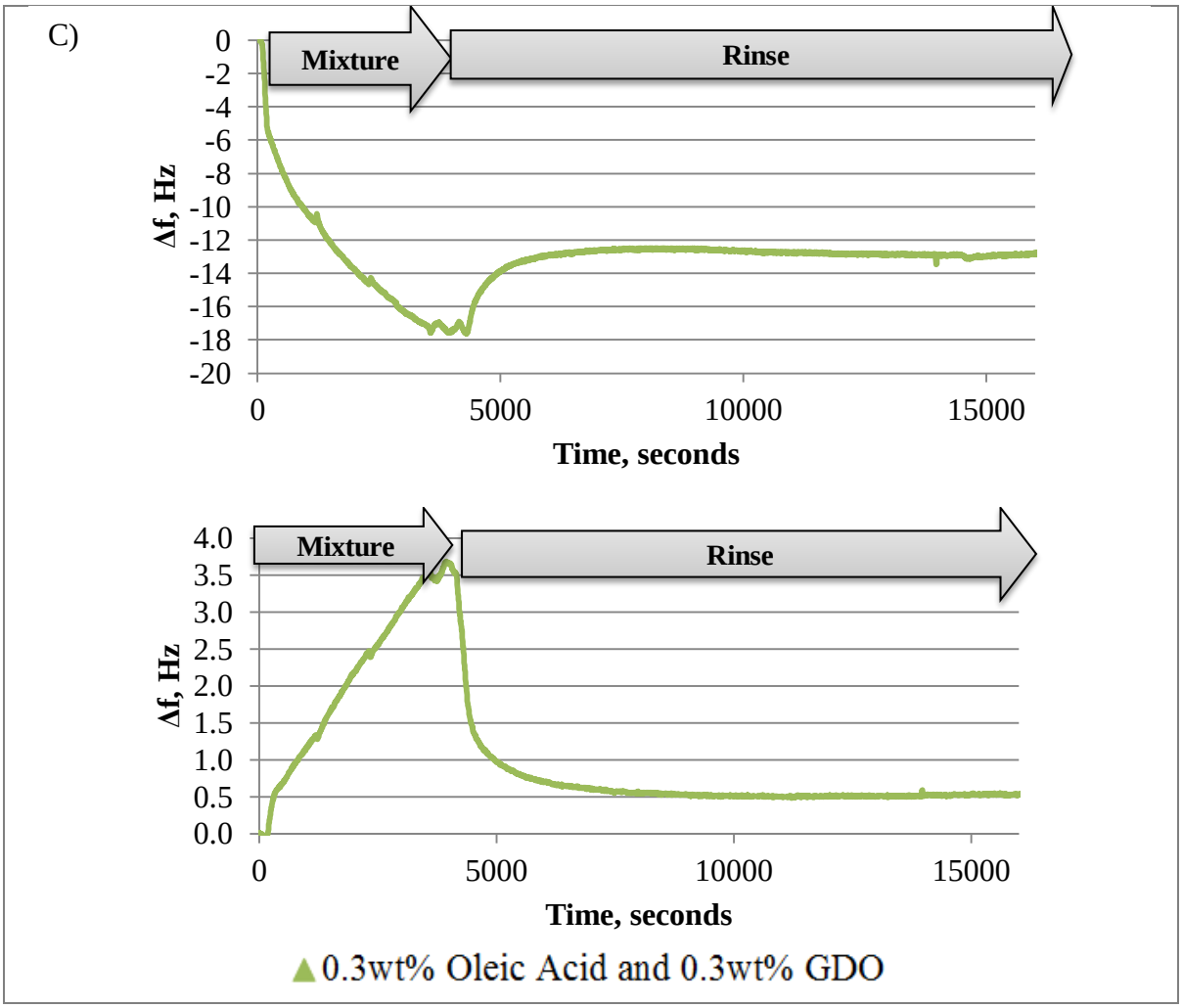

Figure 27: Representative frequency and dissipation measurements for binary GDO and oleic acid mixtures in real time. A) The red curve is the addition of 0.3 wt% GDO for one hour. Next the solution is switched to 0.3 wt% oleic acid, followed by rinse with isooctane. The blue curve illustrates the reverse. (B) Addition of 0.1 wt% GDO followed by 0.3 wt% oleic acid and finally rinse. All experiments were the surfactants were added sequentially produced rigid monolayer with relatively the same mass. (C) In the binary mixture of both oleic acid and GDO the mass and dissipation were much greater suggesting adsorption may be occurring through a different two step mechanism.

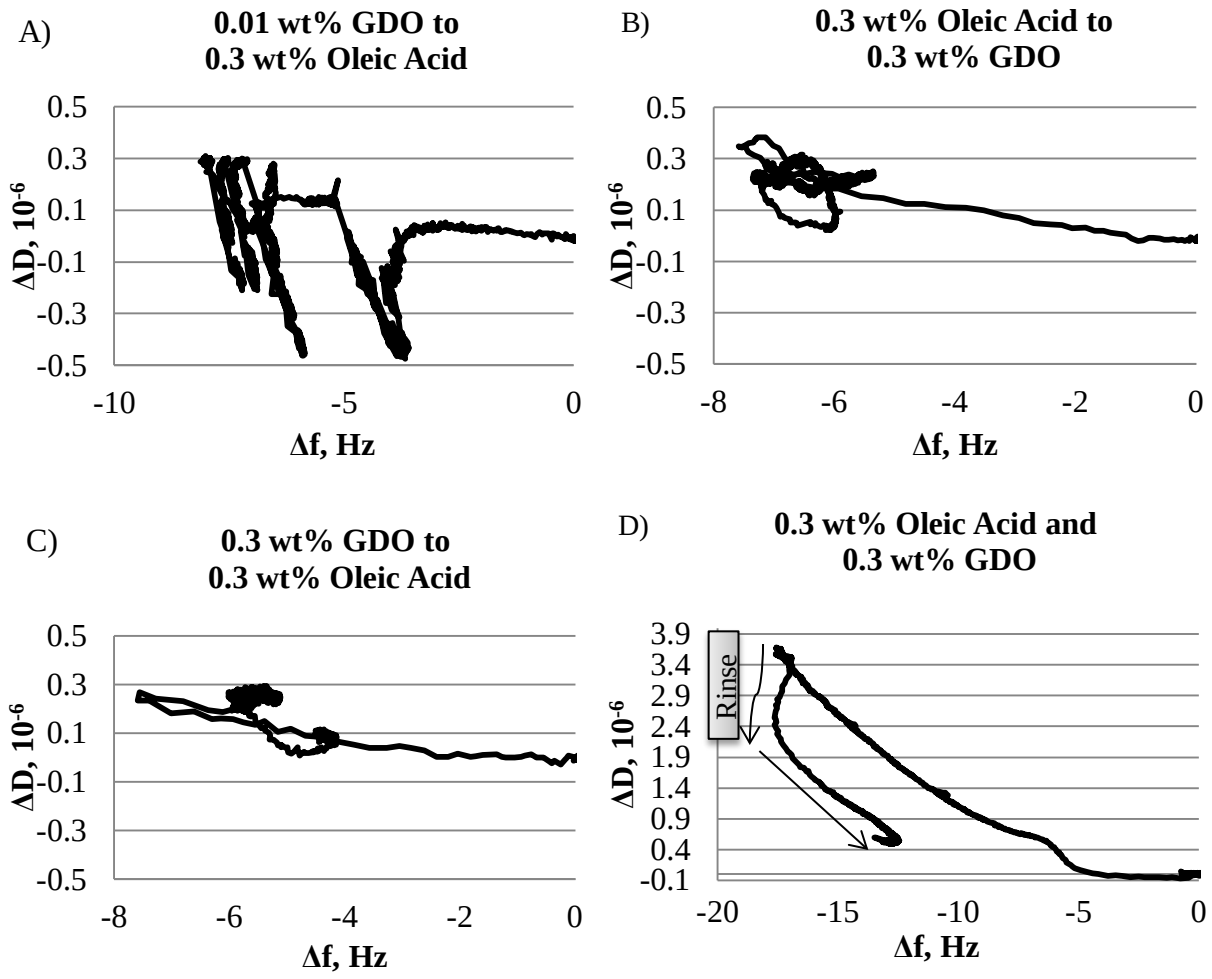

Figure 28: Frequency and dissipation curves for binary surfactant system of GDO and oleic acid. In the sequential systems (A, B, and C), the first surfactant flowed through the QCM cell for 60 minutes then the solution was switched to the second surfactant. After an additional 60 minutes, the sensor was rinsed with solvent. All produced similar rigid monolayers. When the surfactants were added in combination (D) a soft, dissipative film formed and upon rinse returned to a rigid monolayer.

3.4 Adsorption and Steel Corrosion: The ability of oleylamine, oleic acid, octanoic acid, GMO and GDO mixtures to protect iron oxide surfaces from steel corrosion was evaluated using the steel corrosion testing described previously. Photographs of the steel coupons after the two day test are shown in Figure 29. Oleic acid, GMO and oleylamine inhibited corrosion if present in high enough concentration, but octanoic acid proved to be a poor corrosion inhibitor

regardless of concentration. Oleic acid improves steel corrosion at lower concentrations relative to oleylamine and GMO, 0.1 and 1.0 wt% respectively. Octanoic acid was tested at 5 times a reasonable concentration (5.0 wt%) and large amounts of rust were still present at the end of 48 hours. In addition to the difference observed between surfactants, there also appeared to be a difference in performance between the two sides of the steel coupon. The steel is pressed into coupons producing slight differences in the two sides. Six surface roughness measurements were taken of each side of two different steel coupons. The average surface roughness (R_a) is then calculated by taking the average of the absolute values of these measurements. The right side had a slightly higher R_a when compared to the left side. The average R_a of the left was 0.81 µm compared to 1.02 µm for the right side. This greater surface roughness may contribute to the reduction in corrosion protection. The left (smoother) side may allow for the formation of more ordered monolayer leading to improved protection from the water and oxygen necessary to form rust.

In an effort to understand the variation seen in steel corrosion performance of oleic acid, oleylamine and octanoic acid, we measured the adsorption of the surfactants at 25°C in real time using QCM-D. For this testing, 0.1 wt% solutions were made of each surfactant. It is important to test at equivalent weight percent, since many applications are sensitive to increased costs due to higher treat rates. Due to the lower molecular weight of octanoic acid, the solution was twice as concentrated from a molar perspective.

(a)

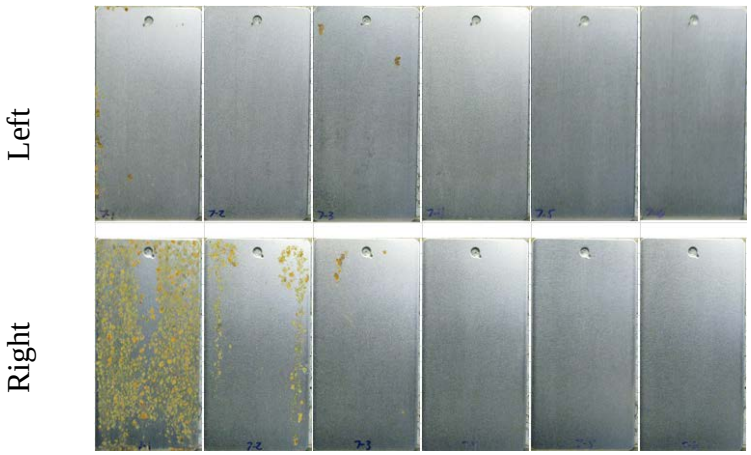

(b)

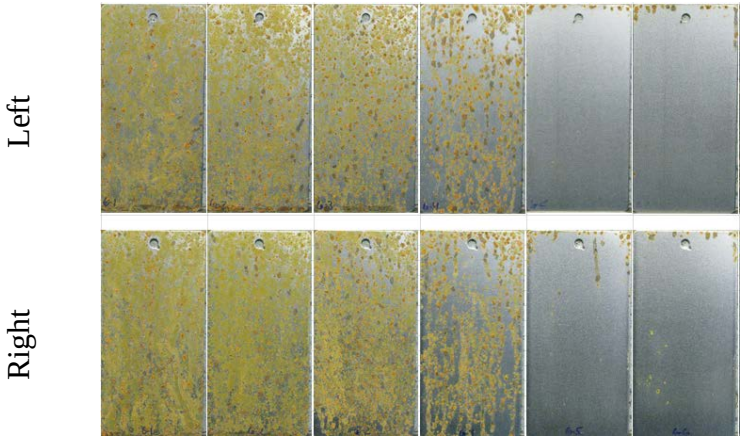

(c)

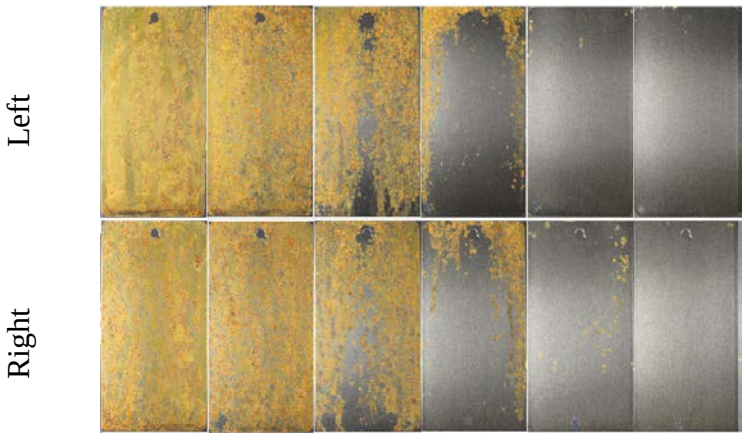

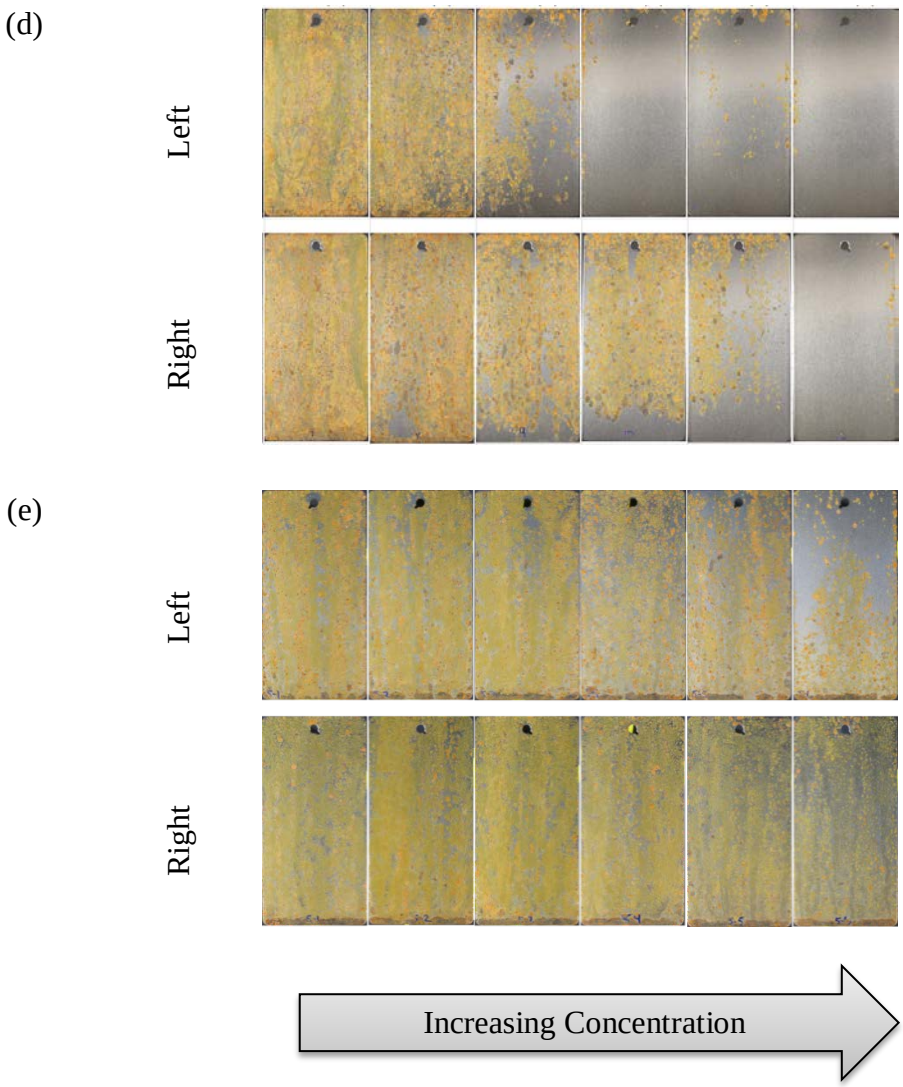

Figure 29: Left (smooth) and right (rough) side of steel corrosion coupons at end of test for (a) oleic acid (b) oleylamine (c) GMO mixture (d) GDO mixture and (e) octanoic acid at six different concentrations. (Concentrations tested for oleic acid, GMO and GDO and oleyl amine: 0.01, 0.1, 0.3, 0.5, 1.0, 1.5 wt% and octanoic acid: 0.01, 0.05, 0.25, 0.5, 1.0, 5.0 wt%).

As mentioned previously, oleylamine and oleic acid exhibited very straightforward adsorption behavior. Upon addition of the sample, frequency decreased (due to added mass) and dissipation increased slightly. The frequency values plateaued fairly quickly indicating there was no additional net change in mass. After two hours of pumping the solution over the sensor, solvent was added to remove any loosely physisorbed surfactant. Addition of solvent, increased frequency and decreased dissipation suggest the removal of loosely adsorbed surfactants from the steel for both surfactants (Figure 30).

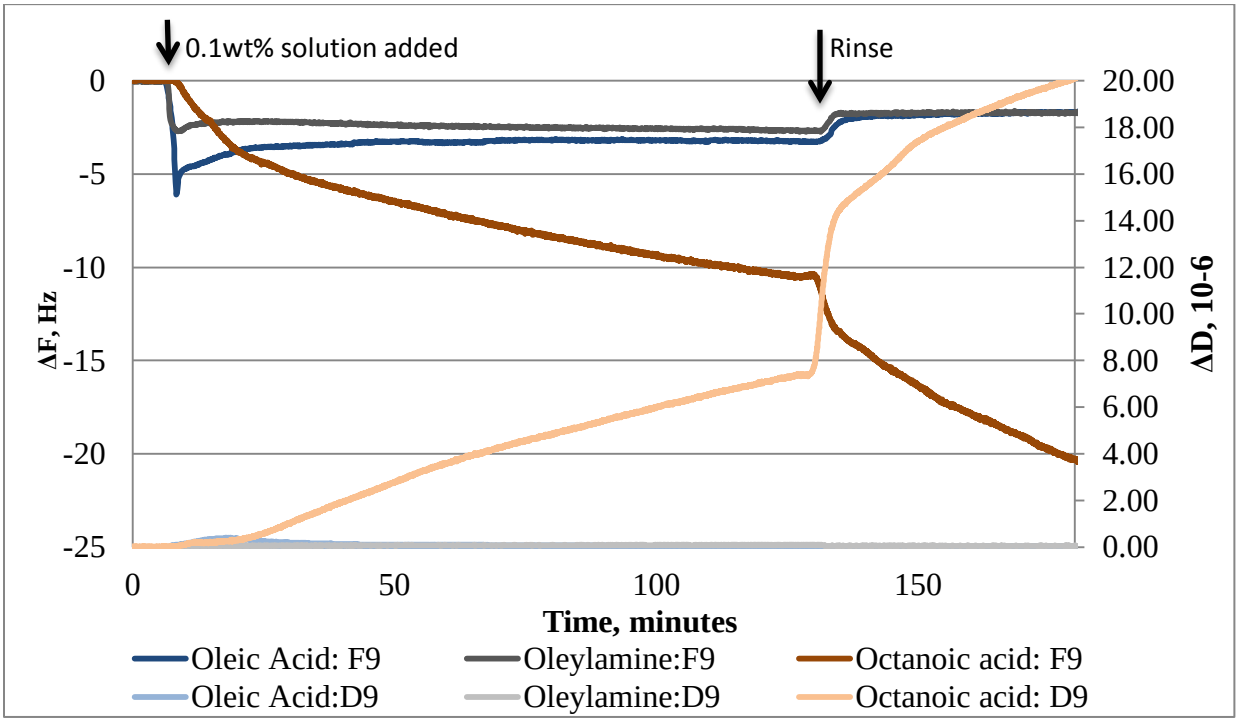

Figure 30: Ninth harmonic frequency and dissipation measurements over time upon addition of oleic acid, oleylamine, or octanoic acid. After two hours the sensors were rinsed with solvent.

The dissipation measured for oleic acid and oleylamine was minimal (< 2% of the frequency), so the Sauerbrey equation is a valid estimation to calculate the adsorbed mass. Frequency and dissipation values were corrected for the viscosity and density difference between the solvent and solution. The adsorbed mass before rinse for oleylamine and oleic acid was 57±7

and 61±4 ng/cm^2, respectively. The measured mass closely corresponds to previously reported values for oleic acid (50 ng/cm^2).[36] At this concentration and under these flow through conditions, the adsorbed masses of oleic acid and oleylamine were not significantly different.

With regard to oleic acid's orientation on the surface, previous work using molecular dynamic simulation predicts the conformation on iron oxide surface would be a mixture of molecules lying flat and upright in oil. As the surface coverage increases, the molecules should become more upright. Also, this modeling did not find a large difference in the structure of the surfactant film when shear was introduced, suggesting the shear introduced from the pump will not have a large impact on results.[37] The measured mass, molecular weight and Avogadro's number was used to calculate the average area per surfactant molecule in the QCM-D experiments (~80 Å^2/molecule). This value falls between the values for perpendicular (25 Å^2/molecule) and parallel (130 Å^2/molecule) orientation to the iron oxide surface.[27] Upon rinse, the data were less repeatable but 37±5 ng/cm^2 of oleic acid remained and 44±8 ng/cm^2 of oleylamine. Once again the values between the surfactants are not significantly different. If the mass is averaged across the entire surface, it would correspond to almost every surfactant molecule being almost parallel to the surface (120±20 Å^2/molecule).

Over the two hours octanoic acid was added, the frequency and dissipation curves for octanoic acid did not plateau. In addition to not reaching equilibrium, upon rinse the change in frequency and dissipation increased further. This increase upon rinse suggests incorporation of solvent due to a decrease in the rigidity of the film and an increase in the mass. The similar chain length of the octanoic acid and iso-octane may contribute to this phenomenon. Higher heats of adsorption have been noted when surfactants are absorbed from solvents of similar chain lengths which have been interpreted as the formation of a mixed surfactant solvent film.[38] The QCM-D

data also supports this interpretation. Due to the high dissipation, the Sauerbrey equation would lead to an underestimation of the mass. The frequency versus dissipation plot in Figure 31 provides insight into the adsorption of octanoic acid.

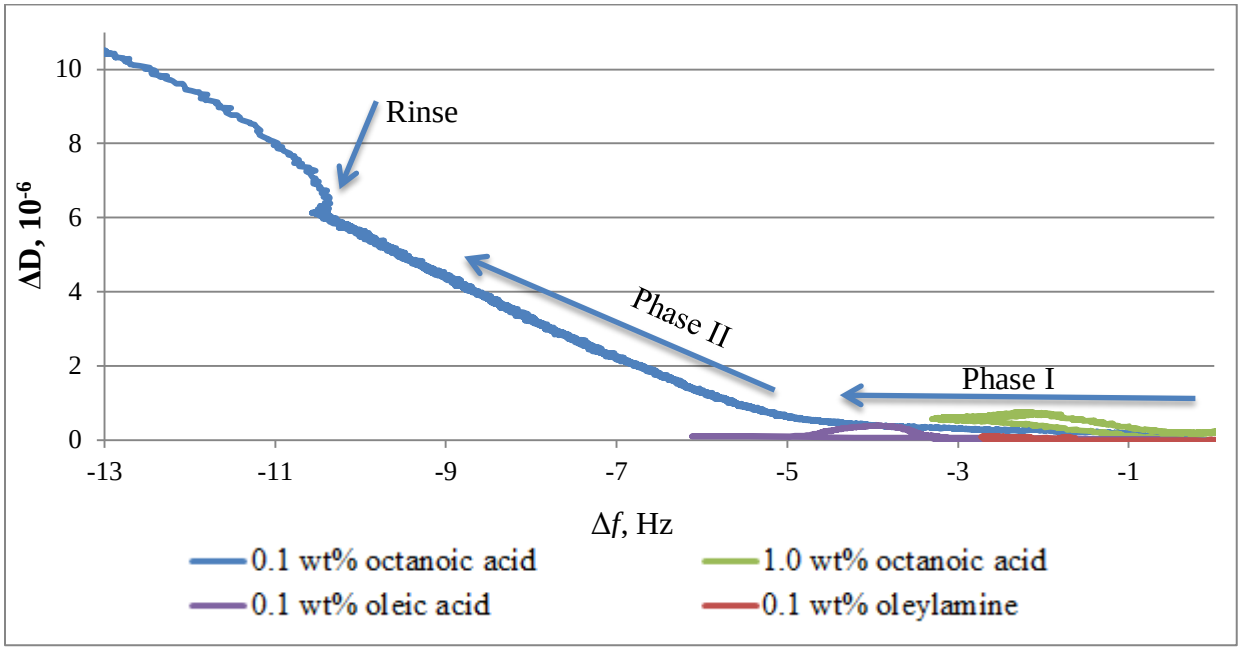

Figure 31: Frequency and dissipation plot of oleic and octanoic acid. A change in slope is indicative of a change in film phase.

The first phase has a very low dissipation and is likely due to the formation of a rigid octanoic carboxylic acid monolayer. Since the dissipation of this phase is minimal, the Sauerbrey equation is once again valid. After correction for changes in bulk properties (viscosity and density), the adsorbed mass was 79 ng/cm^2 (~30 Å^2/molecule). Based on calculations in literature, octanoic acid formed a closely packed, upright monolayer (perpendicular = ~20 Å^2/molecule and parallel = ~60 Å^2/molecule).[27] The second phase could be explained by a mixed solvent/surfactant film, multilayers of octanoic acid, or both. Models comparing stearic and oleic acid have noted that stearic acid forms a more diffuse film that allows the solvent to penetrate

further into the monolayer when compared to oleic acid. Stearic and oleic acid differ only in the cis double bond located between the 9th and 10th carbon. The lack of a double bond and similar alkyl chain length could contribute to octanoic acid's inclination for incorporating solvent compared to oleic acid.

The concentration of octanoic acid was increased by an order of magnitude and retested and these results are shown in Figure 32.

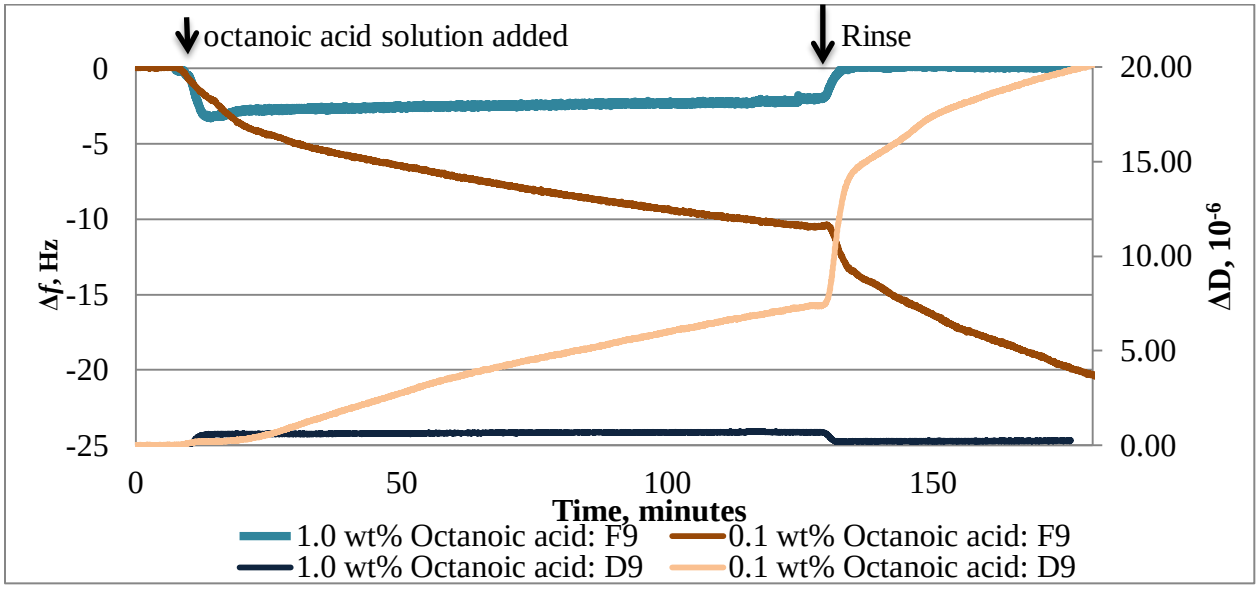

Figure 32: Frequency and dissipation measurements of octanoic acid at two different concentrations over 200 minutes.

This solution exhibited a very different behavior. The mass deposited quickly and as the surfactant/solvent solution continued to flow through the QCM-D the frequency steadily increased. Upon rinse, the frequency returned to around zero and in some cases slightly above zero, suggesting a loss of mass. (A loss of mass has been noted previously in adsorption studies of octanoic acid to steel but no explanation was provided.)[39] A loss of mass has also been noted for thiol SAMs in the presence of oxygen, depending on the solvent. In these experiments in

addition to the loss of mass, dissolved gold was present in the solutions and STM images provide corroboration of these 'holes' that are believed to formed by etching resulting from the strong adsorption of thiols on gold. This explanation has not been completely accepted in literature. [40] The difference in the results for the two concentrations could be due to the preference for formation of aggregates at the higher concentration, especially since the solvent has a similar chain length. Although it is unclear why the adsorption behavior varied with a change in concentration, the data suggests at both concentrations octanoic acid failed to form a monolayer that could prevent the incorporation of solvent or protect the steel surface from corrosion.

Relating the QCM-D data to the steel corrosion results (at 0.1 wt%) suggests a tightly packed, upright monolayer may not necessarily prevent corrosion. In fact, the less perpendicular conformation of oleic acid and oleylamine may be preferable for corrosion resistance. Based on the measured mass, octanoic acid formed a more packed upright film compared to the oleyl surfactants, but this film was more diffuse and permitted the incorporation of solvent and likely water as well. The ability of water to penetrate closely packed hydrocarbon chains of fatty acids monolayers has been noted in previous literature and may explain the differences seen in oleic and octanoic acid in preventing steel corrosion.[41] It is important to note, saturation of the hydrocarbon chains do result in other chemical differences (i.e., pK_a) outside of physical packing on the surface.[42] Corrosion occurs through an electrochemical process initiated by water and air. The degree of unsaturation may contribute to difference in the electrochemical process resulting in difference in steel corrosion protection as well, but that is outside the scope of this work.

In order to understand the differences seen in corrosion prevention for oleylamine and oleic acid, a few adsorption measurements were made at additional concentrations. Adsorption of oleic acid, at six different concentrations ranging from 0.01 to 0.3 wt%, was measured at 25°C.

This concentration range covers typical treat rates for these surfactants in lubricants. The concentrations ranging from 0.10 to 0.3 wt% exhibited similar adsorption behavior. The measured mass plateaued within 10 minutes, which is the time steel coupons are exposed to solution in steel corrosion testing, and upon rinse a small loss in mass was observed. The solution at 0.05 wt% took thirty minutes to reach equilibrium. The lowest concentration never reached equilibrium and created a more dissipative film that incorporated solvent upon rinse (Figure 49 in Appendix).

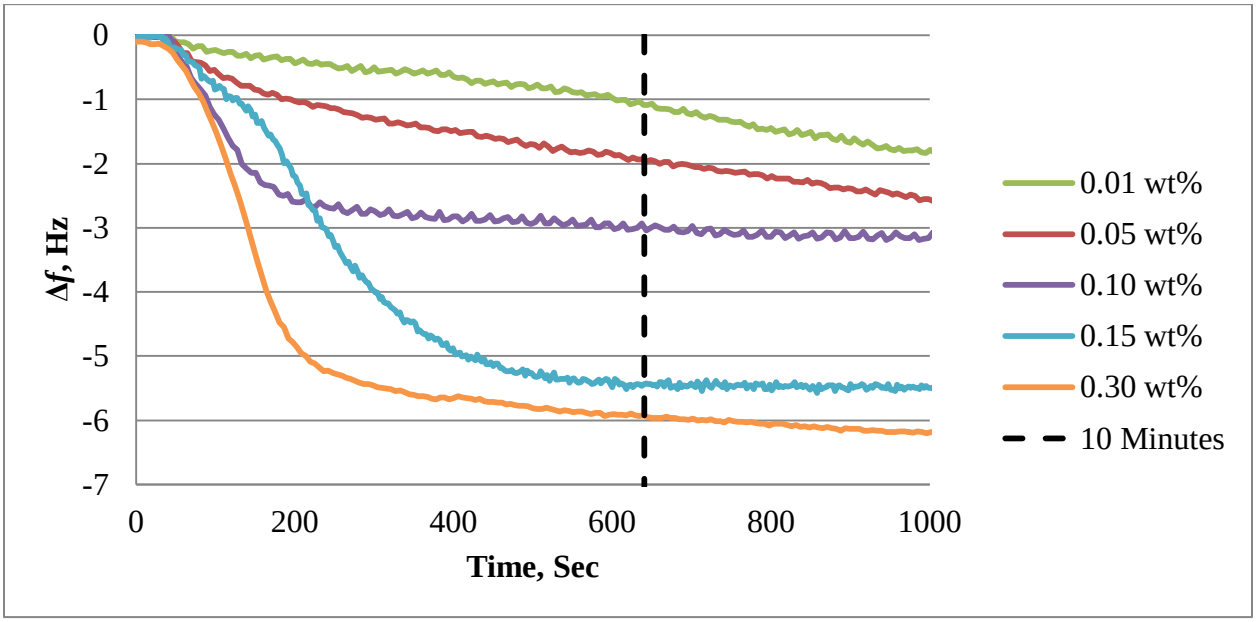

Figure 33: Representative initial frequency and dissipation measurement for oleic acid solutions ranging from 0.01 to 0.30wt%. The dotted line represents the length of time steel coupons are exposed to the solution before corrosion is tested.

The adsorbed mass of oleic acid at equilibrium and after rinse was calculated for the each concentration of oleic acid. If no equilibrium was reached after an hour, the frequency change at one hour was used for the calculation. Results are summarized in Figure 34. Corrections for bulk viscosity were necessary at concentrations at or above 0.10 wt%. The adsorbed mass for the lower concentrations was more variable, especially after rinse, likely due to varying amount of

solvent incorporation. At the concentrations that exhibited more repeatable behavior (≥ 0.08 wt %), improvement in packing was seen as the concentration of oleic acid increased. The increase in packing density indicates the orientation of the oleic acid begins to become more upright. Minimal increase in mass is observed between 0.15 and 0.30 wt% suggesting increasing the concentration past 0.15 wt% has a minor impact on the density of the monolayer. The mass at 0.3 wt% corresponds to 45 ± 13 Å^2/molecule at equilibrium and 62 ± 12 Å^2/molecule after rinse. At this concentration, a monolayer of oleic acid would be oriented between 55 to 75 degrees from the steel surface, if the surfactant was uniform across the surface.

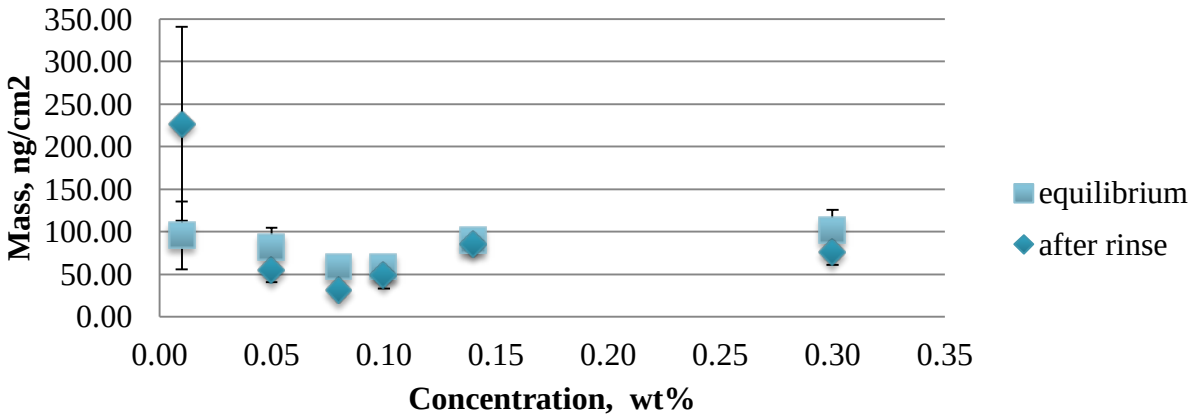

Figure 34: Mass of oleic acid at equilibrium and after rinse at six difference concentrations (0.01, 0.05, 0.08, 0.1, 0.12, and 0.3 wt %). Corrections for bulk viscosity and density changes were made for the data at equilibrium. Error bars represent 95% confidence intervals.

In the steel corrosion testing, at concentration of 0.1 wt%, corrosion resistance begins to improve and at 0.3 wt% minimal or no rust is observed. As mentioned in the kinetics discussion, the experimentally determined desorption rate for oleic acid is so low it appears oleic acid is virtually irreversibly bound under these conditions. The theoretical surface coverage calculated from the equilibrium constant is compared to the percentage of the rust free surface at the termination of the humidity cabinet test. As illustrated in Figure 35, a strong trend appears

between the two values. In order to measure the correlation of these two values, the theoretical surface coverage was plotted against the percentage of the steel coupon that was rust free after test. Regardless of surfactant (GDO or oleic acid) and concentration there as a strong correlation ($R^2 = 0.95$) suggesting this may be a good way to predict steel corrosion performance (assuming the alkyl chain is capable of preventing/reducing diffusion of solvent or water to surface).

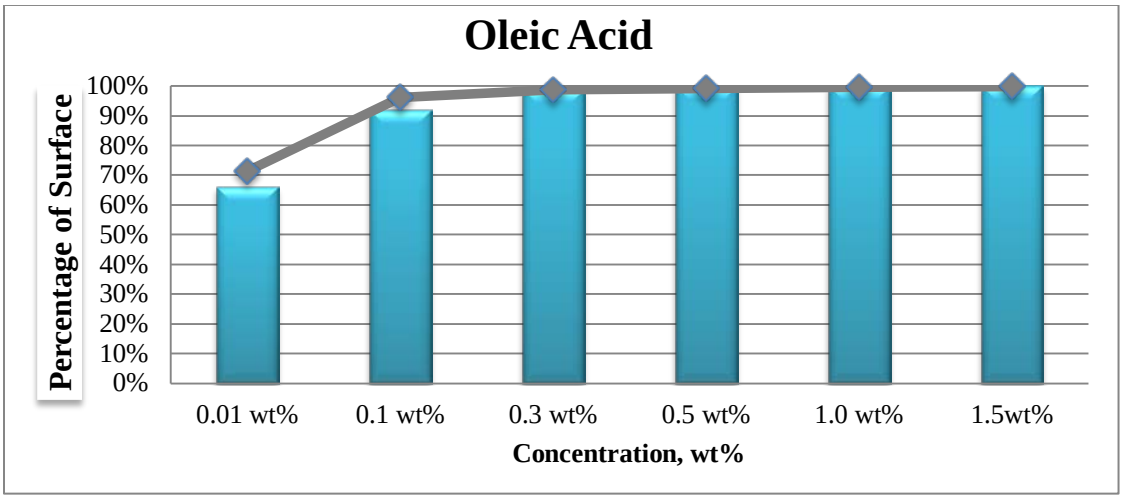

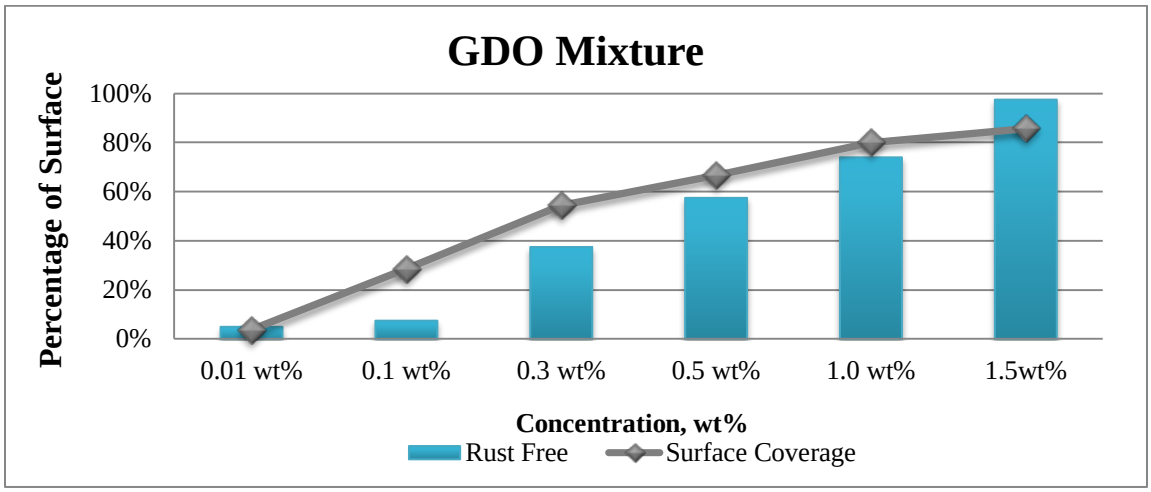

Figure 35: Theoretically calculated surface coverage for oleic acid and GDO at multiple concentrations compared to the percentage of steel surface with no rust upon termination of steel corrosion testing

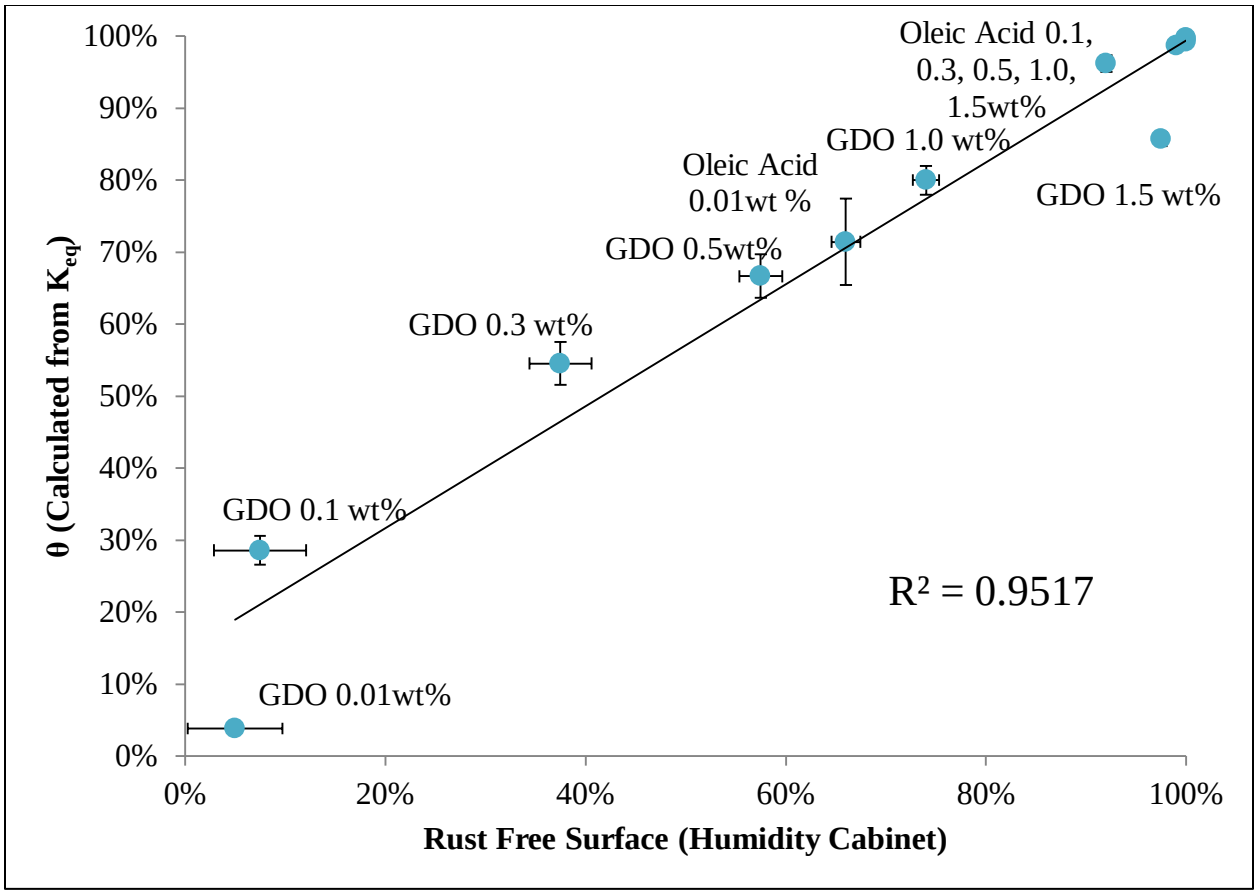

Figure 36: Scatter plot comparing surface coverage calculated from the experimentally determined equilibrium constant and the percentage of surface rust free after corrosion test. Regardless of surfactant (GDO and oleic acid) and concentration there is a strong correlation (R^2 = 0.95).

Oleylamine was tested at three different concentrations: 0.01, 0.10 and 4.07 wt% (Figure 36). There were minimal differences seen between the two lowest concentrations in the ability to prevent corrosion (Figure 29) and adsorption measured on the QCM-D (Figure 36). At 0.01 and 0.10 wt% of oleylamine, there was almost 100% rust on the steel coupons at the end of the corrosion test and only a small shift in frequency (~2.5Hz) and dissipation (~0.1x 10^{-6}) as measured by QCM-D. The highest concentration, 4.07%, is ten times a typical treat rate but was tested in an effort to maximize the density of the monolayer. Greater deposition was measured at this concentration, but the dissipation was much higher so the Sauerbrey equation could not be

used for the conversion to mass. The kinetics of oleylamine adsorption was vastly different than the kinetics of oleic acid adsorption and could explain the differences seen in preventing corrosion. The observed rate constant of oleylamine varied minimally with concentration making an accurate calculation of the rate of adsorption and desorption less precise. Considering solely the order of magnitudes for the rate constants, the rate of adsorption for oleylamine was four orders of magnitude smaller than oleic acid. Also, the rate constant of desorption for oleylamine was an order of magnitude greater than adsorption for oleylamine. These differences in kinetics could explain the inferior steel corrosion protection of oleylamine.

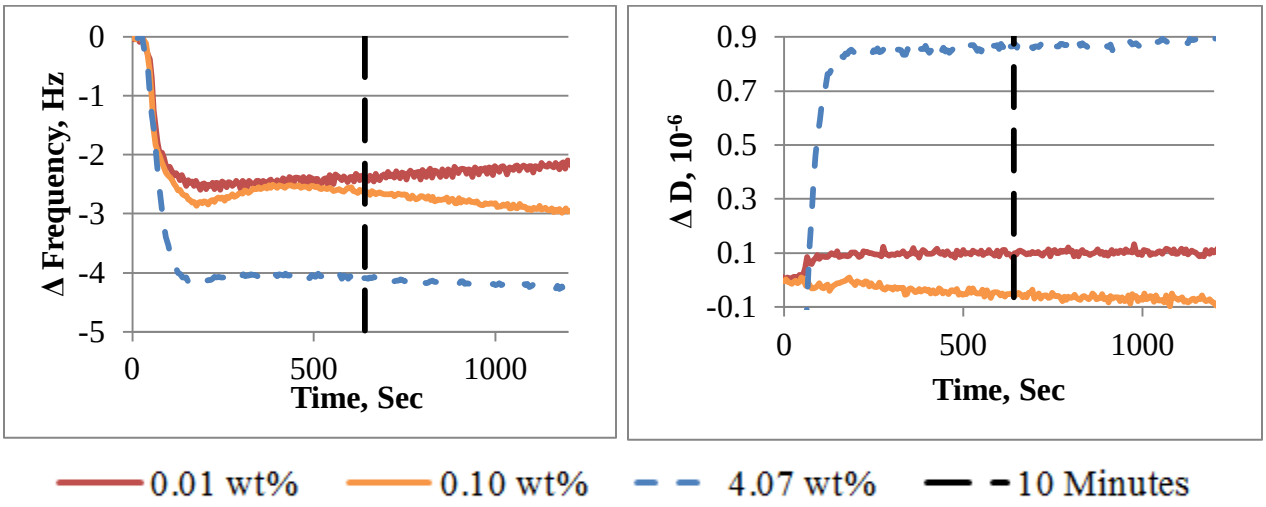

Figure 37: Representative initial frequency and dissipation measurement for oleylamine solutions ranging from 0.01 to 4 wt%. The dotted line represents the length of time steel coupons are exposed to the solution before corrosion is tested. The highest concentration (4.07 %) required very large corrections for changes in bulk properties.

In the flow through system of the QCM-D, there is an abundance of surfactant over the length of the experiment. This may explain why the concentration differences observed in the steel corrosion testing are not apparent when looking at the mass at a single concentration (0.1 %). Also, comparing the mass and packing of the surfactants doesn't provide a complete explanation. The weak adsorption of oleylamine and strong adsorption of oleic acid to iron oxide

suggested by the kinetics correlates with oleylamine's inability to protect iron oxide surface from corrosion at low concentrations. If a better correlation to the steel corrosion test is required, it may be best to duplicate the QCM-D experiments under more similar conditions. After the solution is pumped into the chamber, the pump could be turned off for ten minutes followed by a rinse with a solvent.

Comparing the QCM-D to the steel corrosion results, there appears to be a few insights into the ability of a surfactant to prevent corrosion of steel. First, the surfactants need to form sufficient coverage before exposure to a warm, humid environment (10 minutes in this bench test). Based on the QCM results, this depends on the polar group and concentration of surfactant. Second, the surfactant needs to align in a direction that prevents the incorporation of water which is largely controlled by the alkyl chain. If the alkyl chain is too short (octanoic acid) or the concentration too low, solvent (and likely water) intermix with the surfactant leading to corrosion of the steel. Third, strong adsorption with minimal desorption (as demonstrated by the kinetics) is required to protect the steel surface from corrosion. As demonstrated by oleylamine, this later point can also be overcome if enough surfactant is present.

3.5 Adsorption and Friction of Surfactants on Iron Oxide Surface: In an effort to understand the correlation between surfactant structure and friction performance, we compared the QCM-D results to HFRR measurements. It is well known that the adsorption of surfactants on to steel results in the formation of a monolayer capable of reducing friction.[43] Consistently seen throughout literature, saturated surfactants are more effective at reducing friction when compared to their unsaturated analogues.[44] One example of the effect of chain unsaturation on friction was reported by Lundgren.[45] He compared the friction of stearic, oleic and linoleic acid using a surface force apparatus to measure frictional forces. Linoleic acid generated the highest

CoF and stearic acid the lowest. One predominant theory is that this is directly related to the ability of the surfactants to form a compact monolayer. Oleic acid contains a *cis* double bond in the center of the tail capable of disrupting the packing. If two cis double bonds are present, linoleic acid, the packing is further disrupting and the friction is at its highest.[45]

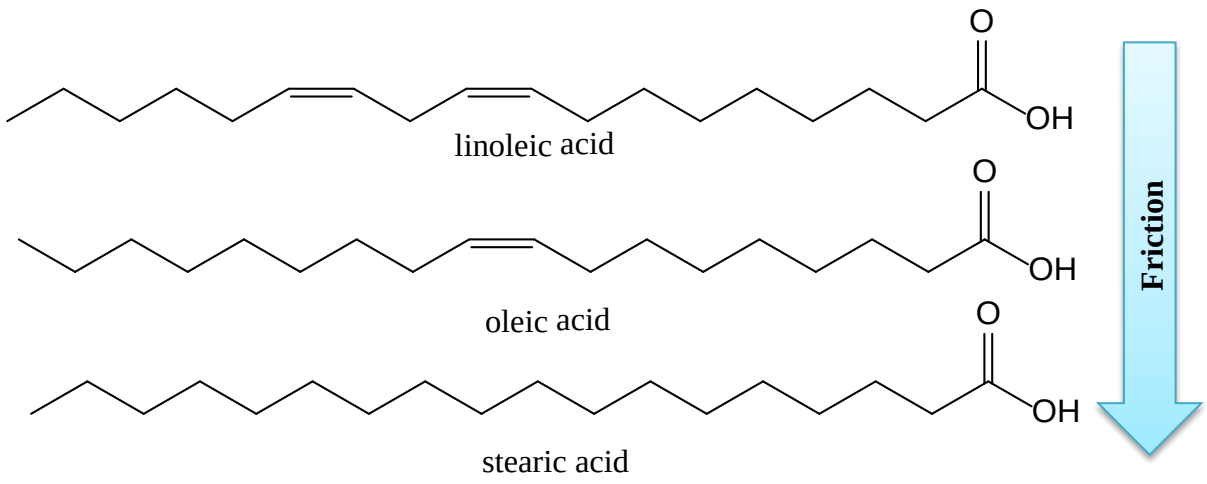

Figure 38: Saturation of the alky chain of surfactants directly affects their ability to lower friction

As discussed previously, the glycerol monoester surfactants produced a more compact monolayer (at 2mM) compared to the other surfactants tested (Figure 19). As discussed previously, this result is somewhat surprising due to the bulkier structure of glycerol esters compared to oleylamine and oleic acid. One possible explanation is the ability of glycerol monoleate to form intermolecular hydrogen bonds. The intermolecular interactions that occur in oleic acid and oleylamine monolayer are largely van der Waal interactions between the alkyl tails. The stronger intermolecular interactions of hydrogen bonding versus van der Waal interactions may contribute to the denser more organized packing.

As mentioned, the glycerol esters produced larger more dissipative films. If these adlayers can be maintained under boundary conditions, in theory, it could increase the distance between the surface and thus lower friction relative to the surfactants that form a single monolayer. Boundary friction was measured of each solution at 25 °C and 50 °C to determine if the difference observed in adsorption would have an impact on friction (Figure 38).

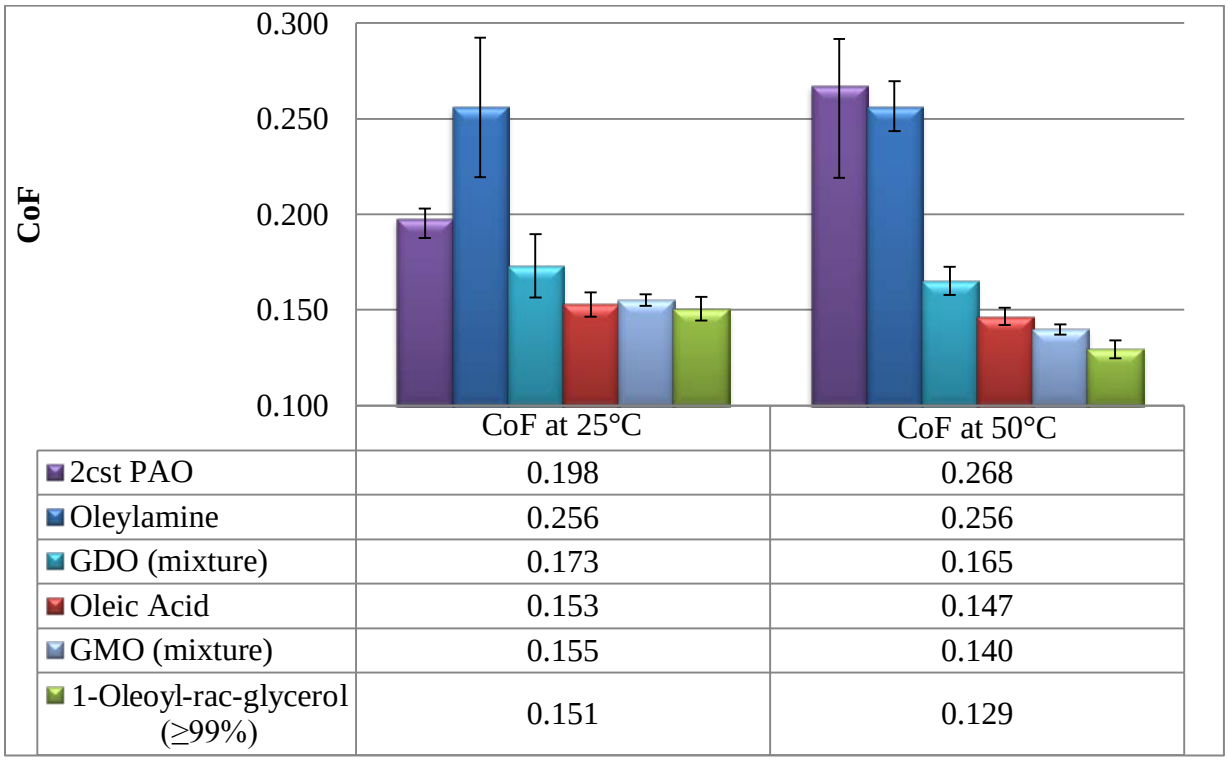

	CoF at 25°C	CoF at 50°C
2cst PAO	0.198	0.268
Oleylamine	0.256	0.256
GDO (mixture)	0.173	0.165
Oleic Acid	0.153	0.147
GMO (mixture)	0.155	0.140
1-Oleoyl-rac-glycerol (≥99%)	0.151	0.129

Figure 39: Boundary CoF measured in HFRR experiments of 2 mM solutions of surfactant and 2 cst PAO base oil at 25 and 50 °C. Error bars represent the 95% confidence interval.

The measured friction values at 25 °C for oleic acid, 1-oleoyl-*rac*-glycerol, and the GMO (mixture) were indistinguishable suggesting the adlayer could not be maintained under these conditions and concentration. Comparatively, glycerol dioleate exhibited slightly higher friction and oleylamine significantly higher friction. The friction of the oleylamine solution was actually

greater than the 2cst PAO alone. In addition to higher friction values, the repeatability of the measurements was relatively poor, producing confidence intervals 4 to 10 times larger. Reflecting on the Stribeck curve discussed previously, as the viscosity of the base oil decreases (due to higher temperature) the two surfaces will come closer in contact and friction will increase. Due to this closer proximity of the surfaces, greater differentiation in friction is measured between the surfactants at the higher temperature. The ability of a surfactant to lower friction is often attributed to its ability to form a tightly packed monolayer.[45] In order to determine if the packing measured using QCM-D correlated with the HFRR friction results, a scatterplot comparing the CoF to the average area per molecule is illustrated in Figure 39.

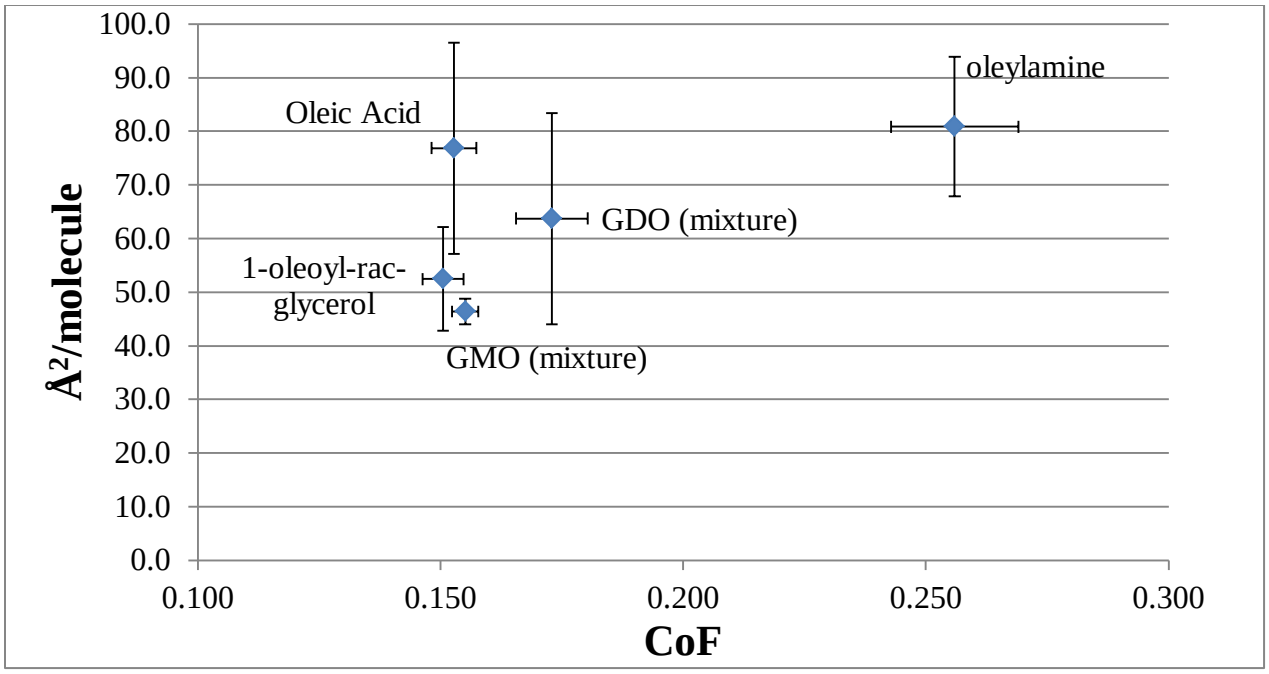

Figure 40: Scatterplot of the boundary friction at 25°C to the average molecular area per molecule.

Comparing the experimentally determined packing and CoF suggests under these conditions there was no correlation. GMO and 1-oleoyl-glycerol pack more efficiently than oleylamine and also are more effective at reducing friction. However, compared to oleic acid, glycerol

monooleate produces a more compact monolayer and is essentially the same at reducing friction at this concentration. Friction was measured under dynamic sliding conditions, so the strength of the bond holding the surfactant to steel may explain the difference in friction. Oleic acid is capable of forming strong covalent bonds with steel, so under sliding conditions the monolayer may be maintained. GMO forms hydrogen bonds with the surface which are not as strong, but intermolecular hydrogen bonds stabilize the monolayer and may enable it to remain intact under pressure and sliding. GDO also hydrogen bonds with steel, but only forms dimers so not as resilient under dynamic conditions. The variation in the friction measurements for GDO and oleylamine was also quite a bit larger relative to the other surfactants, suggesting the amount of surfactant removed for the weaker bound monolayer is highly variable. Examining friction over time (instead of the average) is further support that the initial adsorbed layer cannot be maintained under these conditions (Figure 40). GDO and oleylamine are able to effectively reduce friction initially at 25°C, but after 60 seconds of sliding friction begins to increase.

(a)

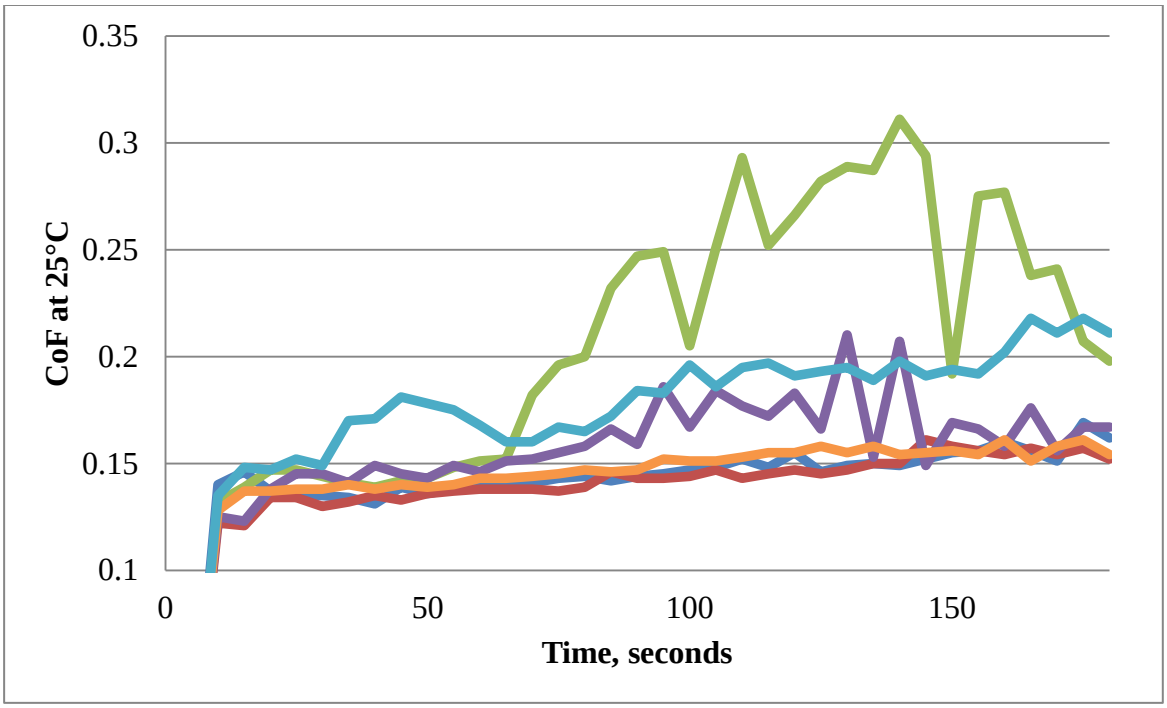

(b)

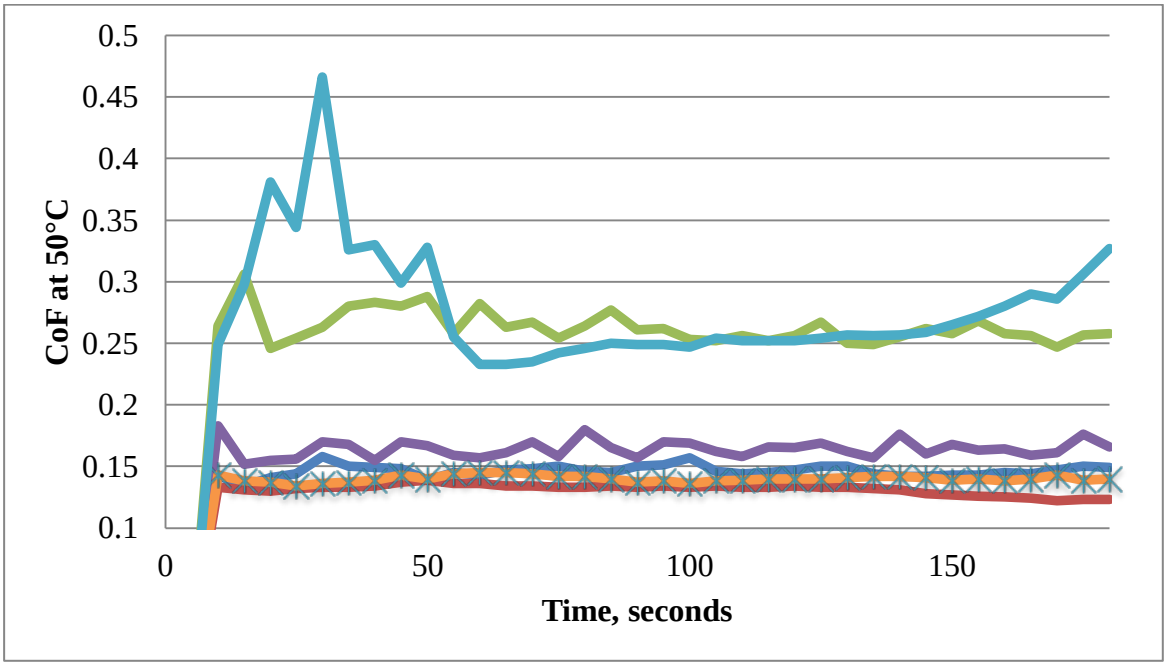

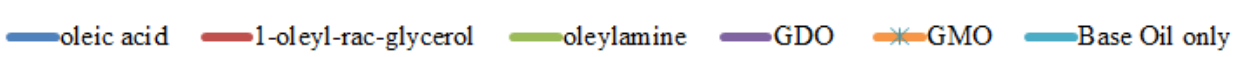

Figure 41: CoF measured using HFRR over time at 25°C (a) and 50°C (b) for 0.1 wt% solutions. As stated previously, the reservoir temperature stabilized at 25 °C for 90 seconds, than the rig reciprocates under 4 N of pressure, 1 mm path length, and 20 Hz. Friction measurements were taken every 5 seconds for 3 minutes. The fluid temperature was then raised to 50 °C and the same procedure and measurements repeated.

In an effort to further investigate friction, CoF was measured for each surfactant across a wide concentration range at 25 and 50 °C (Figure 41). For all measured surfactants the CoF reached a minimum and plateaued. The raw friction data was fit to a first order decay equation to mathematically calculate the minimum frictional values with confidence.

$$CoF = (Y_0 - Plateau)e^{-kx} + Plateau \quad (20)$$

x = concentration (wt %)
Y_0 = y-intercept (unitless)
$Plateau$ = minimum CoF (unitless)
k = rate constant (1/wt %)

The concentration each surfactants reached a minimum varied, but did occur at lower concentrations at higher temperatures, for the majority of the surfactants. The minimum CoF for each surfactant and 95% confidence intervals are depicted in Figure 42.

Considering the confidence interval, all surfactants reduce friction equivalently if a large enough concentration is present at 25 °C. At the higher temperature, the base oil contributes less to the overall friction and further differentiation is observed. The concentration at which each surfactant reaches maximum reduction in friction was determined by the fit of Equation 20 and is listed in Table 11. GMO (pure and mixture) and oleic acid reduced friction by 50 % at concentrations below 0.02 wt%. The concentration that these surfactants reached maximum reduction in friction was half the concentration of GDO and oleylamine. As mentioned previously, these differences could be due to the degree of stability of the monolayer when pressure and sliding are applied and the reduced time required for the surfactant to readsorb (kinetics).

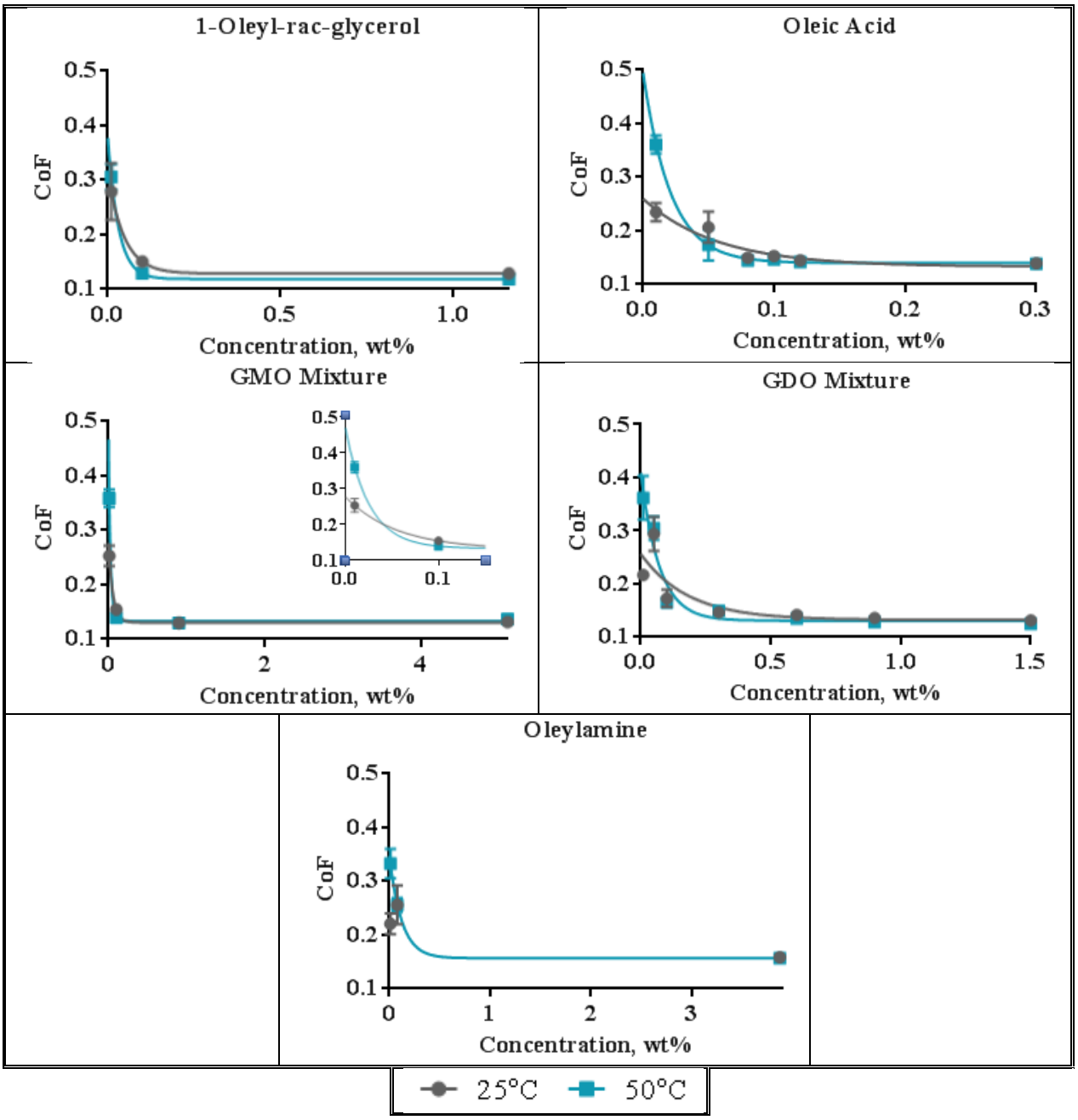

Figure 42: Boundary friction measured for surfactants across multiple concentrations. Error bars represent 95% confidence intervals. Line represent the fit to first order decay (Equation 20).

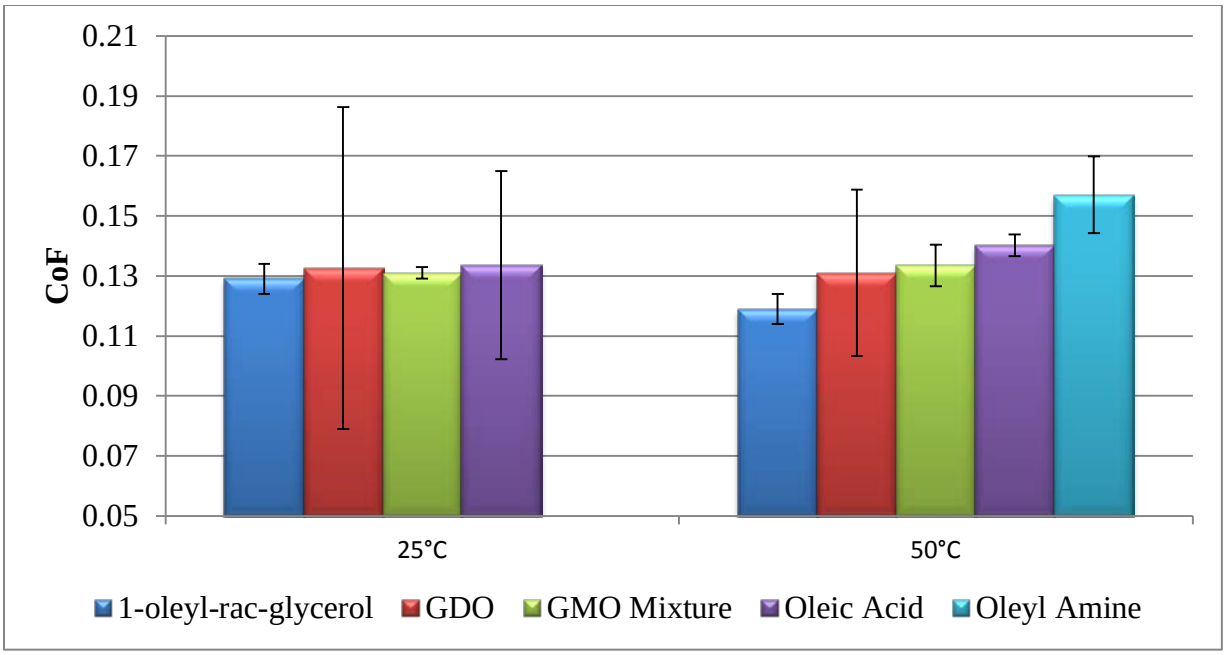

Figure 43: Minimum CoF and 95% confidence intervals for surfactants

Table 11: Minimum concentration required to reach 99.9% reduction in friction. Due to the large variation in oleylamine CoF there is not enough data to determine value for oleylamine at 50°C.

Surfactant	25°C	50°C
GDO Mixture	0.30 wt%	0.20 wt%
GMO Mixture	0.15 wt%	0.10 wt%
1-Oleoyl-*rac*-glycerol	0.15 wt%	0.10 wt%
Oleic Acid	0.12 wt%	0.08 wt%
Oleylamine	0.40 wt%	---

At higher concentrations, if the less stable SAMs are removed there is an abundance of more surfactant ready to reabsorb. Figure 43 compares the experimentally determined equilibrium constants to the concentration of surfactant required to reach minimum friction. The higher equilibrium constants require lower concentration suggesting correlation, but more data (ideally at higher temperatures) is needed to make strong conclusions on the relationship of these parameters.

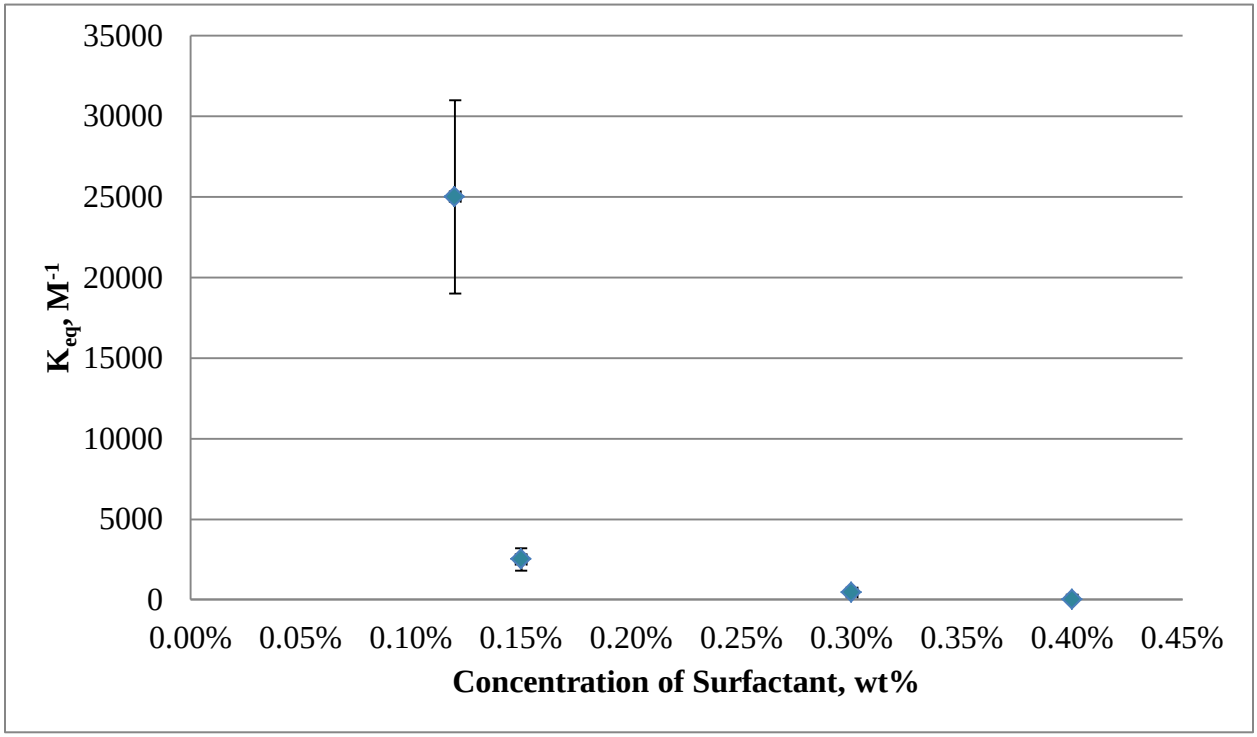

Figure 44: Equilibrium constants of surfactants plotted against the minimum concentration required for maximum reduction in friction.

CHAPTER 4: Summary and Future Work

The objective of this work was to understand if the QCM-D technique could be applied to transportation lubricant systems. In order for this technique to be useful, it needs to provide insight into the adsorption occurring at steel surfaces that can be related to the macroscopic performance. Using QCM-D, the adsorption of multiple common friction modifiers (from iso-octane) was monitored in real time. The adsorption of surfactants was investigated qualitatively by characterizing the morphology of the adsorbed layer and determining if adsorption occurred through a single or multi-step process. Utilizing the Sauerbrey equation, the mass of adsorption and packing of the surfactant was calculated. Finally, the Langmuir isotherm model was applied to quantify the kinetics of adsorption across the concentration regimes of interest. After thorough investigation of simple (single) systems, the adsorption of binary systems (sequentially and simultaneously) was investigated. QCM-D provided some qualitative insight suggesting mixed systems provide very different adsorption, but since the sensor is not specific to a single analyte it can provide limited insight without a second technique to visualize the surface. Lastly, the QCM-D results were compared to the ability of the surfactant to prevent steel corrosion and reduce friction (HFRR). Packing information and film morphology provided limited insight into performance, but kinetics was strongly correlated to both corrosion prevention and friction reduction. Considering lubricants systems function in environments of constant sliding, surfaces often do not have time to reach equilibrium so understanding the kinetics will continue to be critical.

Future work: Due to the complexity of lubricant systems, it will critical to continue to work towards a better understanding of the chemical interactions occurring on the steel surfaces. First, much of this work was done at 25°C due to the temperature limitations of the module available. High temperature cells exist that are capable of maintaining temperatures as high as 150°C. High temperatures are often seen in the actual applications, so understanding its effect on adsorption and quantifying thermodynamic parameters would augment our current understanding of these interactions. Second, as described previously, at higher concentrations, the mechanism for adsorption of the glycerol oleates differed from the lower concentration solutions. Also, in the GMO and GDO mixtures odd frequency and dissipation shifts occurred initially at higher concentrations of GMO. Characterizing the aggregation that occurs in these solutions and its effect on adsorption could resolve much of the questions and complete our understanding of these systems. Lastly, identifying and setting up a secondary technique that is capable of visualizing the interactions and bonding occurring at the surfaces would help to support the QCM-D. A reflective IR technique, Polarization Modulation-Infrared Reflection-Adsorption Spectroscopy (PM-IRRAS), can be utilized on steel surfaces and is capable of characterizing the binding on surfaces as well as the orientation of SAMs adsorbed to the surface. Combing the QCM-D in combination with this technique would provide a more complete picture of bonding occurring on steel surfaces under static environments. Also in addition to these techniques, AFM can be utilized to probe the tribofilm under dynamic (sliding) conditions. Combing the QCM-D with these techniques will only further our understanding.

Literature Cited

Literature Cited

1. Kondo, Y.; Koyama, T.; Sasaki, S., *Tribological Properties of Ionic Liquids*. 2013.
2. Herdan, J. M., Friction modifiers in engine and gear oils. *Lubrication Science* **2000,** *12* (3), 265-276.
3. Derevjanik, T. S. *Detergent and friction modifier effects on metal/metal and clutch material/metal frictional performance*; 0148-7191; SAE Technical Paper: 2001.
4. Atkins, P.; DePaula, J., Physical Chemistry. In *Physical Chemistry*, Seventh ed.; W.H. Freeman and Company: New York, 2001; pp 754-759.
5. Dill, K. A.; Brombert, S., *Molecular Driving Forces: Statistical Thermodynamics in Chemistry and Biology* Garland Science: New York, NY, 2003.
6. Levy, O.; Markovits, G. Y.; Perry, I., Thermodynamics of aggregation of long chain carboxylic acids in benzene. *J. Phys. Chem.* **1975,** *79* (3), 239-242.
7. Atkins, P.; DePaula, J., Physical Chemistry. In *Physical Chemistry*, Seventh ed.; W.H. Freeman and Company: New York, 2001; pp 988-1000.
8. (a) Schessler, H. M.; Karpovich, D. S.; Blanchard, G. J., Quantitating the Balance betweenEnthalpic and Entropic Forces in Alkanethiol/Gold Monolayer Self Assembly. *J. Am. Chem. Soc.* **1996,** *118* (118), 9645-9651; (b) Nuzzo, R. G.; dubois, L. H.; Allara, D., Fundamental Studies of Microscopic Wetting on Organic Surfaces. 1. Formation and Structural Characterization of a Self-Consistent Series of Polyfunctional Organic Monolayers. *J. Am. Chem. Soc.* **1990,** *112*, 558-569.
9. Greenfield, M. L.; Ohtani, H., Packing of Simulated Friction Modifier Additives under Confinement. *Langmuir* **2005,** *21* (16), 7568-7578.
10. Fujiwara, H., *Spectroscopic ellipsometry: principles and applications*. John Wiley & Sons: 2007.
11. Dixon, M. C., Quartz Crystal Microbalance with Dissipation Monitoring: Enabling Real-Time Characterization of Biological Materials and Their Interactions. *Journal of Biomolecular Techniques* **2008,** *19*, 8.
12. Kortüm, G., *Reflectance spectroscopy: principles, methods, applications*. Springer Science & Business Media: 2012.
13. Pattnaik, P., Surface plasmon resonance. *Appl Biochem Biotechnol* **2005,** *126* (2), 79-92.
14. Galgoczy, R.; Roca-Cusachs, P.; Alcaraz, J., Atomic Force Microscopy. *eLS* **2013**.
15. Frey, B. L.; Corn, R. M.; Weibel, S. C., Polarization-Modulation Approaches to Reflection-Absorption Spectroscopy. *Handbook of Vibrational Spectroscopy* **2001,** *2*, 1042-1056.
16. (a) Abdelmaksoud, M.; Bender, J. W.; Krim, J., Nanotribology of a vapor-phase lubricant: A quartz crystal microbalance study of tricresylphosphate (TCP) uptake on iron and chromium. *Tribology Letters* **2002,** *13* (3), 8; (b) Giurgiutiu, V.; Friedman, H.; Bender, J.; Borg, T.; Yost, M.; Newcomb, W.; Black, A.; Bost, J.; Stewart, C., Electromechanical impedance sensor for in vivo monitoring the body reaction to implants. *J Invest Surg* **2004,** *17* (5), 257-70; (c) Naderi, A.; Iruthayaraj, J.; Pettersson, T.; Makuska, R.; Claesson, P. M., Effect of Polymer Architecture on the Adsorption Properties of a Nonionic Polymer. *Langmuir* **2008,** *24*, 6676-6682; (d) Cho, N.-J.; Frank, C. W.; Kasemo, B.; Hook, F., Quartz crystal microbalance with dissipation monitoring of supported lipid bilayers on various substrates. *Nature Protocols* **2010**,

1096-1106; (e) O'Sullivan, C. K.; Guilbault, G. G., Commercial quartz crystal microbalances-theory and applications. *Biosensors & Bioelectronics* **1999,** *14*, 8.
17. Wilson, J., D. ; Buffa, A. J.; Lou, B., *College Physics*. Pearson Education, Inc.: New Jersey, 2003; p 5.
18. Sauerbrey, G., Verwendung von Schwingquarzen zur Wägung dünner Schichten und zur Mikrowägung. *Z. Physik* **1959,** *155* (2), 206-222.
19. Voinova, M. V.; Jonson, M.; Kasemo, B., 'Missing mass' effect in biosensor's QCM applications. *Biosensors and Bioelectronics* **2002,** *17* (10), 835-841.
20. Kanazawa, K. K.; Gordon, J. G. I., The Oscillation Frequency of a Quartz Resonator in Contact with a Liquid. *Analytica Chimica Acta* **1985,** *175*, 99-105.
21. Rodahl, M.; Höök, F.; Krozer, A.; Brzezinski, P.; Kasemo, B., Quartz crystal microbalance setup for frequency and Q-factor measurements in gaseous and liquid environments. *Rev Sci Instrum* **1995,** *66* (7), 7.
22. Abudu, A.; Goual, L., Adsorption of Crude Oil on Surfaces Using Quartz Crystal Microbalance with Dissipation (QCM-D) under Flow Conditions†. *Energy & Fuels* **2009,** *23* (3), 1237-1248.
23. Kanazawa, K.; Cho, N.-J., Quartz Crystal Microbalance as a Sensor to Characterize Macromolecular Assembly Dynamics. *Journal of Sensors* **2009,** *2009*.
24. Voinova, M. V.; Rodahl, M.; Jonson, M.; Kasemo, B., Viscoelastic Acoustic Response of Layered Polymer Films at Fluid-Solid Interfaces: Continuum Mechanics Approach. *Physica Scripta* **1999,** *59* (5), 7.
25. Jaiswal, A., Introduction to Data Analysis. Qsense: Linthicum Heights, MD, 2011.
26. Bain, C. D.; Troughton, E. B.; Tao, Y.-T.; Evall, J.; Whitesides, G. M.; Nuzzo, R. G., Formation of Monolayer Films by the Spontaneous Assembly of Organic Thiols from Solution onto Gold. *J. Am. Chem. Soc.* **1989,** *111*, 321-335.
27. Wheeler, D. H.; Potente, D.; Wittcoff, H., Adsorption of Dimer, Trimer, Stearic, Oleic,Nonanoic and Azelaic Acids on Ferric Oxide. *Journal of the American Oil Chemists' Society* **1971,** *48*, 125-128.
28. (a) Simič, R.; Kalin, M., Adsorption mechanisms for fatty acids on DLC and steel studied by AFM and tribological experiments. *Applied Surface Science* **2013,** *283*, 460-470; (b) Loehle, S.; Matta, C.; Minfray, C.; Le Mogne, T.; Martin, J.-M.; Iovine, R.; Obara, Y.; Miura, R.; Miyamoto, A., Mixed Lubrication with C18 Fatty Acids: Effect of Unsaturation. *Tribology Letters* **2014,** *53* (1), 319-328; (c) Loehlé, S.; Matta, C.; Minfray, C.; Mogne, T. L.; Iovine, R.; Obara, Y.; Miyamoto, A.; Martin, J. M., Mixed lubrication of steel by C18 fatty acids revisited. Part I: Toward the formation of carboxylate. *Tribology International* **2015,** *82, Part A* (0), 218-227.
29. Davidson, J. E.; Hinchley, S. L.; Harris, S. G.; Parkin, A.; Parsons, S.; Tasker, P. A., Molecular dynamics simulations to aid the rational design of organic friction modifiers. *Journal of Molecular Graphics and Modeling* **2006,** *25* (4), 495-506.
30. (a) Reimhult, E.; Höök, F.; Kasemo, B., Intact Vesicle Adsorption and Supported Biomembrane Formation from Vesicles in Solution: Influence of Surface Chemistry, Vesicle Size, Temperature, and Osmotic Pressure†. *Langmuir* **2003,** *19* (5), 1681-1691; (b) Reimhult, E.; Höök, F.; Kasemo, B., Vesicle adsorption on SiO2 and TiO2: Dependence on vesicle size. *J. Chem. Phys.* **2002,** *117* (16), 7401-7404.
31. Shrestha, L. K.; Shrestha, R. G.; Abe, M.; Ariga, K., Reverse micelle microstructural transformations induced by oil and water. *Soft Matter* **2011,** *7* (21), 10017.

32. Bus, J.; Groeneweg, F.; vanVoorst Vader, F., Effect of hydrogen bonding on water in oil emulsion properties. *Progress in Colloid & Polymer Science* **1990,** *82*, 9.
33. Reimhult, E.; Larsson, C.; Kasemo, B.; Höök, F., Simultaneous Surface Plasmon Resonance and Quartz Crystal Microbalance with Dissipation Monitoring Measurements of Biomolecular Adsorption Events Involving Structural Transformations and Variations in Coupled Water. *Analytical Chemistry* **2004,** *76* (24), 7211-7220.
34. Karpovich, D. S.; Blanchard, G. J., Direct Measurement of the Adsorption Kinetics of Alkanethiolate Self-Assembled Monolayers on a Microcrystalline Gold Surface. *Langmuir* **1994,** *10* (9), 3315-3322.
35. Davis, M. M., *Acid-Base Behavior in Aprotic Organic Solvents*. National Bureau of Standards: 1968; Vol. NBS monograph 105, p 170.
36. (a) Lundgren, S. M.; Persson, K.; Kronberg, B.; Claesson, P. M., Adsorption of fatty acids from alkane solution studied with quartz crystal microbalance. *Tribology Letters* **2006,** *22* (1), 15-20; (b) Lundgren, S. M.; Persson, K.; Mueller, G.; Kronberg, B.; Clarke, J.; Chtaib, M.; Claesson, P. M., Unsaturated fatty acids in alkane solution: adsorption to steel surfaces. *Langmuir* **2007,** *23* (21), 10598-602.
37. Doig, M.; Warrens, C. P.; Camp, P. J., Structure and Friction of Stearic Acid and Oleic Acid Films Adsorbed on Iron Oxide Surfaces in Squalane. *Langmuir* **2014,** *30* (1), 186-195.
38. Groszek, A. J., Heats of Preferential Adsorption of Boundary Additives at Iron Oxide/Liquid Hydrocarbon Interfaces. *A S L E Transactions* **1970,** *13* (4), 278-287.
39. Hackerman, N.; Roebuck, A. H., Adsorption of Polar Organic Compounds on Steel. *Industrial & Engineering Chemistry* **1954,** *46* (7), 1481-1485.
40. (a) Schonenberger, C.; Sondag-Huethorst, J. A. M.; Jorritsma, J.; Fokkink, L. G. J., What are the "holes" in self-assembled monolayers of alkanethiols on gold? *Langmuir* **1994,** *10* (3), 611-614; (b) Cao, Z.; Zhang, L.; Guo, C.-Y.; Gong, F.-C.; Long, S.; Tan, S.-Z.; Xia, C.-B.; Xu, F.; Sun, L.-X., Evaluation on corrosively dissolved gold induced by alkanethiol monolayer with atomic absorption spectroscopy. *Materials Science and Engineering: C* **2009,** *29* (3), 1051-1056.
41. Zisman, W. A., Relation of the Equilibrium Contact Angle to Liquid and Solid Constitution. In *Contact Angle, Wettability, and Adhesion*, American Chemical Society: 1964; Vol. 43, pp 1-51.
42. Kanicky, J. R.; Shah, D., O., Effect of Degree, Type, and Position of Unsaturation on the pKa of Long-Chain Fatty Acids. *Journal of Colloid and Interface Science* **2002,** *256*, 201-207.
43. (a) Hardy, W. B.; Doubleday, I., *Boundary Lubrication. The Paraffin Series*. 1922; Vol. 100, p 550-574; (b) Bowden, F. P.; Gregory, J. N.; Tabor, D., Lubrication of Metal Surfaces by Fatty Acids. *Nature* **1945,** *156*, 97-101.
44. Beltzer, M., Assessing Adsorption of Conventional Friction Modifying Molecules by Relative Contact Potential Difference Measurements. *Journal of Tribology* **1992,** *114* (4), 675-682.
45. Lundgren, S. M.; Ruths, M.; Danerlöv, K.; Persson, K., Effects of unsaturation on film structure and friction of fatty acids in a model base oil. *Journal of Colloid and Interface Science* **2008,** *326* (2), 530-536.

APPENDIX

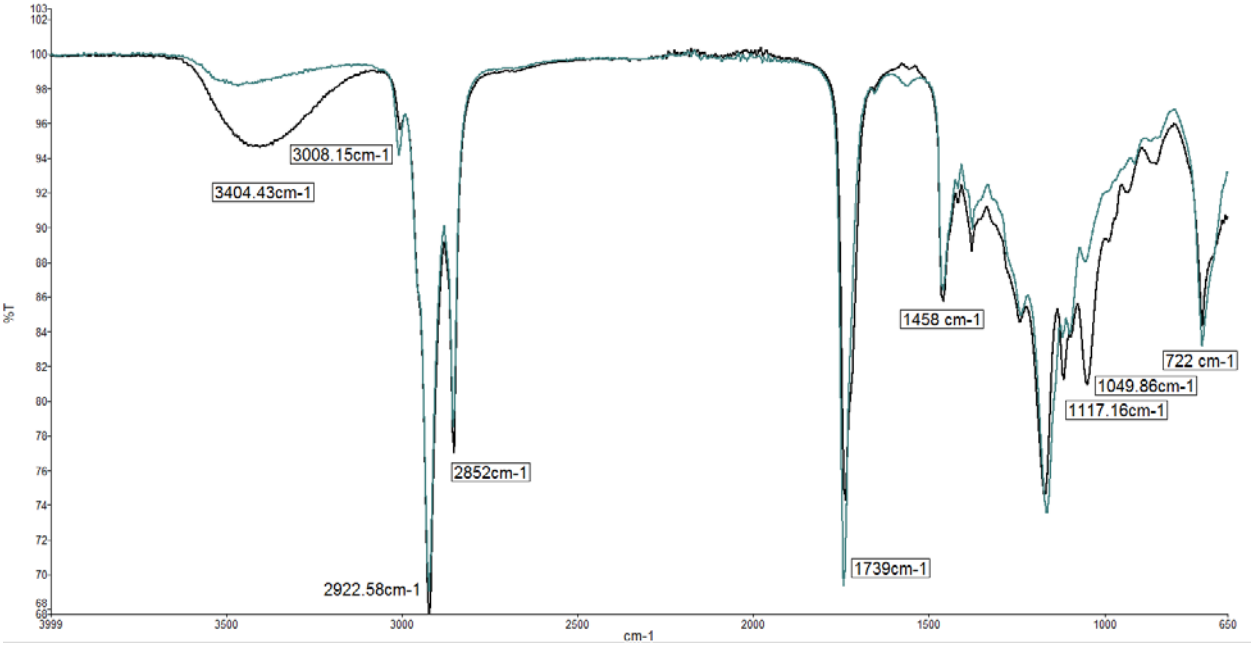

Figure 45: IR of glycerol oleate mixtures

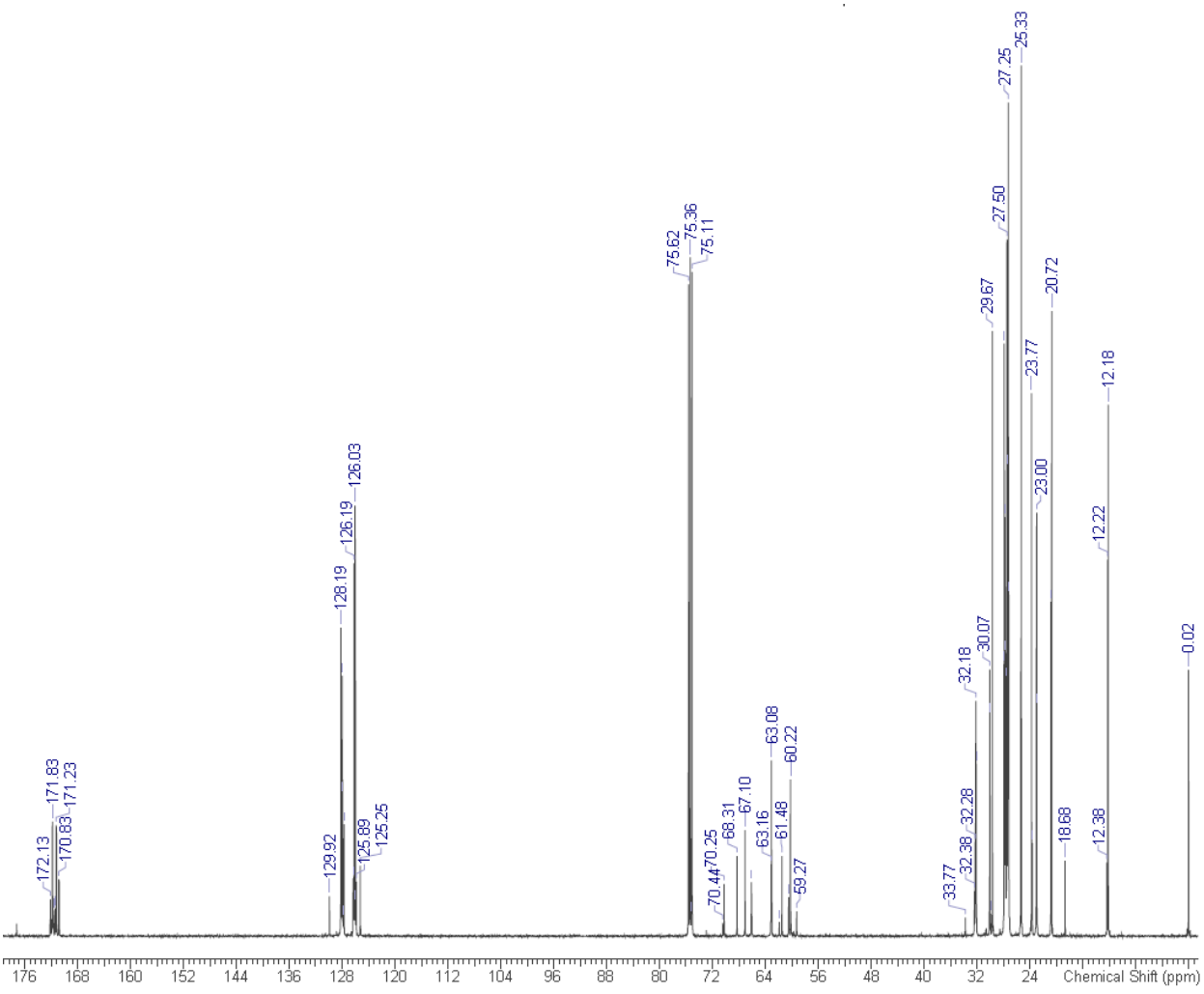

Figure 46: ^{13}C NMR spectrum of glycerol dioleate mixture

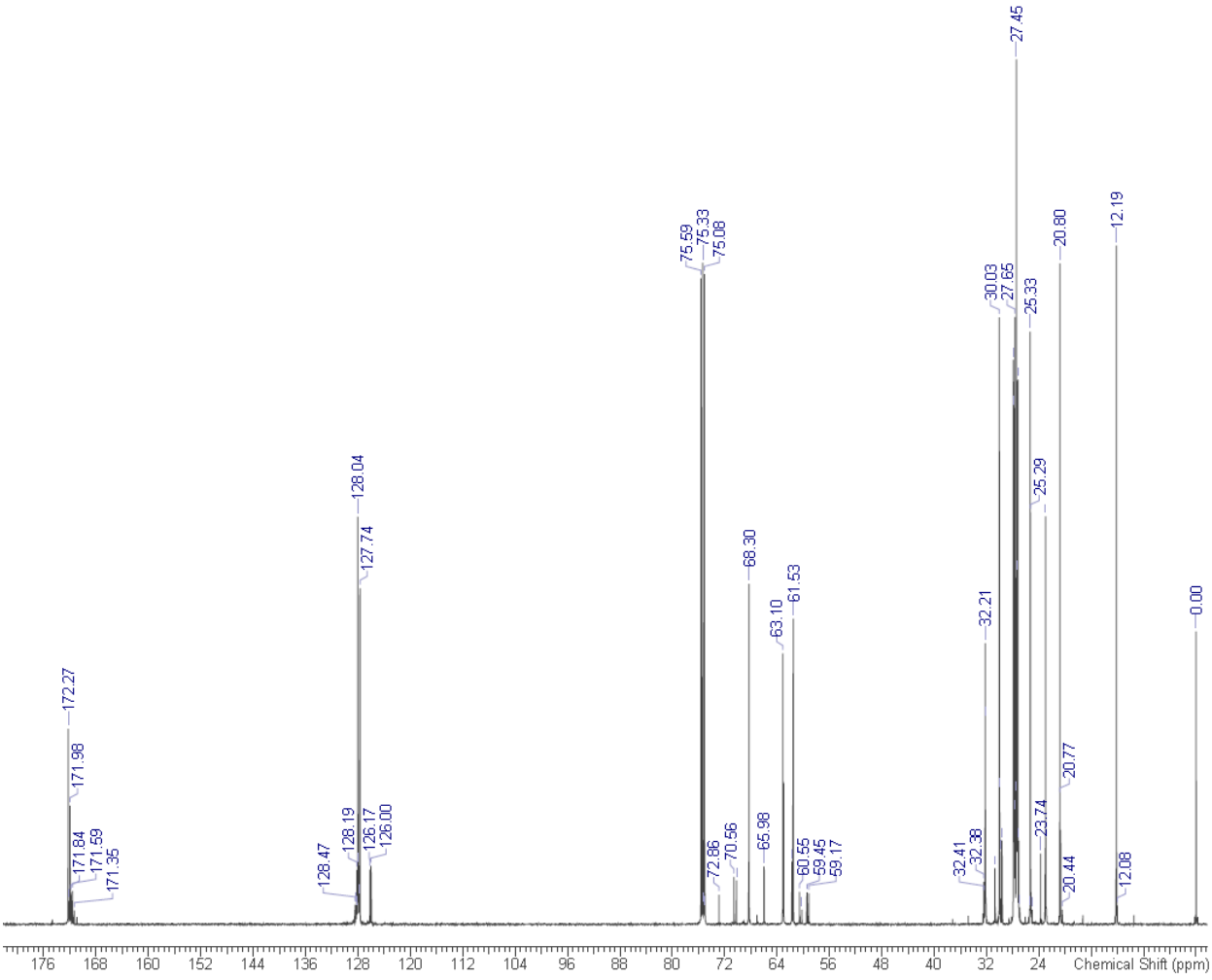

Figure 47: ^{13}C NMR spectrum of glycerol monoleate mixture

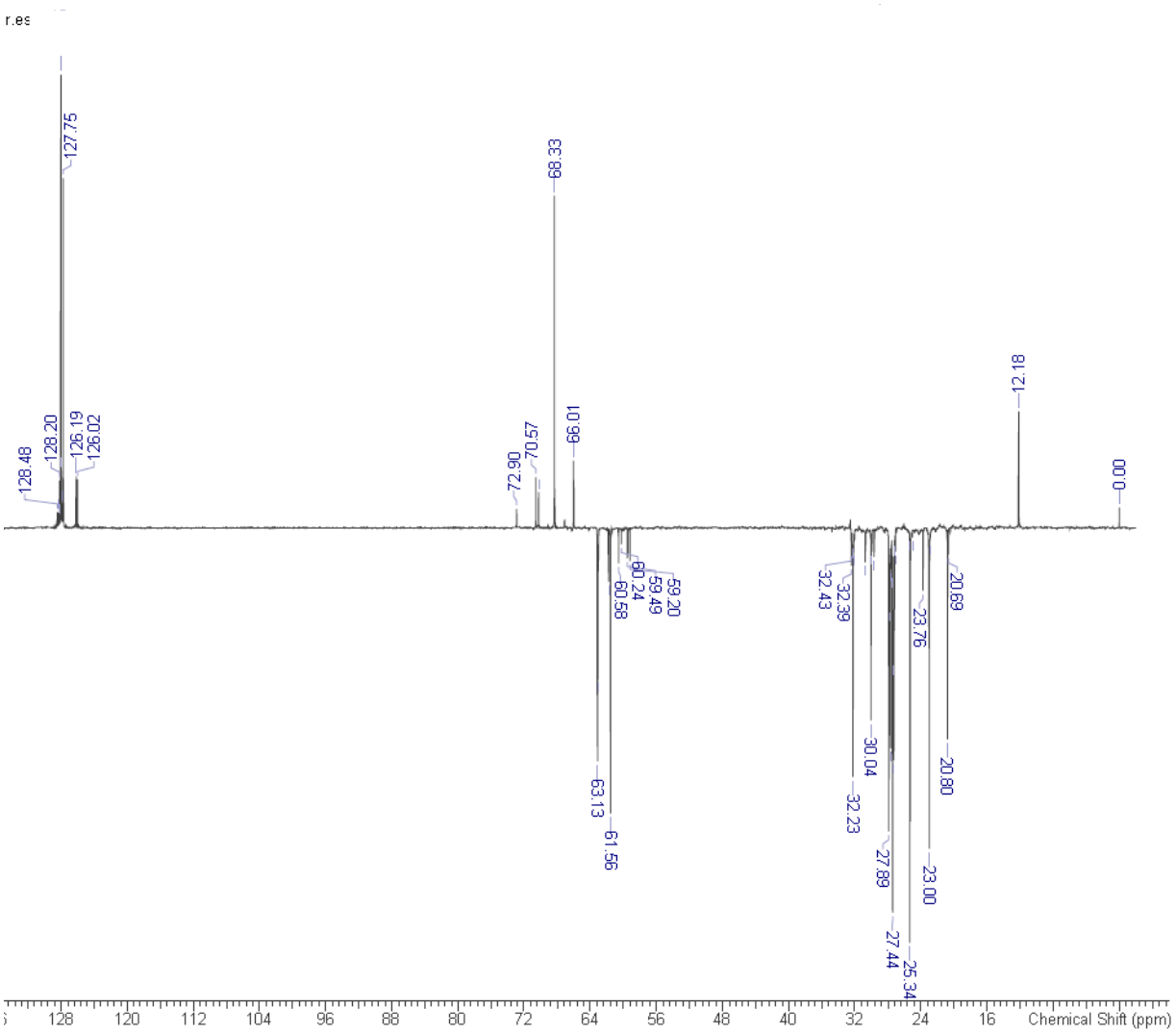

Figure 48: DEPT-135 spectrum of glycerol monoleate mixture

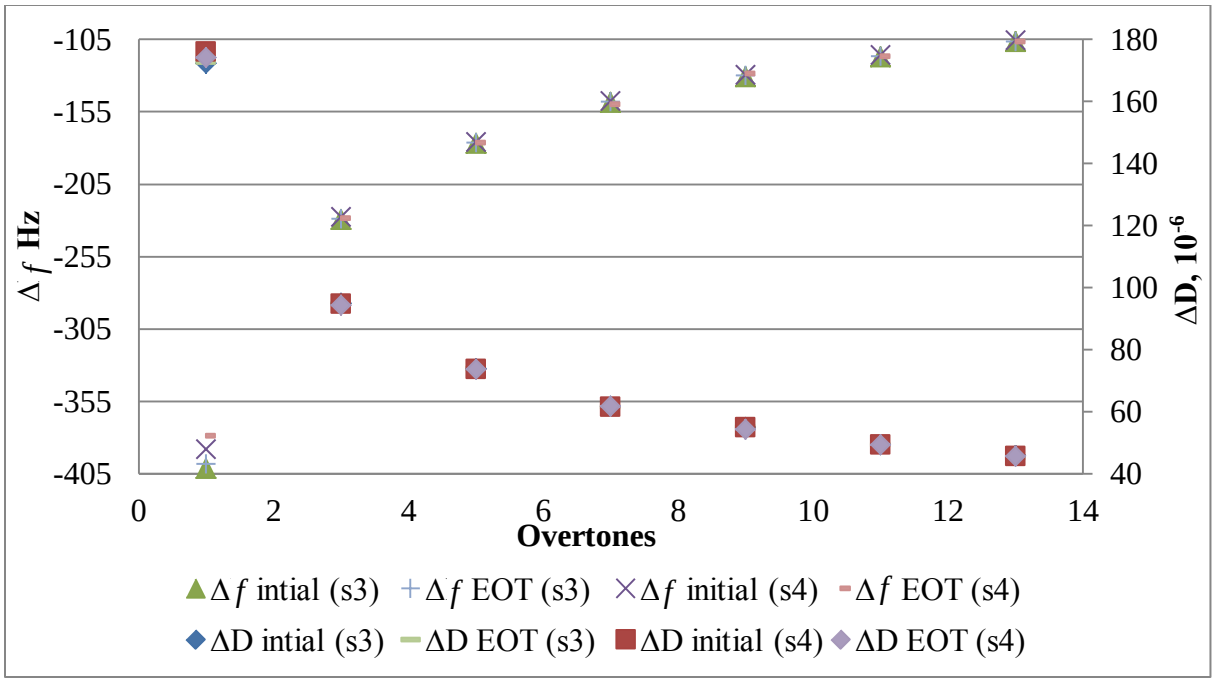

Figure 49: Initial frequency and dissipation shift measured from air to iso-octane by two different crystals (s3 and s4). These values were then compared to the same crystals after the adsorption of fatty acids and cleaning (End of Test, EOT). The frequency returned to within 0.9% and dissipation within 0.4%.

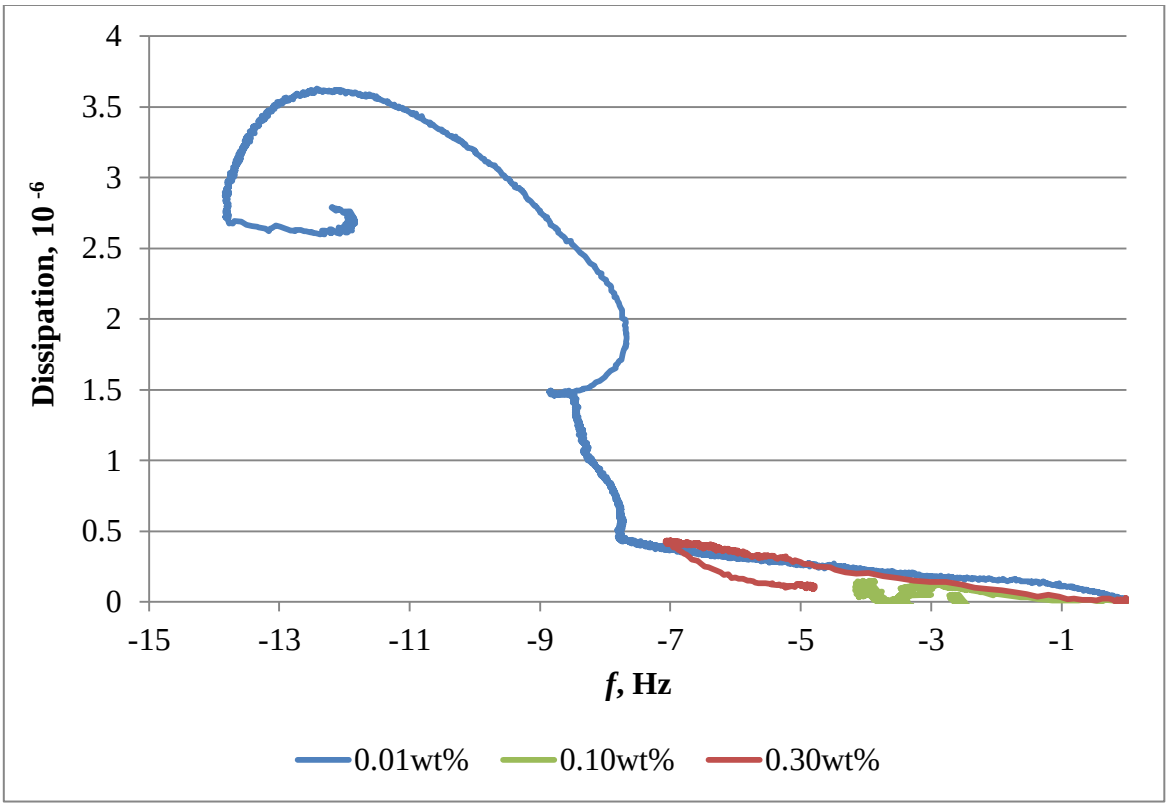

Figure 50: Frequency and dissipation curve of oleic acid at three different concentrations. Initial adsorption occurs through same mechanism, but at the lower concentration the film begins to become dissipative. Upon rinse two different mechanisms occur. The higher concentration (red) removes phyisorbed oleic acid illustrated by the decrease in frequency and dissipation upon rinse. The lowest concentration incorporates solvent into film illustrated by the increasing the dissipation and frequency. Physisorbed oleic acid may be removed at the same time but the two phenomena cannot be distinguished in this data.